Salinity distribution in the upper layers of the Bay of Bengal and its response to climatic events

Thesis submitted to the
Cochin University of Science and Technology
in partial fulfilment of the requirements for the degree of
DOCTOR OF PHILOSOPHY
in
PHYSICAL OCEANOGRAPHY

Under the Faculty of Marine Sciences
by
ANOOPA PRASAD C
(Reg. No. 4318)

Naval Physical and Oceanographic Laboratory
Kochi - 682 021

December 2017

to my parents

Declaration

I hereby declare that the thesis entitled, "**Salinity distribution in the upper layers of the Bay of Bengal and its response to climatic events**" is an authentic record of the research work carried out by me and no part thereof has been presented for the award of any degree or diploma in any University or Institution.

Kochi-21   Anoopa Prasad C
December, 2017   (Reg. No. 4318)

Certificate

This is to certify that the thesis entitled, "**Salinity distribution in the upper layers of the Bay of Bengal and its response to climatic events**" is an authentic record of research work carried out by Ms. Anoopa Prasad C under my supervision and guidance at Naval Physical and Oceanographic Laboratory, Kochi-21, in partial fulfilment of the requirements for the award of Ph.D. degree of the Cochin University of Science and Technology in the Faculty of Marine Sciences and no part of it has previously formed the basis for the award of any degree in any university. All the relevant corrections and modifications suggested by the audience during the pre-synopsis seminar and recommended by the Doctoral committee have been incorporated in the thesis.

Kochi-21   Dr. P V Hareesh Kumar
December, 2017   (Research Guide)
                                        Associate Director & Scientist 'G'
                                  Naval Physical and Oceanographic Laboratory
                                                  Kochi- 21

Acknowledgements

Preface

The Bay of Bengal (BoB) located in the northeastern Indian Ocean is forced by seasonally reversing monsoon winds. The huge amount of freshwater influx due to heavy rainfall and river runoff associated with the summer monsoon makes the BoB one of the very low salinity basin in the tropical oceans. The freshwater flux increases the near surface stratification, inhibits vertical mixing and maintains high sea surface temperature. This strong near surface stratification is ideal for deep convection and rainfall. These features makes the bay dynamic and hence draws interest of researchers from around the world. The goal of the thesis is to improve the understanding of the salinity variability in the upper layers of the BoB with emphasis on the oceanic and atmospheric processes leading to this variability on different timescales. Moreover, characterization of the watermasses, various processes that contribute to the saltening of the BoB and the salinity variability associated with the climatic events are addressed.

Analysis of salinity based on the existing climatologies reveal a seasonal cycle in the surface salinity with intense freshening of the northern part of the basin during the summer monsoon season, which subsequently spreads along the coastal periphery. Therefore, the temperature-salinity for 61 years (1950-2010) is analyzed on different spatio-temporal scales with special emphasis on the variability along the coastal periphery of the BoB. The inadequate salinity data prevented the study of its variability around this seasonal picture with a good spatial coverage. To have proper judgment of the mechanisms driving the seasonal and inter-annual salinity variability, the climatology is supplemented with global observational programs like Argo and RAMA. Moreover data from exclusive field experiments such as BOBMEX, WOCE, and other ships of opportunity are utilized. Unlike in the earlier studies, all these data sets were utilized to identify the three watermasses in the upper layers of the BoB, which seems to be very essential to understand the dynamics of the bay and to describe their evolution and generation mechanisms. Subsequently, how the continuous freshening in BoB is supplemented or balanced with high salinity water from subsurface level is investigated. Contrary to earlier assumption that the saltening of the BoB occurs by lateral advection from the rest of the Indian Ocean, it is revealed that the vertical exchange with the subsurface saltier waters also plays a significant role in increasing surface salinity. Finally, the responses of salinity to climatic events like Indian Ocean Dipole, El Niño/La Niña and flood/drought monsoon years are discussed.

Contents

List of Abbreviations

APDRC	Asia Pacific Data Research Center
Argo	Array for Real-Time Geostrophic Oceanography
AS	Arabian Sea
ASCAT	Advanced Scatterometer
AVISO	Archiving Validation and Interpretation of Satellite Oceanography
BoB	Bay of Bengal
BOBMEX	Bay of Bengal Monsoon Experiment
DMI	Dipole Mode Index
EICC	East India Coastal Current
ENSO	El-Niño Southern Oscillation
IOD	Indian Ocean Dipole
NDW	Northern Dilute Watermass
nIOD	negative Indian Ocean Dipole
pIOD	positive Indian Ocean Dipole
QuikSCAT	QuicK SCATterometer
RAMA	Research Moored Array for African-Asian-Australian Monsoon Analysis and Prediction
SBBW	Southern Bay of Bengal Watermass
SEAS	southeastern Arabian Sea
SLA	Sea Level Anomaly
SMC	Summer Monsoon Current
SODA	Simple Ocean Data Assimilation
SSS	Sea Surface Salinity
SST	Sea Surface Temperature
TW	Transition Watermass
WICC	West India Coastal Current

List of Figures

Chapter 1

Introduction

Bay of Bengal (BoB) is a semi-enclosed tropical basin in the northeastern part of the Indian Ocean. Apparently due to the geographical location, the bay comes under the influence of the seasonal reversal of winds known as monsoon. Basically, the reversal of wind direction is due to the differential heating between land and ocean. The winds blow from the southwest during summer monsoon (June-September) and from the northeast during winter monsoon (November-February) (Fig. 1.1 a, b). In general, the summer monsoon winds are much stronger than the winter monsoon winds. In addition, the summer monsoon is associated with heavy rainfall. The transition between the monsoons occurs in March-April and October with weak winds.

In response to these monsoon winds, the BoB exhibits a seasonal cycle in the hydrographic structure and circulation pattern. The surface circulation in the BoB is characterized by an anti-cyclonic northwestern gyre centered at 15°N during winter and cyclonic during summer. With the onset of southwest monsoon, the circulation becomes more dynamic and is in general anti-clockwise. In this season, the southern Bay (5°-10°N) is fed by the eastward flowing Summer Monsoon Current (SMC). The SMC (Fig. 1.1d) advect high salinity water from the Arabian Sea (AS) into the BoB (Vinayachandran et al., 1999; Jensen, 2001) till September and dissipates by October. Potemra et al. (1991) reported strong cyclonic circulation around 18°N in the northern bay. During this period, the East India Coastal Current (EICC) flow poleward along the southern part (south of 15°N) and equatorward in the north (Shetye et al., 1991). Moreover, the EICC plays a significant role in connecting the BoB with equatorial Indian Ocean and AS (Shankar et al., 2002; Durand et al., 2009; Shenoi, 2010). In winter, a westward flowing current, known as the North Equatorial Current/Winter Monsoon Current is present in the equatorial region (Fig. 1.1c). This current is noticed between November and April with its peak in February. During the period November to January, the EICC flow equatorward all along its path and by February reverses its direction everywhere north of 10°N. Subsequently, during February-May the BoB exhibits an anti-cyclonic gyre with a poleward EICC (Shetye et al., 1993; Shenoi, 2010).

During the transition period between the monsoons, Kelvin waves are triggered in the equatorial region. Yu et al. (1991) have shown that the eastward propagating Kelvin wave, on reflecting from the eastern boundary (off Sumatra

coast), propagates along the coastal waveguide of the BoB as a coastal Kelvin wave, radiating westward propagating Rossby waves into the interior bay and influences the western boundary region of the BoB (McCreary et al., 1996; Shetye et al., 1996). Besides, McCreary et al. (1993) have shown that the winds along the eastern boundary of the BoB also trigger similar Kelvin waves, which influences West India Coastal Current (WICC). Out of two pairs of upwelling and downwelling Kelvin wave, the second downwelling Kelvin wave formed in October-December enters the Arabian Sea, whereas the two upwelling Kelvin waves (January-March and August-September) and first downwelling Kelvin wave (April-June) are confined to the coastal waveguides of the BoB (Rao et al., 2009). The remote wind forcing from the equatorial Indian Ocean and eastern rim of the BoB in the form of coastal Kelvin waves leads to seasonal reversal of EICC that precedes wind reversal by several months (Yu et al., 1991; McCreary et al., 1993, 1996; Shankar et al., 1996). The spatio-temporal variability of the EICC is generated by remote forcing, in union with local wind forcing and intrinsic hydrodynamic instabilities (Durand et al., 2009; Chen et al., 2012; Cheng et al., 2013).
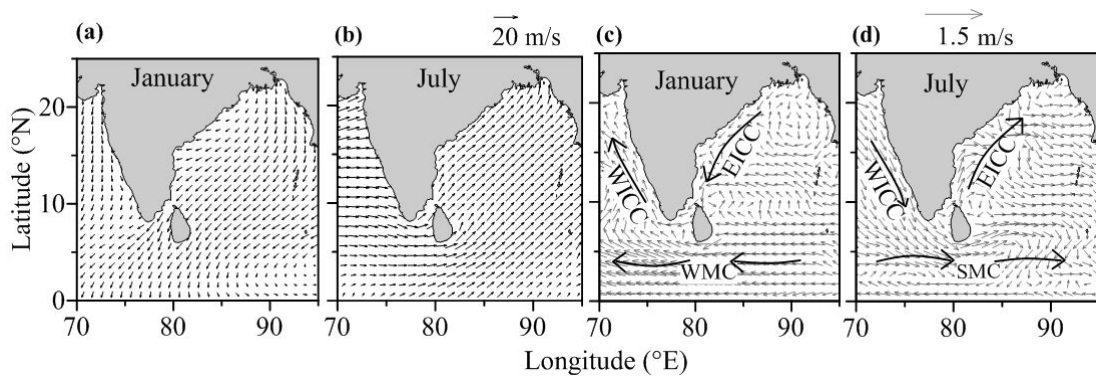
Fig. 1.1 Mean wind direction from QuikScat and surface circulation from SODA during winter monsoon (January) (a) and (c) and summer monsoon (July) (b) and (d). WMC-Winter Monsoon Current, SMC- Summer Monsoon Current, EICC- East India Coastal Current, WICC- West India Coastal Current.

Moreover, EICC has several meso-scale features in the form of cyclonic and anti-cyclonic eddies (Durand et al., 2009) which further complicates the circulation pattern in the BoB. The spatial scale of these features ranges from a few tens of kilometers to few hundreds of kilometers, while their temporal scale ranges from few weeks to few months (Robinson, 1983). If the spatial dimension of eddies is of the order of the Rossby deformation radius (~100 km) then they are called meso-scale eddies. In the northern hemisphere, eddies with clockwise circulation are called anti-cyclonic (warm water and high sea level at the center) and cyclonic are those with

anti-clockwise circulation (cold water and low sea level at the center). Water converges in an anti-cyclonic eddy and diverges in cyclonic eddy, leading to downwelling and upwelling respectively at their centers.

The combined use of *in situ* and altimetry observations reveals that eddies are recurrent features in the BoB throughout the year (Ali et al., 1998; Gopalan et al., 2000; Prasanna Kumar et al., 2004, 2007; Kurien et al., 2010; Nuncio and Prasanna Kumar, 2013; Hareesh Kumar et al., 2013). Along the western periphery of the BoB, the presence of eddy off Vishakhapatnam during March-April and October-November resulted in strong cross-shore temperature gradient (Ramasastry and Balaramamurty, 1957). Later, Rao and Sastry (1981) associated the nutrient distribution with cyclonic and anti-cyclonic flow. However, high stratification in the upper layers inhibited the cold core eddy signal to be seen in the surface temperature and salinity field during the southwest monsoon (Babu et al., 1991). Cyclonic eddies play a key role in transferring nutrients from subsurface depths into the euphotic zone and enhances the biological productivity by more than double compared to the non-eddy region (Gomes et al., 2000; Madhupratap et al., 2003; Prasanna Kumar et al., 2007; Nuncio and Prasanna Kumar, 2013). On the other hand, the intense warm core eddies enhances the heat potential and often positively feedback to cyclone intensification (Goni 2008; Ali et al., 2007). Therefore several studies on cyclonic and anti-cyclonic eddies have shown that their presence alters the hydrography and biogeochemistry of the BoB (Prasanna Kumar et al., 2004; Nuncio, 2007).

Another aspect that influences the circulation along the western boundary of the BoB during the summer monsoon, is the upwelling along the southern part of the east coast of India (Shetye et al., 1991; Gopalakrishna et al., 2002) Here, the upwelling commences as early as in March which is confined very close to the coast (mostly within 40 km) and episodic (LaFond and LaFond, 1968; Murty and Varadachari, 1968; Shetye et al., 1991). Even with the southwesterly winds, upwelling is not very intense along the western boundary of the BoB. This is due to the equatorward flow of the freshwater plume in the north which could overwhelm the offshore Ekman transport (Gopalakrishna and Sastry, 1985; Shetye et al., 1991; Gopalakrishna et al., 2002). Utilizing the data collected along a 13ºN transect from 87ºE to Chennai, Vinayachandran and Kurian (2007) observed that the upwelled water was marginally cooler (<0.5ºC) and saltier (0.25) than that outside the

upwelling band. Recent study by Sil and Chakraborty, (2015) illustrated downwelling in the northern BoB during winter monsoon with the arrival of northeast wind.

1.1   A review on the salinity variability in the upper layers of Bay of Bengal

The BoB receives a large quantity of freshwater through rainfall and runoff from rivers like Ganges, Brahmaputra, Godavari, Mahanadi, Cauvery, Irrawaddy, and Krishna (1.625 x 10^{12} m^3/yr; Subramanian, 1993) leading to lowering of salinity of the bay, particularly in its northern part. In such a freshwater dominant environment, salinity, rather than temperature, plays a governing role on density variation in the upper layers. The freshwater advect southward along the coastal periphery of the eastern BoB during the summer monsoon. Only during the northeast monsoon, the remnants of freshwater in the northern BoB flow southwards along the western periphery of the BoB (Shetye et al., 1996; Anoopa and Hareesh Kumar, 2015). The spreading of the freshwater into the interior of the bay affects the circulation pattern and the thermohaline characteristics in the entire basin (Han et al., 2001). This is supported by the field measurement programs (Sengupta et al., 2006; D'Addezio et al., 2015; Pant et al., 2015) and modeling studies (Han and McCreary, 2001; Howden and Murtugudde, 2001; Jensen, 2003; Benshila et al., 2014; Akhil et al., 2014; Wilson and Riser, 2016). These studies have stressed the importance of low salinity waters of BoB origin in the modification of salinity structure in the Arabian Sea and equatorial Indian Ocean.

North of 15°N, the freshwater pool is confined to the upper 30 m with a strong halocline below, thereby increasing the upper layer stratification (Prasanna Kumar et al., 2002; Sengupta et al., 2006; Sengupta et al., 2016) and hindering vertical mixing between the surface and deep waters. Studies (Shetye et al., 1991; Shetye, 1993; Rao et al., 1994) have shown that the strong haline stratification affects the biological, biogeochemical processes and results in the occurrence of oligotrophic conditions. In addition, the strong vertical stratification reduces the effects of storm-induced surface cooling, which may in turn support strengthening of tropical cyclones (Sengupta et al., 2008; Neetu et al., 2012; Vincent et al., 2012).

Another consequence of freshwater flux into the head of the BoB is the formation of a shallow, salinity-stratified mixed layer above the deeper isothermal layer (Shetye et al., 1996; Rao and Sivakumar, 2003; Thadathil et al., 2007). The layer

between the shallow mixed layer and the isothermal layer is called the barrier layer (BL; Lukas and Lindstrom, 1991). The BL hampers the vertical exchanges of heat and momentum between the upper mixed layer and the thermocline (Lucas et al., 2016). The presence of BL leads to high SST throughout the basin (Shenoi et al., 2002; de Boyer Montégut et al., 2007), which is ideal for deep atmospheric convection (Neetu et al., 2012). In the BoB BL develop during October-November and peak during December-March (Thadathil et al., 2002; Rao and Sivakumar, 2003; de Boyer Montégut et al., 2007). Besides, BL occur in conjunction with temperature inversions (Thadathil and Gosh, 1992; Thadathil et al., 2002; Girishkumar et al., 2013; Drushka et al., 2014).

During summer monsoon, the sea surface salinity increases by 14.5 units (Salinity is expressed in the Practical Salinity Scale, i.e. in grams of salt per kilogram of seawater, hence without units) between the head of the bay and the southern bay at 5ºN, i.e. from about 20 to about 34.5 (Murty et al., 1992). The comparatively saline water in the southern BoB is partly due to the intrusion of SMC which brings saltier Arabian Sea water (Murty et al., 1992; Vinayachandran et al., 1999). Even though BoB receives intense freshwater discharge during June to September, this water reaches the interior bay only by October-November. Here, the surface salinity exhibits a decrease from south to north (34 at 7°N to 32 at 16°N) and drops by 3 units at 17°N during the post-monsoon season. Similar pattern of variation was observed in the coastal regions but the drop was more pronounced between 16°N and 17°N (34 to 21). During pre-monsoon period, i.e. March-May, due to dearth of freshwater the sea surface salinity is relatively high and hence the overall variation in salinity is between 32 and 34. This results in a uni-modal distribution in salinity with peak occurring just prior to the onset of summer monsoon and minimum in October. Therefore, salinity in the BoB is highly heterogeneous and exhibits variability at different spatial and temporal scale due to differences in freshwater flow and heat exchange (Rao and Sivakumar 2003; Benshila et al., 2014). The strong lateral salinity gradient at the surface also leads to salinity fronts (Hareesh Kumar et al., 2013) that give rise to a host of instabilities over a range of spatial and temporal scales.

Some studies have used the available hydrographic data to specifically describe the low saline watermasses in the BoB (La Fond 1958; Gallagher 1966; Emery and Meincke 1986; Murty et al., 1992; Varkey and Sastry 1992; Varkey et al.,

1996; Sarma et al., 1999). Based on the hydrographic survey in the western BoB, La Fond (1958) grouped the surface waters of BoB into three, viz., the Northern Dilute Watermass (NDW), Transition Watermass (TW) and Southern Bay of Bengal Watermass (SBBW). But, it fell short in providing a comprehensive picture of the evolution and formation mechanism of the surface watermasses as the study was localized in space and time. Later, Rao and Jayaraman (1968a) based on their observations in southwestern BoB during northeast monsoon noticed BoB watermass (S<34; σ_t<22) in the surface layers. Rao and Jayaraman (1968b) named the low salinity water in the upper 50 m of the eastern Bay and Andaman Sea (S < 33, σ_t < 21) as Eastern Dilute Water of Indo-Pacific origin. Their study also revealed another watermass in the upper 100 m of the southern Bay and the western and middle parts of the central Bay (S: 33-34, σ_t: 21-22) which resembles the SBBW. Emery and Meincke (1986) described BoB water as the water in the surface layer having salinity from 28 to 35 and temperature in the range 25-29°C. In the northwestern BoB low density water (σ_t <14) with strong horizontal gradient in the surface layer and σ_t >21 at 50 m depth was reported by Sasamal (1989). He associated low density with low salinity which resulted in surface density distribution similar to that of salinity. Shetye et al. (1993) observed variations in T-S due to freshwater influx during summer monsoon. Varkey et al. (1996) documented the characteristics of the Bay of Bengal Low Salinity Water (BBLSW) in the northern Bay and Andaman Sea with T = 27°C, S = 33 and σ_t ~ 21.2. Sarma et al. (1999) observed wide scatter in the upper layers of T-S structure due to freshwater influx and prevailing surface currents along 18°N and 90°E. Utilizing high resolution regional model, Benshila et al. (2014) described the seasonal salinity structure and identified the pathways of the northern bay freshwater based on passive tracer experiments. Studies subsequent to La Fond (1958) regarded the surface watermasses of BoB as a single entity without considering its classification, despite the fact that surface water exhibit wide variation from one region to another due to differences in freshwater inflow and heat exchange. Also, the information regarding the spatio-temporal variation of watermasses and generation are comparitively limited. However, none of these studies provide a comprehensive picture of the structure of watermasses in the BoB as they evolve round the year or provide a quantitative estimate. Another aspect associated with BoB watermass is its advection into the southeastern Arabian Sea (SEAS) during winter. Earlier studies based on data from synoptic transects (Thadathil and Ramaraju 1987; Shetye et al.,

1996; Hareesh Kumar and Mathew 1997) described its transport into the SEAS. The availability of temperature and salinity data at higher spatio-temporal resolution helps to discern the origin of BoB water that is advected into the SEAS.

At subsurface depths (~150 m), Arabian Sea Watermass is identified in the southern bay towards equator (Murty et al., 1992; Jensen, 2001; Vinayachandran et al., 2013). The watermasses below 100-150 m depth in the central and southern BoB are Equatorial Surface Water (ESW) with σ_t of 22.5, Persian Gulf Water (PGW) below 300 m depth (σ_t ~26.81) overlying the Red Sea water (RSW) characterized by σ_t ~27.19 (Varkey and Sastry, 1992). The existence of PGW in the BoB was reported initially during the IIOE (Rochford, 1964; Varadachari et al., 1968). Sastry et al. (1985) also observed the existence of PGW in the bay between 200-900 m; however, he interpreted the broad salinity maximum as a possible mix of PGW and RSW. Later studies, whether observational or model-based, suggested that PGW and RSW are confined to the Arabian Sea (Shenoi et al., 1993; Han and McCreary, 2001). Recently, Jain et al. (2016) elucidated the presence of PGW in the depth ranges of 200-450 m and RSW throughout the bay at depth between 500 and 1000 m.

1.2   Inter-annual variability in the salinity structure

Studies on inter-annual salinity variability in the BoB are very much limited due to the scarcity of sufficient long term measurements. However over the past few years, consistent progress in salinity observation system in the BoB has enabled its monitoring on longer temporal and larger spatial resolution. Rao and Sivakumar (2003) noticed pronounced seasonal variability of sea surface salinity (SSS) in the coastal regions of the northern BoB. Beyond this seasonal variability, much less is known about salinity variations at inter-annual timescales. However studies in the recent past (Grunseich et al., 2011; Chaitanya et al., 2015; Pant et al., 2015) shows that SSS varies on inter-annual timescales which are induced by two dominant modes of tropical coupled ocean-atmospheric variability, the El Niño/Southern Oscillation (ENSO) (Tziperman et al., 1998) and the Indian Ocean Dipole (IOD) (Saji et al., 1999). El Niño refers to the anomalous warming of the tropical eastern Pacific Ocean and similar warming in western equatorial Indian Ocean leads to IOD. Salinity variation contributes greatly to IOD formation through positive feedbacks that enhance temperature variations and drive IOD circulation across the tropical Indian Ocean. Although signature of salinity cannot be directly observed in the atmosphere,

feedbacks act indirectly on the atmospheric component of the dipole (Murtugudde and Busalacchi, 1998). The effect of salinity on SST anomalies is to create areas of enhanced or reduced convection, resulting in precipitation anomalies across the equatorial Indian Ocean (Webster et al., 1999). These precipitation anomalies also act to increase or decrease SSS anomalies, thus completing a feedback. Rao and Sivakumar (2003) brought out the inter-annual variability of SSS and its variability during El Niño episodes using the historic data along two major shipping lines in the tropical Indian Ocean. Their study showed that the southeastern BoB has considerable salinity variability associated with El Niño years. Based on ocean numerical models, Thompson et al. (2006) demonstrated the IOD influences on the upper ocean circulation of the BoB. The surface circulation is anomalously anti-cyclonic during a positive IOD and affects the freshwater transport between the equatorial Indian Ocean and BoB. This circulation pattern induces fresh anomalies in the eastern bay (Thompson et al., 2006; Jensen, 2007). Conversely, during a negative IOD event, the BoB circulation is anomalously cyclonic and induces salty anomalies in the eastern bay (Thompson et al., 2006). Using a numerical model, Jensen (2007) examined the watermass exchanges between the Arabian Sea and BoB during El Niño, La Niña and IOD events and concluded that transport from the Arabian Sea (BoB) to BoB (Arabian Sea) is enhanced (decreased) during El Niño and IOD years.

Using a coupled model Vinayachandran and Nanjundiah (2009) reported large amount of freshwater input into the BoB during summer monsoon and its redistribution decides the spatial pattern of salinity. While during winter monsoon, salinity variations are induced by horizontal advection and also showed that the SSS anomalies are high during the IOD years. Recently, Pant et al. (2015) showed that enhanced precipitation associated with positive Indian Ocean Dipole (pIOD) lead to enhanced freshening in the northern BoB. Their study also emphasized that, IOD rather than ENSO controls the inter-annual variability of salinity in the BoB. Recent literatures also illustrate that during IOD phases BL is prominently affected. For instance during the positive phase, upwelling Kelvin wave shoals the isotherms and reduces the barrier layer thickness which in turn strengthens the air-sea interactions (Qiu et al., 2012; Cai et al., 2013). While studying the upper ocean salinity stratification in the BoB and its role on air-sea interactions, Shenoi et al. (2002) and Neetu et al. (2012) stressed the importance of exploring and quantitatively estimating

the salinity variability on inter-annual scale especially during climatic events like IOD and El Niño/La Niña.

Even though several studies were made to understand the complex nature of the circulation and hydrography of the BoB, research voids exist due to the limitation of data availability. With the recent observational programs, reliable data sets are now available for extensive research in this area. One of the precinct that has to be addressed is the comprehensive documentation of the watermasses in the surface layers of the BoB, their evolution and formation mechanism. Even though BoB is known as a low salinity basin, the mechanisms for maintaining the salt balance of the basin are not fully explored. The modeling study of Akhil et al. (2014) shows that vertical mixing of surface fresh waters with underlying saltier waters is the primary driver of the saltening phase. Their study also implies that erosion of the freshwater tongue along the east coast of India is due to vertical processes rather than horizontal advection. Chowdary et al. (2016) emphasizes the significance of accurate representation of vertical processes in general circulation models so that they simulate realistic surface and subsurface salinity structure in the BoB. Except few studies (Vinayachandran et al., 2013) carried out recently, the significance of vertical processes in increasing surface salinity were hardly dealt previously. Though some studies on inter-annual variability of salinity in the BoB are made, its quantitative estimates during the climatic events like IOD and El Niño/La Niña are not well addressed. All these research areas are quite important to understand the salinity variability in the upper layers of the BoB due to its potential role in the upper ocean dynamics. The thesis is an attempt in this direction to explain and document salinity variability in the BoB on different spatio-temporal scales and to address some of the aspects mentioned above utilizing recently available wide spectrum of datasets.

1.3 Objectives

The prime objectives of the present work are

(i) To study the salinity variability in the BoB on different spatio-temporal scales and its causative factors,

(ii) To document the evolution, characteristics and formation mechanism of the major watermasses in the surface layers,

(iii) To understand and describe the saltwater pumping and it's possible mechanisms and

(iv) To decipher the influence of major climatic events on salinity variations.

1.4 Thesis layout

The work is presented in seven chapters. A detailed literature review on the studies related to the topic of investigation is presented in the first chapter. The second chapter deals with a detailed description of the various data sets utilized in the thesis and the methodology employed for the data analysis. In Chapter 3, the basin scale variability of salinity in the BoB on different time scales is examined. Chapter 4 describes the evolution of prominent watermasses in the upper layers of BoB and delineation of forcing. The salt water pumping in the BoB and their possible causative factors are documented in Chapter 5. The response of salinity variations to climatic events like Indian Ocean Dipole, El Niño / La Niña and different regimes of summer monsoon are described in Chapter 6. Finally, in Chapter 7, summary and conclusion of the work is presented. The thesis concludes with bibliography at the end.

Chapter 2

Data and Methodology

2.1 Introduction

A suite of oceanographic and atmospheric data supplemented by the satellite information is essential to understand the variability of temperature and salinity in the BoB and its response to the atmospheric forcing. The hydrographic data from various climatology and *in situ* sources forms the framework of the present work. In addition, satellite derived datasets such as sea level anomaly (SLA), wind, current, precipitation, river discharge, evaporation and net heat flux are used to study the response of salinity to these factors more precisely than before.

2.2 Study Area

The BoB is bounded by India and Sri Lanka to the west, Bangladesh to the north, and Myanmar and the Andaman and Nicobar Islands to the east. The geographical domain of BoB extending from 0 to 25°N and 75°E to 95°E (Fig. 2.1) is chosen as the study region of the present work. The continental shelf along the east coast of India is very narrow in the south and gradually widens towards the north with an average width and depth of about 40 km and 30 m respectively. The coastline has interesting geo-morphological features such as a northeast-oriented coastline from the southern end of the peninsula to 10ºN. Beyond it, rather abruptly, the coastline orientation changes to southwest-northeast direction. The bottom topography is almost U-shaped as the southern bay is deeper (~4000 m) and opens to the Indian Ocean. Another unique feature of the Bay is the Swatch of no ground also known as Ganges Trough. It has a moderately flat sea floor of 5 to 7 km wide with its walls at 12° inclination. This Swatch of no ground feeds the Bay of Bengal Fan, the largest submarine fan in the world, by turbidity current. This Fan is approximately 3000 km long, 830-1430 km wide and in excess of 16 km wide. Another feature of the BoB is the Ninety degree East Ridge, which runs in a north-south direction approximately along 90°E.

2.3 Data

In addition to temperature salinity also plays a key role in understanding the ocean dynamics, ocean circulation, and climate change, hence makes both these variables very significant. In a basin like BoB, where the upper ocean dynamics are very complex, information on ocean current, SLA, river runoff, marine meteorological parameters along with the satellite information are also essential to

13

make any specific conclusions. Therefore, in the present work, the climatology of temperature and salinity are supplemented with the *in situ* measurements from the drifting and moored buoy, dedicated field surveys in the BoB and remote sensing data. The other data sets used are the climatology of currents, SLA, river runoff data at the head BoB, satellite derived wind data and heat flux components. The particulars of all the data used in the thesis are given in Table 2.1. Also detailed descriptions of these datasets are given in the subsequent sections.
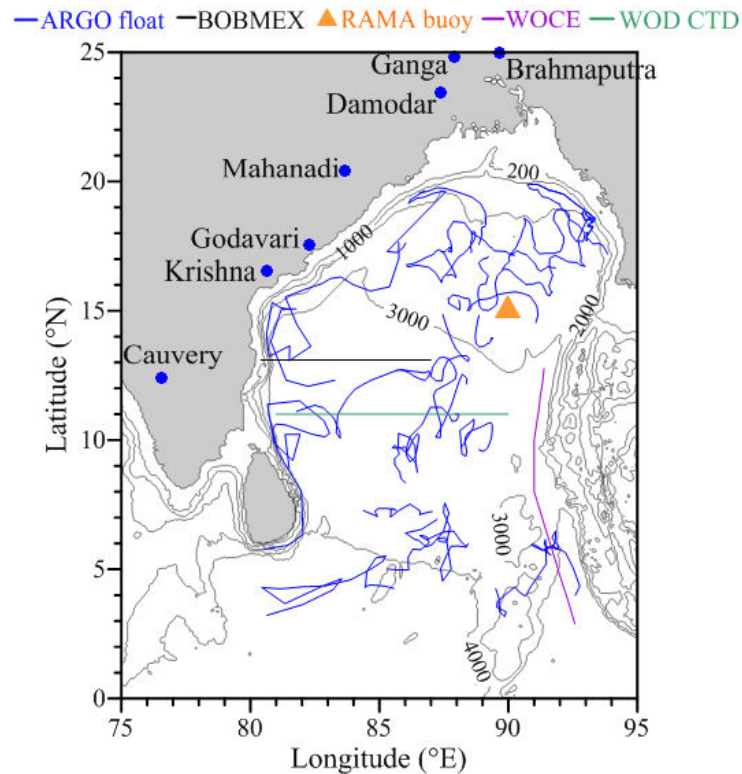
Fig. 2.1 Study area with locations of data from various sources. Argo float (blue line), RAMA buoy (orange triangle), BOBMEX (black line), WOCE (violet line), and WOD CTD (green line). Locations of major river discharge are indicated by blue dots.

2.3.1 Temperature - Salinity

The prime source of temperature and salinity data used in the present work is from the World Ocean Atlas 2013 (WOA 13) and Simple Ocean Data Assimilation (SODA). This is augmented with other data from drifting and moored buoys, dedicated field experiments conducted by various national organizations and satellites. The T-S data are first checked for duplications and subsequently, a large number of quality check procedures were performed. The verified profiles were interpolated to the desired depth levels using standard Lagrangian interpolation.

Table 2.1 Data sets utilized in the study

Parameter	Source	Period/ Temporal resolution	Spatial resolution
T-S	SODA (www.soda.tamu.edu/)	1950-2010 Monthly	0.5°x 0.5°
	WOA 13 (www.nodc.noaa.gov/OC5/woa13/	Climatology	0.25°x 0.25°
	Argo www.coriolis.eu.org	2010-2016 5/10 days	
	RAMA www.pmel.noaa.gov/tao/	2008-2014 Daily	
	BOBMEX-99	July 1999	
	WOCE	February 1995	
SLA	AVISO blended www.aviso.oceanobs.com	1993-2016 7 days	0.33° x 0.33°
Surface current	SODA www.soda.tamu.edu/	1950-2010 Monthly	0.5° x 0.5°
River discharge	SAGE (nelson.wisc.edu/sage/data-and-models/riverdata/	Climatology	
Wind	QuikSCAT apdrc.soest.hawaii.edu/datadoc/qscat_mon_clima.php	Climatology Monthly	0.25° x 0.25°
Wind stress	ASCAT apdrc.soest.hawaii.edu/datadoc/ascat.php	2014 Daily	0.25°x 0.25°
Precipitation	TMI apdrc.soest.hawaii.edu/datadoc/trmm_tmi_mon.php	1998-2010 Monthly	0.25°x 0.25°
Evaporation	OAFlux oaflux.whoi.edu/data.html	1998-2010 Monthly	1° x 1°
Net heat flux	OAFlux oaflux.whoi.edu/data.html	1998-2010 Daily	1° x 1°
Cyclone track	JTWC www.ncdc.noaa.gov/ibtracs/index.php?name=ibtracs-data	2013-2014	

(i)   Climatology and ocean reanalysis

The temperature and salinity from WOA and SODA forms the key source of data. WOA is a set of objectively analyzed climatology of *in situ* temperature and salinity based on data from 1955-2012 for the entire World Ocean (Locarnini et al., 2013; Zweng et al., 2013). The monthly data has a spatial resolution of 0.25 x 0.25 degree and has 57 depth levels (0 - 1500 m) in the vertical. WOA is used to describe

the general temperature-salinity distribution in the bay and for evaluating the efficacy of SODA data.

SODA is an ocean reanalysis data consisting of monthly averaged temperature and salinity fields for the entire global ocean at 0.5°x0.5°x40 level (5.01 - 5375 m). Values of temperature and salinity at 5.01 m depth are considered as SST and SSS respectively. The assimilation methodology is described in Carton et al. (2005) and Carton and Giese (2008). In the present study, the temperature and salinity profile of 61 years spanning from 1950 to 2010 are used to study the long term temperature-salinity distribution. In addition the watermasses in the upper layers of the bay is explored based on the monthly climatology estimated from SODA.

The efficacy of SODA data for oceanographic researches in the Indian Ocean has been documented by several researchers (Thompson et al., 2006; Grunseich et al., 2011; Giese and Ray, 2011). Studies (Fousiya et al., 2015; Chowdary et al., 2016) have shown the reliability of WOA data in model data comparison. Initially, before the SODA data is utilized for any analysis, it is worthwhile to evaluate the SODA salinity data. For this rationale, the surface salinity difference ($\Delta S = S_{WOA} - S_{SODA}$, Fig. 2.2) between WOA (S_{WOA}) and SODA (S_{SODA}) are estimated.

In the coastal periphery of BoB, ΔS is positive throughout the year except in May (Fig. 2.2). During June-August when the circulation is clockwise in the BoB, positive values are observed along the northeastern coastal periphery (~2.25 in August) and it shifts to the northwestern boundary from September till April when the circulation pattern reverses its direction. There is considerable difference in salinity between the two datasets, but, limited to regions where freshwater plays a dominant role with higher values in the WOA. On the other hand, negative ΔS occur in the interior of the northern BoB (north of 10°N and away from coastal boundaries) during January-May and later spreads southward (upto 5°N), but extreme values (~2.5) occur during the period August-February. The difference is only marginal (0.25) in rest of the regions irrespective of whether ΔS is positive or negative, suggesting good agreement between WOA and SODA. One noticeable observation is that, even though ΔS is marginal, it is mostly positive near the equator to 5°N while it is negative north of 5°N. In a nutshell, the difference between WOA and SODA data are large in the coastal regions of the BoB and in the northern BoB, where the freshwater plays a

dominant role in the ocean dynamics. In rest of the bay, the comparison reveals consistency between the two datasets.
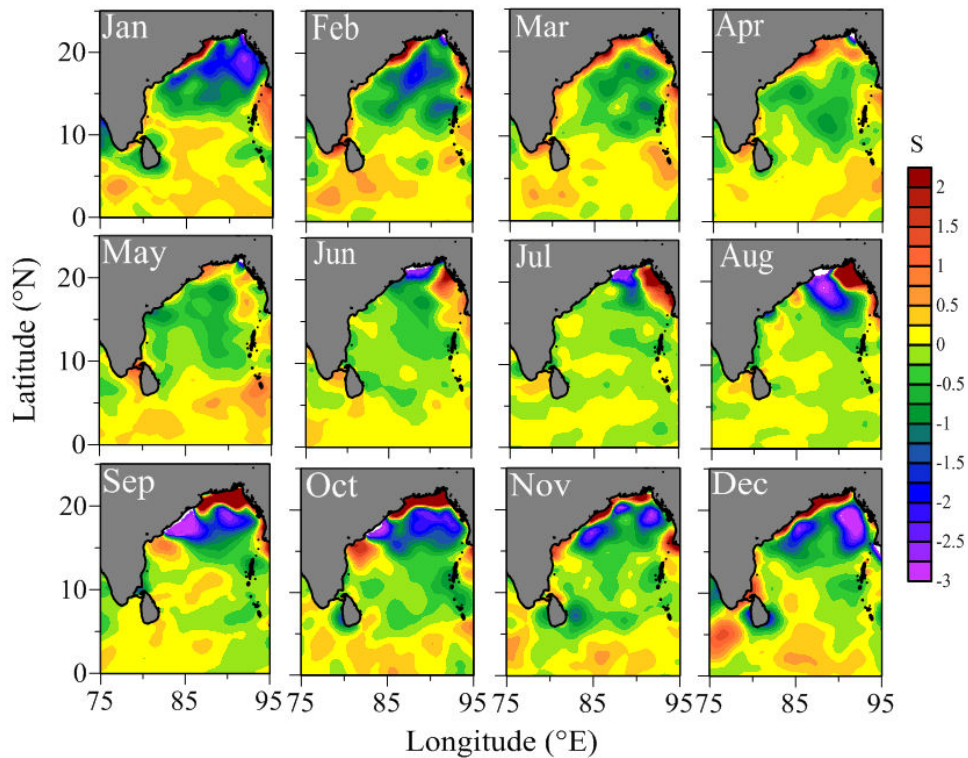
Fig. 2.2 Difference in sea surface salinity (ΔS) between WOA and SODA data. Violet to Green colour indicates negative values and Yellow to Red colour positive values.

(ii)   Drifting buoys

Array for Real-Time Geostrophic Oceanography (Argo) is a drifting buoy program that envisages real-time sampling of the temperature and salinity profiles of the global oceans at an approximate spatial resolution of 300 km (Ravichandran et al., 2004). The accuracy of temperature, salinity and pressure sensors on the typical Argo float is $0.005°C$, 0.01 and 5 dbar respectively. The temporal cycle of the float is 5 or 10 days and the vertical resolution of the profile is 10 m in the upper 200 m. Temperature and salinity values at 4 m depth are considered as SST and SSS respectively. Argo floats for the period 2010-2016 are used in the present work to detect the saltening in the upper layers of the BoB. In the vertical, the data is available at irregular depth which is further interpolated at every 5 m.

(iii)   Moored buoys

Research Moored Array for African-Asian-Australian Monsoon Analysis and Prediction (RAMA) is designed specifically to study the large scale ocean-atmosphere interactions. These buoys provide daily time series of temperature collected from

17

surface (1 m) to 500 m depth and of salinity from 1 m to 100 m depth. The vertical profiles from these buoys are further interpolated onto a common 5 m resolution. Daily data from the RAMA buoy (Fig. 2.1) located at 0°N, 1.5°N, 4°N, 8°N, 12°N and 15°N along 90°E is utilized to describe and document the temporal variation and eddy induced variability of salinity in the BoB.

The daily surface salinity data from RAMA buoy are averaged into monthly means due to data gaps and compared with salinity data from SODA (Fig. 2.3). The spread in the SSS between the SODA and RAMA buoy are examined and subsequently the root mean square (RMS) error between the two data are computed. In most of the cases, the error is found to be less than 0.25 except at 15°N where it is around 0.65. The validation with salinity from RAMA buoy shows that the SODA data depict the salinity changes in the open ocean reasonably well.
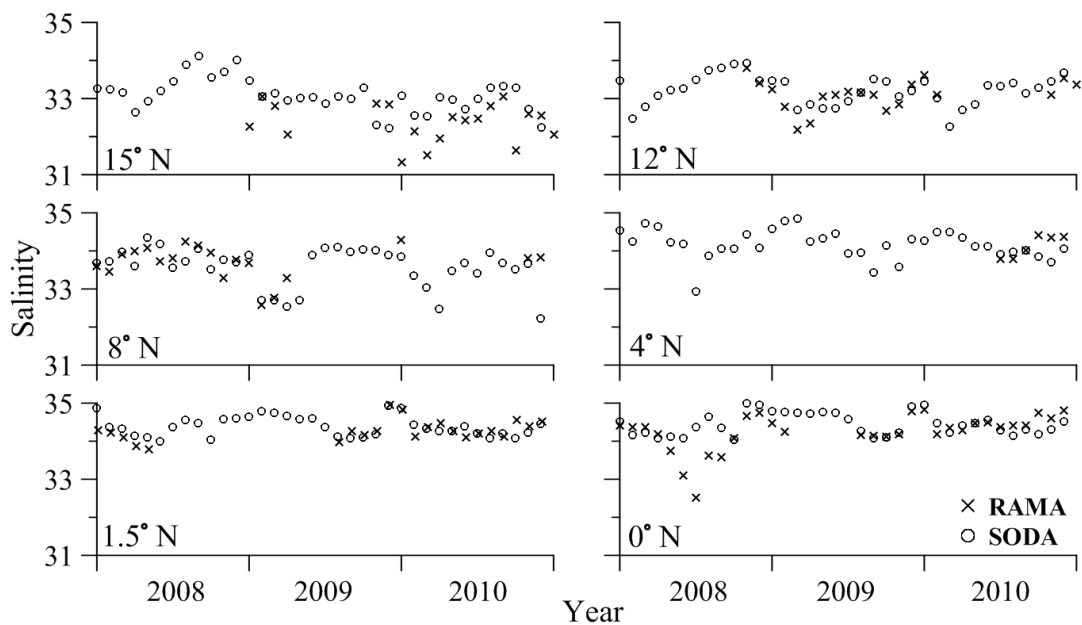
Fig. 2.3 Comparison of sea surface salinity obtained from SODA (circle) and RAMA buoy (cross).

(iv) Field measurement programs

The climatology and moored/drifting buoy data are supplemented with the dedicated field experiments conducted in the BoB. The data sets considered includes Bay of Bengal Monsoon Experiment (BOBMEX-99) and Word Ocean Circulation Experiment (WOCE).

(a)   Bay of Bengal Monsoon Experiment (BOBMEX-99): BOBMEX-99 was executed during July September 1999 as a part of the national program called Indian Climate Research Programme (ICRP). Hydrographic survey was conducted onboard the research vessel INS Sagardhwani in the BoB (along 13°N between 81°E and 87°E with stations at 0.5º intervals) between 15 July and 30 August 1999 in four phases. In this work, the data collected from 28 to 30 July 1999 is utilized to examine the influence of eddies on salinity variability. A detailed description of the BOBMEX-99 observational program is given in Bhat et al. (2001).

(b)   World Ocean Circulation Experiment (WOCE): WOCE was a component of the international World Climate Research Program aimed to establish the role of the World Ocean in the Earth's climate system. WOCE's field phase was between 1990 and 1998, followed by an analysis and modeling phase that ran until 2002. Temperature and salinity data collected onboard R/V Knorr along the track I09 during February 1995 is utilized in this study.

2.3.2 Sea level anomaly (SLA)

The merged SLA data from AVISO (Archiving, Validation, and Interpretation of Satellite Oceanographic data) is used to detect meso-scale features and propagating waves and understand the salinity variability associated with these. The dataset is a merged product from five satellites i.e., Topex/Poseidon (October 1992 to July 2002), ERS1 (January 1994 and March 1995), ERS2 (June 1996 to June 2003), Jason-1 (December 2001-July 2013), Jason-2 (launched in June 2008 and continuing), Envisat (March 2002 to April 2012), Cryosat-2 (launched in April 2012 and continuing) and Saral/AltiKa (launched in March 2013 and continuing). The weekly data available at 1/3 degree spatial resolution for the period September 1993 to December 2016 is used to prepare the monthly mean climatology of SLA. From the SLA, the zonal (u) and meridional (v) geostrophic current components are estimated as

$$u = -\frac{g}{f}\frac{\partial \eta}{\partial y} \qquad\qquad (1)$$

$$v = \frac{g}{f}\frac{\partial \eta}{\partial x} \qquad\qquad (2)$$

where η is elevation, g is gravity and f is the Coriolis parameter.

2.3.3 Ocean currents

The information of ocean currents is very much essential to understand the salinity variability, especially in a basin like BoB. Therefore, current data from SODA are utilized in this work. SODA current consists of monthly zonal and meridional velocity for the global ocean with a resolution of 0.5 x 0.5 degree at 40 depth levels. The surface current (5.01 m) data from 1950 to 2010 is used to prepare monthly mean climatology and to examine the role of advection on salinity variability in typical years for the BoB.

2.3.4 River runoff

The monthly mean climatology of river discharge of the major rivers, viz. Ganges, Brahmaputra, Mahanadi, Godavari, Krishna and Cauvery in the BoB are obtained from the Center for Sustainability and the Global Environment (SAGE) river discharge database. The period of record for each station is variable, from 5 to 74 years. Several researchers (Rao et al., 2009; Vinayachandran et al., 2012; Lu et al., 2015) have used the river discharge data from SAGE as freshwater forcing.

2.3.5 Atmospheric data

(i)   Wind speed and wind stress curl: In order to understand the general wind pattern of the BoB, the monthly climatological QuikSCAT zonal and meridional components of wind data were utilized. In addition, daily zonal and meridional wind stress from Advanced Scatterometer (ASCAT) having a spatial resolution of 0.25^{o}x0.25^{o} for the period 2014 is analyzed to document the variability in the oceanic response due to the cyclones. From wind stress, the curl ($\nabla \times \tau$) is computed using the relation

$$\nabla \times \tau = \frac{\partial \tau_Y}{\partial x} - \frac{\partial \tau_X}{\partial y} \tag{3}$$

where τ_x and τ_y are zonal and meridional components of wind stress.

(ii)   Precipitation (P): The Tropical Rainfall Measuring Mission's (TRMM) Microwave Imager (TMI) is a passive microwave sensor designed to measure rain rates over a wide swath under the TRMM satellite. The daily precipitation data for the period January 1998 to December 2010 at $0.25°$x$0.25°$ resolution is used to compute the monthly climatology and decipher its impact on salinity distribution.

(iii)   Evaporation (E): E from Objectively Analyzed Air-Sea Fluxes (OAFlux) at 1°x1° resolution along with P is utilized to estimate the freshwater flux. For consistency, the TMI precipitation data is re-gridded to as that of E.

(iv)   Net heat flux: Monthly averages of net heat flux (Q_N) at 1°x1° resolution for the period January 1998 to December 2009 is also obtained from the OAFlux to estimate the monthly climatology for analyzing the net heat flux distribution in the BoB.

(v)   Cyclone track data: The Joint Typhoon Warning Centre (JTWC) provides detailed information regarding the passage of cyclones. JTWC maintains an archive of tropical cyclone track data, commonly referred to as best tracks. In early May 2013, an area of disturbed weather formed over the southern BoB. Cyclone Viyaru consolidated into a depression by May 10. The cyclone Hudhud formed as a low pressure area over Andaman Sea on 7th October 2014 and strengthened to a "very severe cyclonic storm" on 10th October. It was centered near 15ºN and 86.8ºE around 470 km east-southeast of Visakhapatnam. These two cyclones are considered to understand its impact on salinity variability.

2.4   Methodology

2.4.1 Turner angle (*Tu*)

To classify the mixing regimes in the ocean, the concept of *Tu* as suggested by Turner (1973) is implemented in the present work.

$$Tu = \tan^{-1} \frac{R_\rho + 1}{R_\rho - 1} \qquad (4)$$

Here R_ρ is the density ratio or stability ratio which is a measure of the relative contributions of temperature and salinity to the stratification.

$$R_\rho = \frac{\alpha \partial_z T}{\beta \partial_z S} \qquad (5)$$

$\partial_z T$ and $\partial_z S$ are the vertical gradients of temperature and salinity, α is the coefficient of thermal expansion, β is the coefficient of saline contraction and ρ is the density of seawater.

$$\alpha = -\frac{1}{\rho} \frac{\partial \rho}{\partial T} \qquad (6)$$

21

$$\beta = \frac{1}{\rho}\frac{\partial \rho}{\partial S} \qquad\qquad (7)$$

In general, *Tu* varies between −180° to 180°. Stable condition prevail for -90°< *Tu* < 90° and unstable condition for 90°< *Tu* <-90°. The water column is doubly stable when −45° < *Tu* < 45° as both temperature and salinity contribute to a stable density (Fig. 2.4). 45° < *Tu* < 90° represent salt fingering regime (warm and saline over cool and fresh water, i.e., salinity destabilizing), while −90° < *Tu* < −45° represent diffusive convection regime (cool and fresh over warm and saline water, i.e., temperature destabilizing).
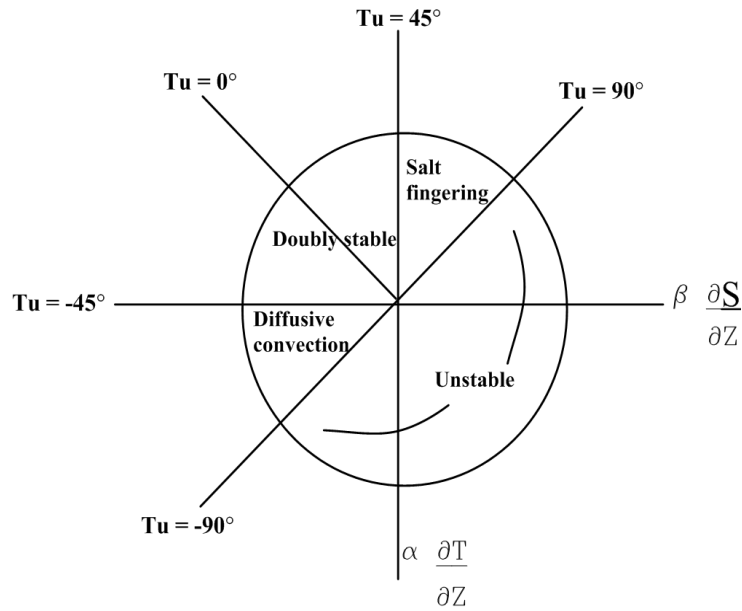
Fig. 2.4 Schematic diagram of the Turner angle

2.4.2 Okubo-Weiss parameter (W)

To identify eddies in the BoB, Okubo-Weiss parameter (W) is used (Okubo 1970; Weiss 1991). W represents the balance between the magnitude of vorticity and deformation (Veneziani et al., 2005) and gives the relative contribution of these two parameters.

$$W = S_n{}^2 + S_s{}^2 - \omega^2 \qquad\qquad (8)$$

Here,

$$S_n = \frac{\partial u}{\partial x} - \frac{\partial v}{\partial y} \qquad\qquad (9)$$

22

$$S_s = \frac{\partial v}{\partial x} + \frac{\partial u}{\partial y} \qquad\qquad (10)$$

$$\omega = \frac{\partial v}{\partial x} - \frac{\partial u}{\partial y} \qquad\qquad (11)$$

S_n, S_s and ω are stretching deformation rate, shearing deformation rate, and vorticity respectively. The u and v components of geostrophic currents estimated from equations (1) and (2) are used to compute S_n, S_s and ω. Regions with W < 0 are vorticity-dominated regions and correspond to the eddy core, while W > 0 indicates strain-dominated regions corresponding to the periphery of the eddy (circulation cell). Hence, W is used to identify the eddy core as interconnected regions of vorticity dominated over strain surrounded by a region of strain dominated over vorticity. The core edge is identified as closed lines with W = 0.

2.4.3 Dipole Mode Index (DMI)

In general, an index based on SST is used to define the DMI (Saji et al., 1999). In the present work, a salinity index based on salinity anomaly (ΔS) is implemented. ΔS is defined as the difference in surface salinity between the individual year and the climatology from SODA for the period 1950-2010. Similar to DMI (Saji et al., 1999), salinity anomaly index is calculated as the difference in ΔS averaged over 10°N - 10°S, 50°E - 70°E in the western equatorial Indian Ocean and 0°-10°S, 90°E - 110°E in the southeastern equatorial Indian Ocean. The computed salinity anomaly index is smoothed by 3 month running mean and normalized by its standard deviation (σ). For a year to be considered as dipole, salinity anomaly index must be greater than 1σ and should continue for at least 2 to 3 months. In addition, DMI based on SST anomaly is also calculated from SODA data following Saji et al. (1999). The pIOD and nIOD events identified based on analysis of DMI and salinity anomaly and that also concurs with earlier studies (Grunseich et al., 2011; Endo and Tozuka, 2015) are presented in Table 2.2.

2.4.4 Oceanic Nino Index (ONI)

The ONI, generally used to characterize the ENSO signal, is defined as the 3 month running mean of the sea surface temperature anomaly (SSTA) in the central Pacific Ocean (5°N-5°S,120°-170°W) (Barnston et al., 1997). In the present work, the ONI data is obtained from the National Oceanic and Atmospheric Administration

(NOAA) Climate Prediction Center (www.cpc.ncep.noaa.gov). The El Niño (La Niña) years are defined as the years in which ONI is above 0.5°C (below 0.5°C) for a minimum of 5 consecutive months. The El Niño/La Niña and co-occurred events during 1950 to 2010 are listed in Table 2.2.

Table 2.2 Years of pIOD, nIOD, co-occurred pIOD+El Niño and nIOD+ La Niña during 1950 to 2010

pIOD	nIOD	El Niño	La Niña	pIOD + El Niño	nIOD + La Niña
1961	1956	1953	1950	1951	1964
1967	1958	1957	1955	1963	1970
2003	1959	1965	1971	1972	1974
2007	1960	1969	1973	1982	1975
2008	1980	1986	1983	1991	1998
	1981	1987	1988	1994	2010
	1984	2002	1995	1997	
	1989	2004	1999	2006	
	1992	2009	2000		
	1996		2007		
	2005				

2.4.5   Monsoon

The different regimes of the summer monsoon are classified into Normal, Flood and Drought years based on the All-India Summer Monsoon Rainfall (AISMR) anomalies from IMD (www.tropmet.res.in). The All-India area-weighted mean summer monsoon rainfall, based on a homogeneous rainfall data set of 306 rain gauges in India, developed by the Indian Institute of Tropical Meteorology, is widely considered as a reliable index of summer monsoon activity over the Indian region.

Table 2.3 Flood and drought monsoon years during 1950 to 2010

Flood	1956 1959 1961 1970 1975 1983 1988 1994 2007
Drought	1951 1965 1966 1968 1972 1974 1979 1982 1985 1986 1987 2002 2004 2009

2.4.6   Wavelet analysis

The wavelet transform is a useful tool for understanding the temporal variability of signals both in oceanography and meteorology (e.g. Mark, 1995; Emery and Thomson, 2001; Hareesh Kumar and Sanilkumar, 2004). This is mainly because of

the fact that it is very difficult to decompose the temporal variability in any signal using the traditional method. Moreover, the wavelet analysis provides the localized variations of power within a timescale by decomposing a time series in time-frequency space. Hence one can easily determine both the dominant modes of variability and how those modes vary in time. In the present study, the software of Torrence and Compo (1998) (http://paos.colorado.edu/research/wavelets) developed for Morlet wavelet is customized and used for the analysis.

A salinity time series, x_n, with equal time spacing δt and n= 0 ... N−1 has been assumed. Wavelet analysis involves the convolution of a real time series *x(t),* with a set of functions that are derived from a 'mother wavelet'. The commonly used wavelet function ($\Psi_0(\eta)$) is Morlet wavelet, consisting of a plane wave modulated by a Gaussian. $\Psi_0(\eta)$ depends on a non-dimensional "time" parameter η. To be "admissible" as a wavelet, this function must have zero mean and be localized in both time and frequency space (Farge, 1992).

$$\Psi_0(\eta) = \pi^{-1/4} e^{iw_0\eta} e^{-\eta^2}, \tag{12}$$

The continuous wavelet transform of a discrete sequence x_n is defined as the convolution of x_n with a scaled and translated version of $\Psi_0(\eta)$:

$$w_n(s) = \sum_{n=0}^{N-1} x_{n'} \psi * \left[\frac{(n'-n)\delta t}{s} \right] \tag{13}$$

Here the (*) indicates the complex conjugate. By varying the wavelet scale and translating along the localized time index n, one can construct a picture showing both the amplitude of any features versus the scale and how this amplitude varies with time. The subscripts *0* on ψ have been dropped to indicate that ψ has also been normalized. Spatial and temporal variation of selected spectral components in the BoB is estimated based on wavelet analysis.

2.4.7   Software tools

A suite of software packages are used to process, analyze and visualization of various data sets utilized in the present work.

- FORTRAN: A programming language that is suited for numerical computation. It is used extensively for all the computations.

25

- Ferret: An interactive computer visualization and analysis tool. It is used to process large and complex gridded netcdf datasets.

- MATLAB: It facilitates numerical computation as well as graphical display of outputs and in the present work used especially for wavelet analysis.

- SURFER: A contouring and 3D surface mapping software

- GRAPHER: To create 2D plots

- Climate Data Operators: software for standard processing of climate and forecast model output.

Chapter 3

Thermohaline variability on basin scale

3.1 Introduction

The Indian peninsula splits the north Indian Ocean into two basins, the AS in the west and BoB in the east (Fig. 3.2). Geographically both the basins are located in the same latitude band and are semi-enclosed. There are similarities in atmospheric forcing: both are influenced by summer and winter monsoon and receive similar amounts of solar radiation. But, the wind systems are dissimilar during the summer monsoon, with stronger winds in the AS than in the BoB, whereas winds are of comparable intensities during the winter monsoon (Shenoi et al., 2002). However, the most striking difference between the two basins lies in the upper ocean hydrology. The negative water balance associated with excess evaporation over precipitation and intrusion from Red Sea and Persian Gulf makes AS high saline (> 35), whereas higher precipitation than evaporation and the massive river run off (1.625×10^{12} m^3y^{-1}, Subramanian, 1993) into the BoB results in positive water balance (Ramanathan and Pisharody, 1972; Sengupta et al., 2006) making BoB a freshwater basin.

A number of regional studies have discussed the variability of temperature and salinity in the AS and BoB. However, these regional analyses do not always reflect basin-scale tendencies and also may not expose the low-frequency variability of spatial structure. The spatial and temporal averages provide important and valuable information on temperature and salinity variability in these basins. Since its hydrology that makes each basin unique, in this chapter the variability of temperature and salinity in the two basins, viz. the AS and BoB on different time scales are treated separately. For this purpose, the temperature-salinity profile available from SODA for AS (the region between 0°-25°N and 40°-80°E) and BoB (the region between 0°-25°N and 80°-100°E) for a period of 61 years i.e., from 1950-2010 are averaged for each basin. To get an idea about the overall thermohaline distribution in both basins, as a first step, the basin scale averages of temperature and salinity are estimated. In addition, the monthly climatology and monthly average of temperature-salinity for each year for the same space domain is also computed. Understanding long term variability would help in assessing whether the future climate scenario shows a continuation of recent variability and also delineates anomalous years. In order to discern the spatial variability of SST and SSS in the BoB, the monthly climatology distribution based on WOA13 (0.25°x0.25° resolution) is utilized. In addition, the

temperature-salinity variability along the coastal regions is also addressed in this chapter as coastal areas are highly dynamic and strategic.

3.2 Basin scale distribution

Figure 3.1 depicts the basin scale long term averages of sea surface temperature (SST) and sea surface salinity (SSS) along with the Evaporation-Precipitation (E-P) for the AS and BoB. The figure shows that the surface layers of the BoB are fresher and warmer (~33.4; ~28.5°C) than the AS by nearly 2 units and 0.7° C respectively. Shenoi et al. (2002) also found that the BoB was generally warmer than AS. The highly stratified surface layers along with weak winds inhibit vertical mixing in the BoB (Han et al., 2001; Rao et al., 2002; Girishkumar et al., 2013) and contribute towards a warmer basin. The excessive freshwater flux (E-P of -6.5 cm/month) in the BoB is the prime factor for its low salinity whereas the positive E-P (3.3 cm/month) causes AS a comparatively saltier basin.
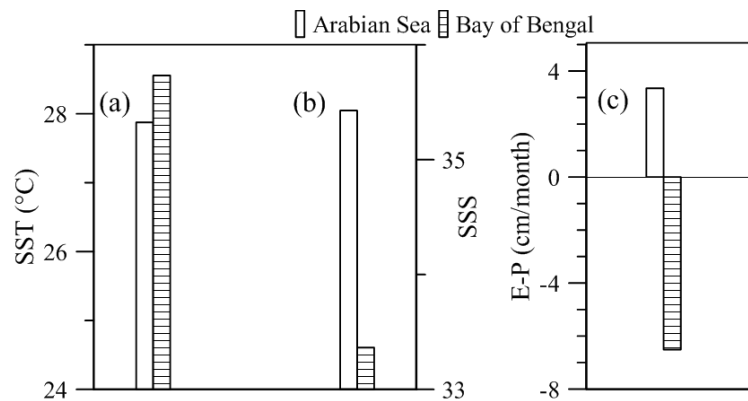
Fig. 3.1 Basin average (a) sea surface temperature (b) sea surface salinity and (c) E-P in the Arabian Sea and Bay of Bengal from 1950 to 2010.

The study is further extended by computing the average profiles of temperature and salinity upto a depth of 1500 m for the two basins (Fig. 3.2). In the present study, the isothermal layer depth (ILD) is defined as the depth at which temperature drops by 1°C from the SST. On a basin scale, ILD is around 40 m in the AS and 45 m in the BoB. On the other hand, the mixed layer depth (MLD), defined as the depth at which sigma-t increases by 0.125 kg/m^3 from the surface, point out that the MLD is always shallower (25 m in AS, 15 m in BoB) than ILD. In the vertical, there is a considerable difference in temperature between the two basins from surface to bottom with varying degree of magnitude. The BoB (26.6°C) is warmer than AS (25.4°C) from surface to a depth of 110 m with maximum difference (1.2°C) at 60 m.

However, below 110 m temperature is higher in the AS (14.7°C) with variation of ~1.2°C at 200 m. In AS, a subsurface maxima (35.5) is observed in the depth ranges of 80-90 m sandwiched between comparatively freshwaters (35.4 at the surface and 34.9 at 1500 m) above and below. On the other hand, in the in the BoB, not only the subsurface maxima is absent in the salinity field but also marked by low salinity water in the surface layers (~33.4) and its continuous increase with depth. The presence of freshwater in the surface layers and its rapid increase to values around 35 units at 200 m leads highly stratified surface layers in the BoB. The opposing effect of freshwater flux in the two basins (Fig. 3.1c) causes a salinity difference of ~2 units at the surface. As the effect of freshwater flux decreases with depth in BoB, the difference in salinity between two basins also decreases (< 0.1 unit beyond 1370 m).
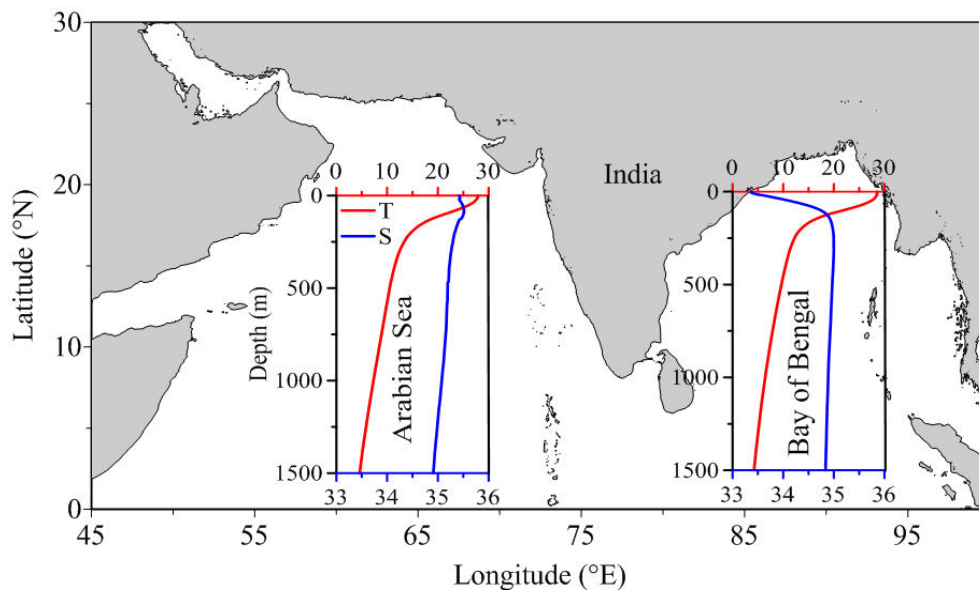
Fig. 3.2 Vertical distribution of temperature (red) and salinity (blue) in the Arabian Sea and Bay of Bengal.

3.2.1 Monthly basin average

To understand the monthly evolution of temperature and salinity in the two basins, the monthly ensemble averages SST and SSS for the period 1950-2010 are estimated (Fig. 3.3). Of the two basins, BoB remains warmer throughout the year. Moreover, both basins exhibits a bimodal distribution in SST with warming phase during the pre- and post monsoon seasons and cooling phase during the southwest monsoon and winter (Fig. 3.3a). In both the basins, SST attains its maximum in May (29.4°C in BoB, 29.1°C in AS); and minimum in January (27.3°C in AS, 27.9°C in BoB). On annual scale, the intense summer cooling in the AS leads to dissimilarity in surface cooling between the two basins in August (1.4°C) while similar patterns of

heating during pre-monsoon leads to minimum difference in May (0.3°C). The surface salinity in the BoB, exhibits a uni-modal distribution with comparatively higher values in June (33.6) and lowest in October (33) (Fig. 3.3b). On the other hand, AS is saltier (> 35.2) throughout the year with maximum occurs in September (35.6) and minimum in March (35.3). In general, there is a difference of ~2 units between the basins throughout the year. The difference is highest in October (2.5) and lowest in March (1.8).
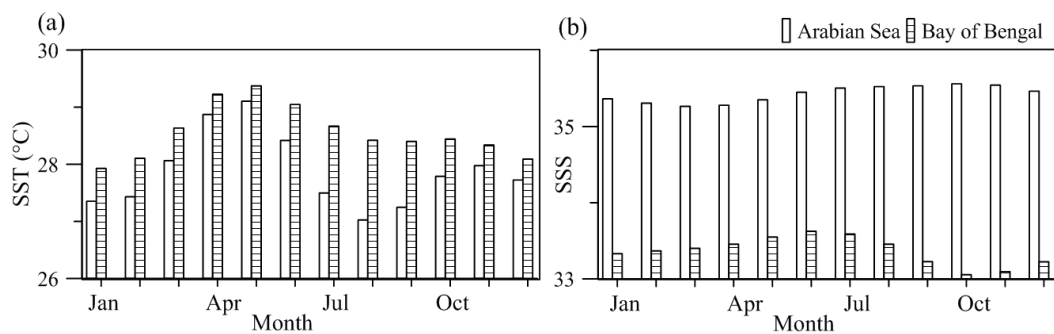
Fig. 3.3 Monthly basin average of (a) sea surface temperature (SST) and (b) sea surface salinity (SSS) in the Arabian Sea and Bay of Bengal
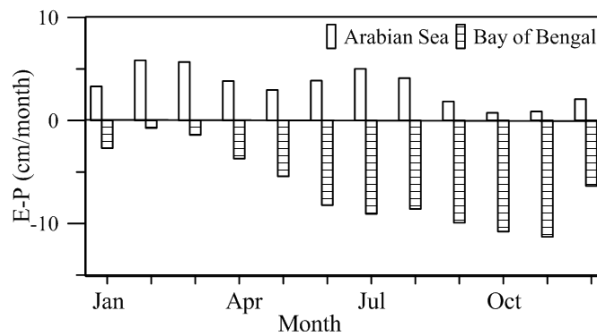
Fig. 3.4 Monthly basin average of evaporation minus precipitation in the Arabian Sea and Bay of Bengal.

Fig. 3.4 shows that E-P is positive in the AS, on the other hand it is negative in the BoB throughout the year The saltier water in the AS is due to excess of evaporation over precipitation as suggested by positive E-P whereas it's vice versa in the BoB (Fig. 3.4). The presence of saltier water in the AS is attributed to excess evaporation over precipitation as suggested by positive E-P whereas it's vice versa in the BoB with negative E-P (Fig. 3.4). The high salinity in February in the BoB is in response to minimum E-P (-0.7 cm/month) and low salinity in October-November is a result of excess of precipitation over evaporation (~ -11 cm/month). In the AS maximum E-P of 5.8 cm/month is observed in February and minimum in October (0.7 cm/month). In nutshell, the same phase in the variation of SST in AS and BoB

suggests that both the basins responded equally to the atmospheric forcing. On the other hand, salinity peaks are in out of phase as the forcing mechanisms are different in the two basins. Rao and Sivakumar (2003) analyses the salt budget of near-surface mixed layer and shows it is primarily governed by freshwater flux, horizontal advection and entrainment across the mixed layer base.

The monthly basin averaged vertical section of temperature and salinity in the two basins is presented in Fig. 3.5 (a) and (b). In general, SST in excess of 28°C is noticed in the BoB except in January with its peak during April-May whereas, in the AS, the SST exceeds 28°C only during pre-monsoon season which extends to a depth of 25 m. Up to 150 m depth levels, the temperature shows more or less similar variability in the AS and BoB (Fig. 3.5a). Beyond 200 m, both the basins show marked differences, with temperature gradient more in the BoB (Fig. 3.5a). In the case of salinity, AS shows a variation of 0.5 units (from 35 to 35.5) between the surface and 500 m (Fig. 3.5b). Moreover, a prominent subsurface maximum is noticed around 75-100 m depth (35.5) due to the presence of Arabian Sea Watermass between January and prior to the onset of summer monsoon. With the commencement of monsoon, the maximum shoals to shallower depth levels and increases the salinity in those depths. In the BoB, comparatively low salinity water (<34) occupies the upper 40 m and it does not increase beyond 35 up to 500 m. The maximum freshening (>33.25) occurs during the period September to December; with gradual increase from January to April (to 33.5). The distinct temperature-salinity relationship in the two basins is essentially reflected in the T-S diagram (Fig. 3.5c).
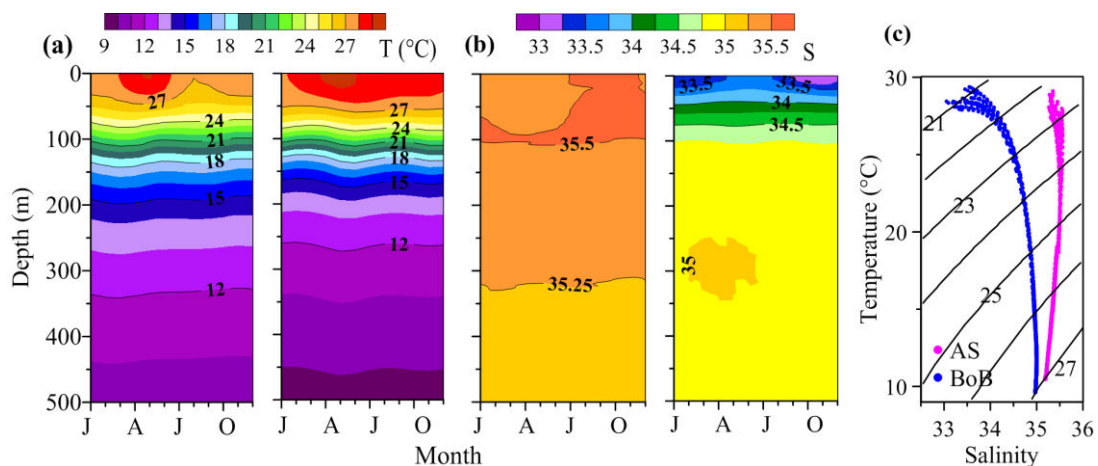
Fig. 3.5 Basin averaged vertical monthly distribution of (a) temperature (b) salinity and (c) T-S in the Arabian Sea (blue) and Bay of Bengal (magenta).

In order to understand the average temperature and salinity within the AS and BoB, these two parameters are vertically averaged for different depth bands. The averaged temperature from surface to 100 m show bi-modal distribution in both basins (Fig. 3.6a) with BoB showing a maximum of ~27°C in June and minimum of 26.2°C in February. The averaged temperature in the AS peaks in April (26.3°C) and dips in August (25.2°C). This temperature distribution indicates warmer BoB than AS in the upper 100 m. The accumulated heat during pre-monsoon season might be trapped in this shallow surface mixed layer in the BoB (Fig. 4.5) thereby making the bay warmer. Also, less mixing of surface warmer water with subsurface water due to presence of barrier layer in the BoB can also enhance the surface warming. The maximum departure between the two basins occurs in August (1.3°C) and minimum in March (~0.22°C). Even though, the averaged temperature between 100 m and 500 m depth levels (Fig. 3.6b) follow similar pattern of variations as in the surface layer, the AS is found to be warmer compared to BoB by 1°C. The strong mixing deepens mixed layer and leads to warmer subsurface layers of the AS. Since the warm subsurface layer in the AS is thicker than BoB, the average temperature of upper 500 m is higher than the BoB (Fig. 3.6c).
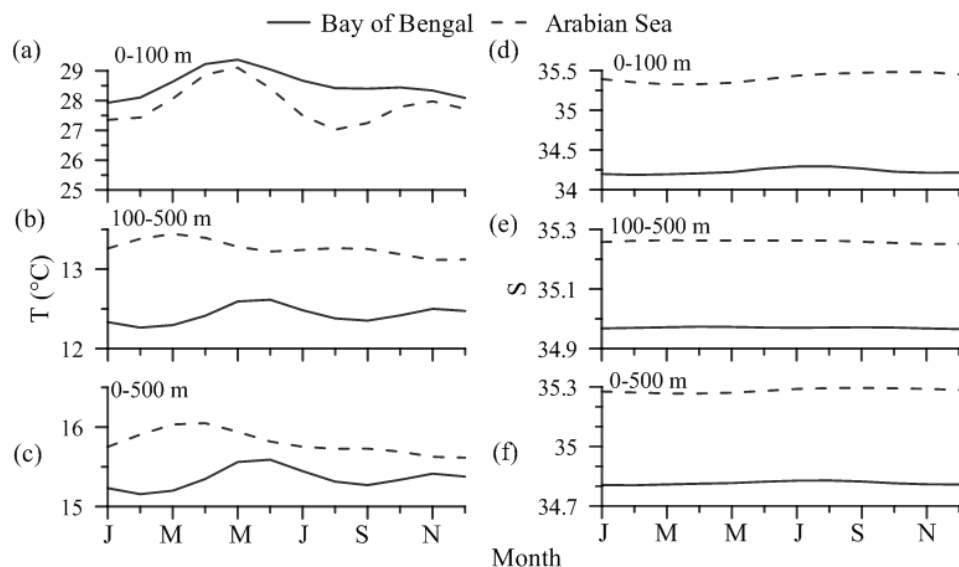
Fig. 3.6 Monthly distribution of vertically averaged temperature (a-c) and salinity (d-f) between (a, d) 0-100 m, (b, e) 100-500 m and (c, f) 0-500 m.

In the case of salinity, AS is saltier than BoB at all the depth levels (Fig. 3.6 d-f), but the differences decreases towards deeper depths. For example, in the surface layer (0-100 m), the AS is more salty than BoB by ~1.2 units (Fig. 3.6d), which is primarily due to massive freshwater flux in the BoB. The departure in salinity

33

between the two basin drops to ~0.3 towards deeper depths as the influence of freshwater is confined to upper few meters.

3.2.2   Inter-annual basin average

The most conspicuous hydrological parameter which differentiates AS from BoB is salinity and this is evident from its spatio-temporal variability i.e., either on basin scale average or monthly basin scale average. In the AS, several studies have been carried out to understand the variability in the temperature and salinity on different time scales. However, such studies are sparse as far as the BoB is concerned. Hence, hereafter, the studies are mainly focused on BoB. As a first step, in order to understand the long term variability in the BoB, the basin averaged SST and SSS anomaly during 1950 to 2010 from surface to 500 m depth are estimated. Since anomaly is the deviation from the mean it is useful in differentiating the unusual events in SST and SSS (Fig 3.7a and b). The SST anomaly is computed as the difference between each monthly basin averaged SST and climatic basin average of SST. Similarly salinity anomaly is also computed.
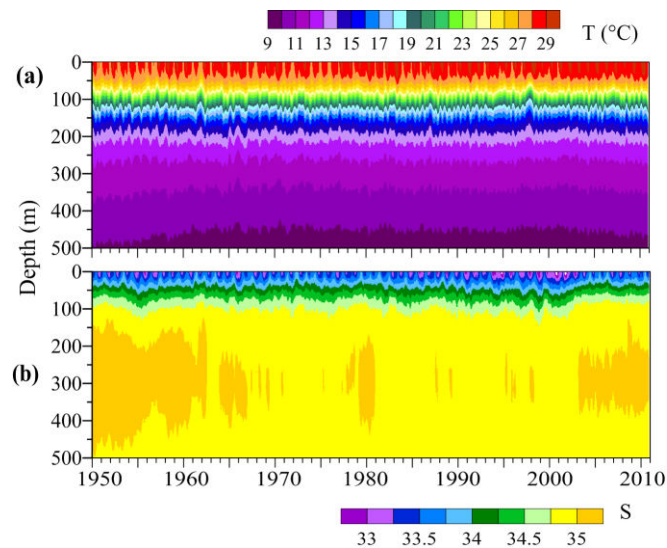
Fig. 3.7 Basin averaged vertical distribution (surface to 500 m) of (a) temperature and (b) salinity in the Bay of Bengal from 1950 to 2010 utilizing SODA data.

The vertical section of temperature shows an isothermal layer of thickness ~45 m followed by thermocline upto a depth of 120 m (gradient of 0.1°C/m) and deeper layer with weak gradient (Fig. 3.7a) embedded with seasonal warming and cooling cycle. In the salinity field, low saline water (>33.25) capped above a highly stratified layer followed by layer where salinity variation is weak (Fig. 3.7b) embedded with seasonal freshening events. At the subsurface level salinity core appears during 1950-

60 and after 2002. The salinity in the surface layers show freshening from 1980 till 2001. One noticeable observation in thermal structure is significant warming post 2001 resulting in comparatively warmer surface layers (excess of 29°C).

Over the last sixty one years (1950-2010), SST anomaly shows an increasing trend of ~0.5°C embedded with seasonal warming and cooling (Fig.3.8a). Dinesh Kumar et al. (2015) utilizing various dataset also corroborate the increase in SST in the BoB. Even in the upper 500 m, vertically averaged temperature for different depth level reflects this warming trend (Fig. 3.7a, 3.9a-e). The number of negative anomaly exceeding 0.5°C are more in number during pre 1980s and those exceeding 1°C are associated with nIOD and La Niña (1955, 1961, 1974-75). Dinesh Kumar et al. (2015) attributed the increasing trend in the SST to the net heat gain in the BoB. The decrease of wind speed over the basin during the past two decades impacts and lowers the latent heat flux and thus contribute to the observed long-term increasing trend in SST (Dinesh Kumar et al., 2015). Rahul and Gnanaseelan (2012) also observed increasing trend in SST. The increasing SST together with increasing wind strength and a relatively lower humidity compensation increased latent heat flux and hence decreased the net heat flux.
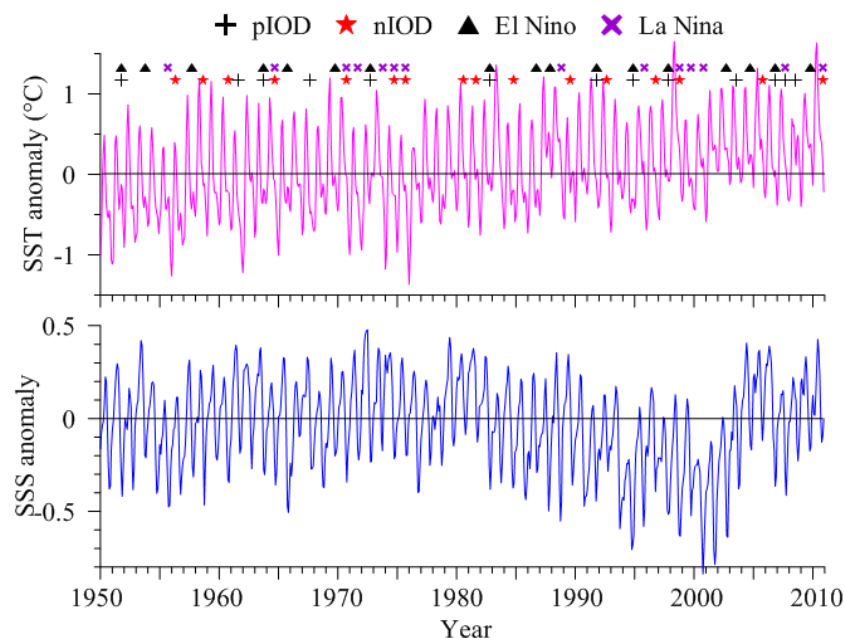
Fig. 3.8 Basin averaged (a) sea surface temperature anomaly and (b) sea surface salinity anomaly in the Bay of Bengal from 1950 to 2010 based on SODA data. Values of temperature and salinity at 5.01 m depth are considered as sea surface temperature and sea surface salinity respectively.

The SSS anomaly exhibits year to year variability with seasonal saltening and freshening (Fig. 3.8b) associated with freshwater flux. The signals of SST and SSS exhibit almost pentadal scale of variability till 1980 with minimum positive peaks in the beginning and end of each five year (1955, 1965 and 1976-78). SSS anomaly from 1980 till 2001 show drop of 1.1 units. These periods are characterized by occurrence of several (8 events) climatic events like La Nina, combined pIOD-El Niño and flood years. The period 1990-2001 show gradual decrease with maximum drop of ~0.7 unit as the incidence of climatic events are more frequent (5 events). This is evident from negative anomaly throughout the year in 1992, 1994, 1997, 2000 and 2001.
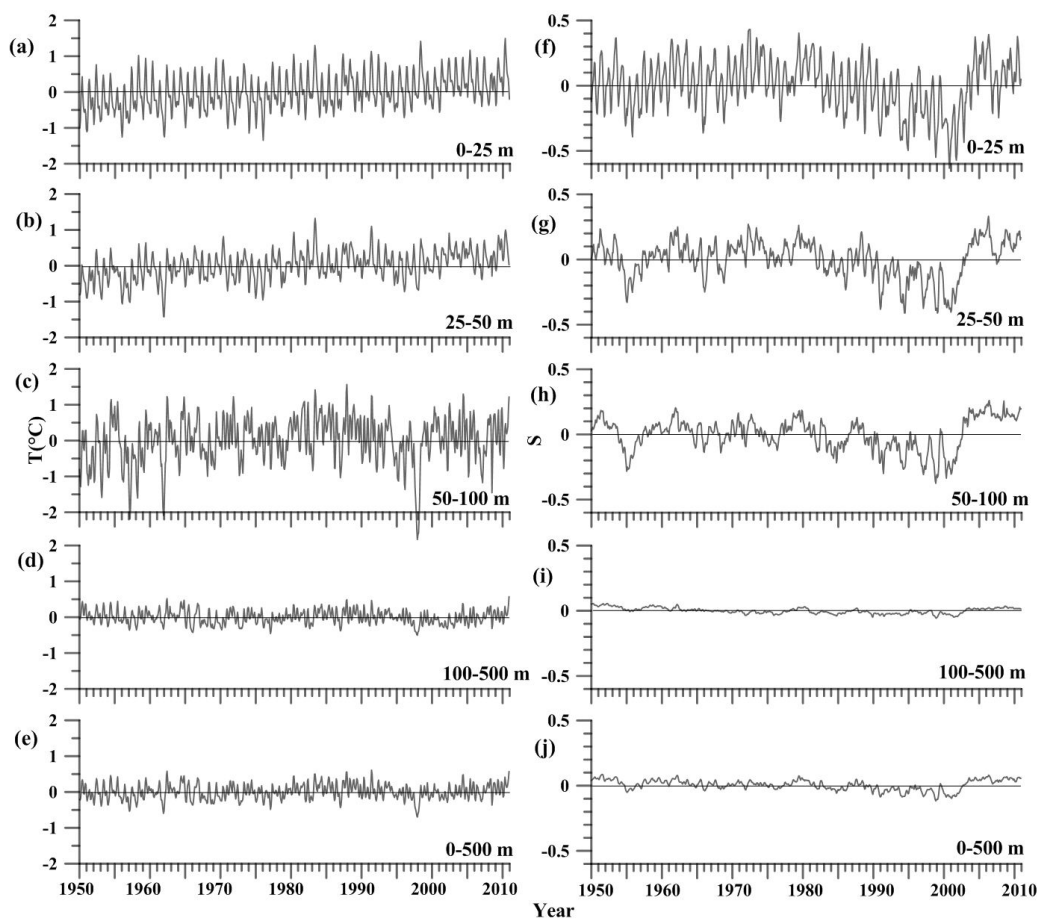
Fig. 3.9 Monthly distribution of temperature anomaly based on SODA data (a-e) and salinity anomaly vertically averaged (f-j) between (a, f) 0-25 m, (b, g) 25-50 m, (c, h) 50-100 m, (d, i) 100-500 m and (e, j) 0-500 m.

Another noticeable observation is absence of subsurface core of salinity in excess of 35 during this period (Fig. 3.7b). The vertically averaged temperature for different depth slab also show similar pattern of variation as observed in salinity. Interestingly the prominent drop (~2°C) is observed only in the 50-100 m level during the period 1990-2000. Therefore cooling in between (50-100) may be due to lateral

advective process. The absence of cooling in the upper 50 m is attributed to warmer and deep isothermal layer (Fig. 3.7a).
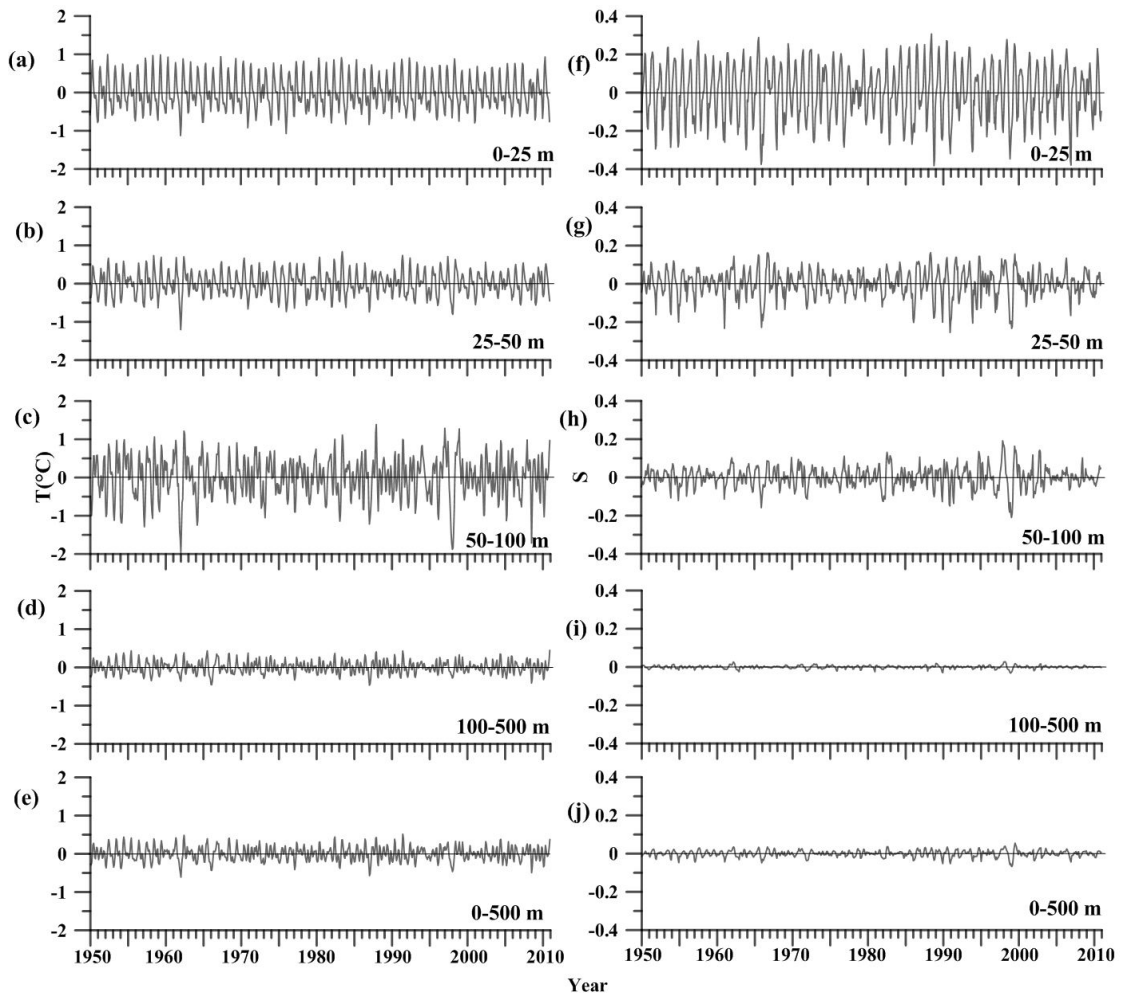
Fig. 3.10 Monthly distribution of temperature anomaly based on SODA data (a-e) and salinity anomaly vertically averaged (f-j) between (a, f) 0-25 m, (b, g) 25-50 m, (c, h) 50-100 m, (d, i) 100-500 m and (e, j) 0-500 m.

Thereafter from 2002 till 2010, SST anomaly increases by 1.2°C (Fig. 3.8a) and the upper 50 m continues to be comparatively warm (temperature in excess of 29°C) which may be due to occurrence of more number of El Niño events (Fig. 3.7a). During this period, there is an overall increase in salinity anomaly (1.2) of the bay with occasional drop. Salinity is higher during 2002, 2004 and 2009 probably due to drought. In the subsurface level, overall increase in salinity (35) (Fig3.8b) is observed. Unlike for the period 1990-2001, temperature of water column upto 100 m show almost uniform increase of 0.3°C. This suggests the dominance of surface layer processes in the upper 100 m water column. In salinity anomaly, occasional drop in 2005-2006 is attributed to flood and combined pIOD-El Niño but this is reflected only in the upper 50 m. The salinity variation below this level is uniform. In conclusion,

the subsurface layers too reflect the impact on surface layer caused due to climatic events but with reduction in magnitude.

The pattern of temperature and salinity anomaly (Fig. 3.10) is totally different when climatic mean is replaced with annual mean. The temperature anomaly (Fig. 3.10 a-e) shows inter-annual variability embedded with seasonal variations. In the 50-100 m zone which is in the thermocline, maximum anomaly is observed (Fig. 3.10c). In the case of salinity anomaly, no discernible freshening events similar to that at surface (Fig. 3.7b) are observed in 0-25 m layer (Fig. 3.10 f). In the subsequent layers, amplitude of anomaly decreases with depth with negligible variation in the 100-500 m layer (Fig. 3.10i).

3.3   Variability along the coastal periphery

The coastal regions of the BoB are highly dynamic and show rapid variability both in the spatial and temporal domain. The sea level variability in these coastal belts is caused by coastal upwelling/downwelling, freshwater influx, currents, tides, and long period waves. To study the variability along the coastal periphery of the BoB, the temperature and salinity distribution for each 1x1 degree grids along the entire coastal boundary of BoB (Fig. 3.11a) are segregated. The SLA along the coastal grids considered for the study is 1° away from the coast. As the offshore length scale of the coastal Rossby wave varies with latitude, a length scale of 1° was chosen (Shankar 2000; Hareesh Kumar and Sanilkumar, 2004). Then temperature and salinity gradient in these grids are computed. To estimate the vertical gradient, the difference between temperature/salinity in the thermocline (MLD + 10 m) and surface layer is calculated. The static stability parameter (E, Pond and Pickard, 1983) is utilized to obtain the vertical stratification for the coastal grids.

In general, the spread in temperature, salinity and their vertical gradients is more in the regions covering the head bay (grids 14-20) and it exhibits a decreasing trend towards either side (Fig. 3.11 b-e,f). The spread in temperature (~5°C) is highest in grid 16-18. Correspondingly salinity in the same grid show maximum spread of 19 units. This is also evident from the maximum standard deviation observed in the SST and SSS. In addition, the maximum vertical stratification is observed in this region due to the massive discharge from various rivers that the upper few meter of the water column. The vertical stratification at the head bay (Fig. 3.11g) are about 3-4 orders of magnitude higher than that in rest of the BoB. The positive gradient in this region

owes its existence to thermal inversion especially during winter, when subsurface temperature is higher than SST. The large spread in theses parameter at head bay suggests large variability in these parameters than in rest of the regions of the BoB.

A noticeable observation at the head bay is the minimum spread in SLA (Fig. 3.11d) which could be attributed to high stratification in those regions. This high stratification may also be one of the reasons for restricting the two Kelvin waves into the eastern BoB. SLA variability is maximum from grid 20-25 along north western boundary of BoB could be associated with presence of cyclonic/anti-cyclonic eddies along with the freshwater influx. The low temperature (26.2°C), freshwater (25) and high vertical stratification in the eastern bay (grid 8-9) is primarily due to the freshening by precipitation and the runoff from Irrawaddy (Subramanian, 1993; Prasad, 1997). The highly stratified layer in these regions minimizes the scatter in the temperature and salinity fields (Fig.3.11 b, c). It is also evident that salinity rather than temperature controls the stability.
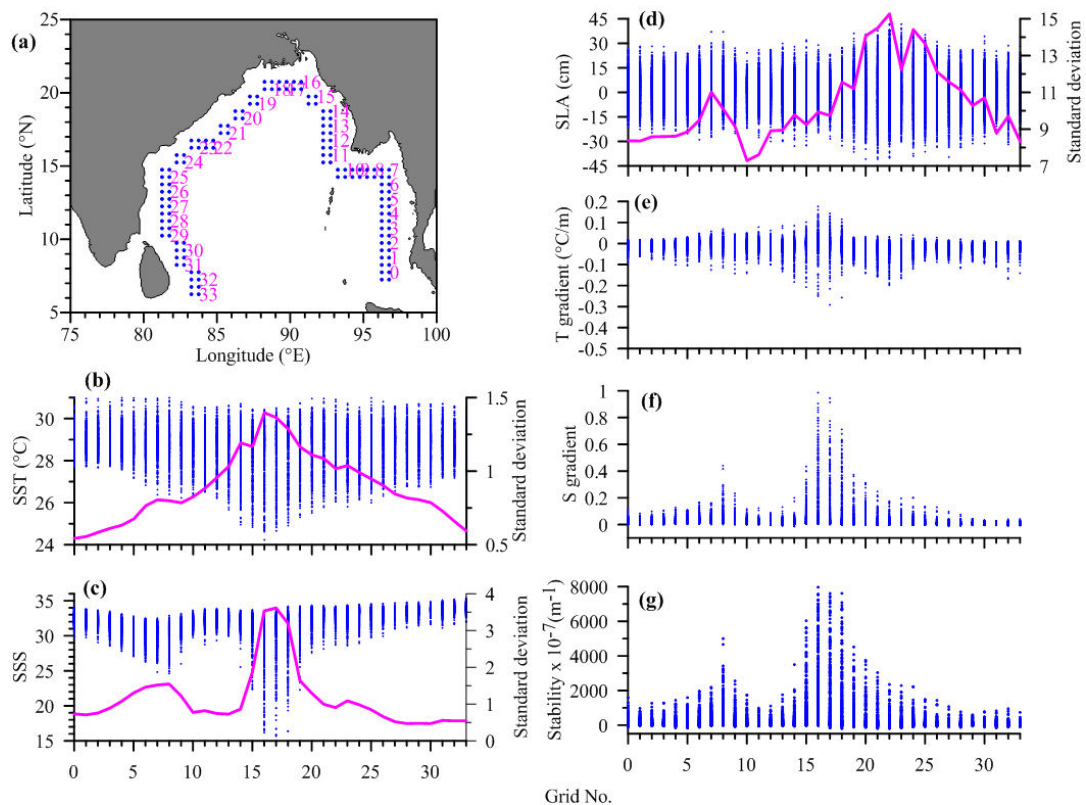
Fig. 3.11 (a) Coastal grid numbered from 0 to 33, variability in (b) sea surface temperature, (c) sea surface salinity, (d) sea level anomaly, (e) temperature gradient, (f) salinity gradient and (g) stability along the coastal boundary of BoB. Magenta line in (b), (c) and (d) are standard deviation of each dataset.

Another observation is that the eastern periphery of the BoB is fresher (salinity <30) and slightly warmer compared to the western periphery (salinity >30). Here, the spread in temperature and salinity is minimum in the southeastern periphery of the BoB (temperature >3°C, salinity <3) compared to its western counterpart (temperature >4°C, salinity >4). The coastal upwelling, meso-scale activities, advection of Arabian Sea Watermass from the AS along with the propagating waves is the probable reasons for making the western bay slightly saltier. Extremely low temperature (~24.5°C) and salinity (~15) is observed at the head bay (grids 16-18) during the peak winter, i.e. December-February and fresher during September-October respectively.

3.4 Temperature and salinity distribution in the surface layer

The monthly distribution of temperature and salinity from WOA13 illustrate spatial variations of these parameters. During pre-monsoon season, SST is characterized by more than 28°C south of 15°N of BoB with highest temperature in May (~30°C). Subsequently with onset of summer monsoon SST decreases to 28.5°C in August (Fig. 3.12). Meanwhile, comparatively low temperature (<28°C) water is noticed around the southern tip of the peninsula and Sri Lanka.
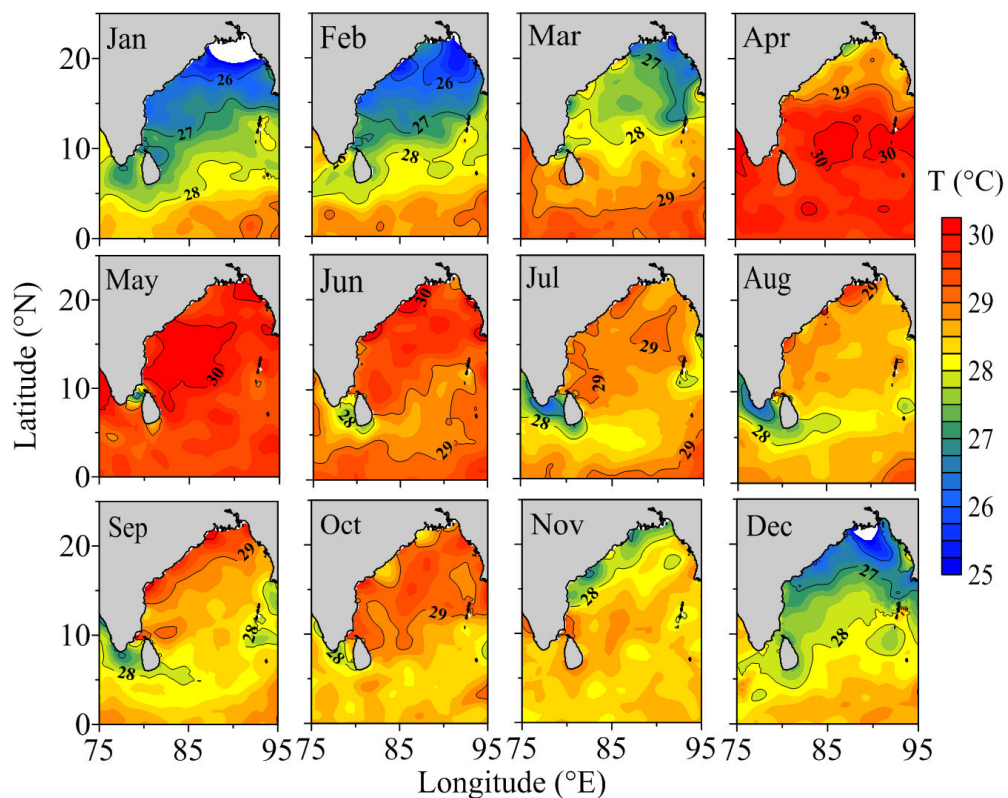
Fig. 3.12 Monthly distribution of sea surface temperature (SST) in the Bay of Bengal. Contour interval is 0.25°C.

During post-monsoon season, surface temperature more than 28°C exist throughout the bay, but along the east coast of India in November it is less than 28°C. In winter, SST is < 26°C in the northern BoB due to cold northeasterly winds and SST increases towards southern BoB. The temperature is ~28°C south of 5°N. The intra-seasonal SST changes can be associated with changes in the surface winds and atmospheric convection over BoB. The spatial distribution gives insight on the zonal and meridional variability of temperature. However, the bimodal distribution as observed in basin averaged is reflected north of 10°N.
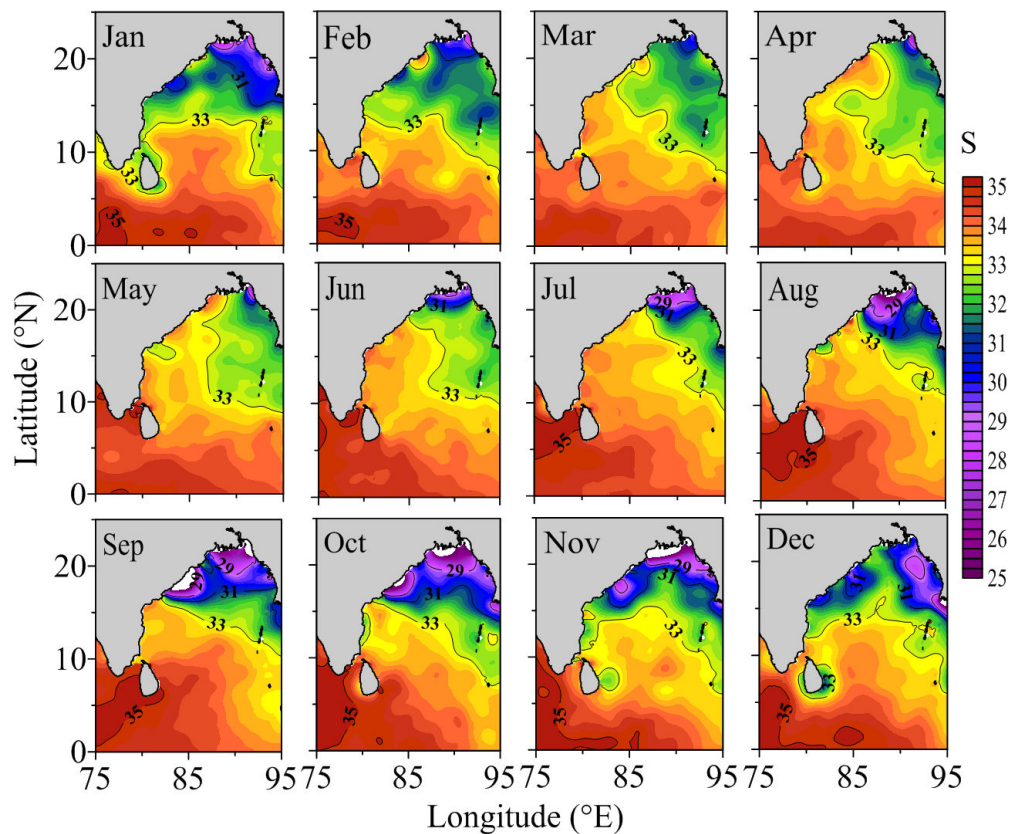
Fig. 3.13 Monthly distribution of sea surface salinity (SSS) in the Bay of Bengal. Yellow to red colour for salinity higher than 33 and violet to green colour for less than 33. Contour interval is 0.25 units.

Fig. 3.13 shows a contrasted pattern of the surface salinity, with fresh water in the northeastern BoB, and saltier water in the central and southern basin. This large-scale gradient exists throughout the year, but is seasonally modulated. During pre-monsoon season, salinity difference of ~0.75 is observed between the north western (33) and northeastern (32.25) BoB. Whereas, south of 10ºN is occupied by water of salinity greater than 33.5. Onset and progress of summer monsoon produces significant changes in salinity structure of BoB, especially in northern and coastal

periphery. This is attributed to huge freshwater influx (Subramanian, 1993) and it flows southward along the eastern coast of BoB. The isohalines orient almost parallel to the eastern bay leading to maximum salinity gradient. With cessation of monsoon, circulation reverses and the freshwater start spreading along the western boundary reaching 17°N in September, whereas in the central and southern Bay comparatively saline water exists (than 33.5). On an annual scale lowest salinity of 25 is observed at the head Bay during October. During winter, the low salinity water advect further south upto 6°N along western boundary of the basin. An increasing trend is observed towards (~ 35) southwestern BoB.

In this chapter, temperature and salinity distribution on different spatio-temporal is explored. The basin averaged temperature-salinity for a period of 61 years (1950-2010) shows warmer and fresher BoB than AS. This trend is observed even on monthly averaged distribution. The inter-annual variability of SST in the BoB exhibit consistent increase post 1980 and the maximum freshening in the span of 61 years is observed during 1990-2000. The anomalous peaks in temperature and salinity are associated with climatic events. The effects of these events are reflected in subsurface level with reduction in magnitude with depth. The variability in coastal area is maximum at the head bay due to huge freshwater flux. However, spatial distribution of SST and SSS in the entire basin are dissimilar zonally and meridionally.

Chapter 4

Evolution of watermasses in the upper layers of Bay of Bengal

4.1 Introduction

The BoB receives large quantity of freshwater runoff from the surrounding rivers during the summer monsoon season, which dilutes the salinity in the upper few meters of the BoB to as low as 26. This feature distinguishes BoB from other tropical oceans. The influx of freshwater along with the prevailing circulation in the northern BoB, causes wide scatter in the upper layer T-S structure (Sarma et al., 1999). Therefore it is important to catogorize the watermasses from their hydrographic properties in order to describe the circulation of the BoB.

Watermass is a body of water with a common formation history and is defined by a specific temperature, salinity and sigma-t (σ_t) characteristics. In 1958, La Fond (1958) provided the first description of the different watermasses of the BoB based on the available hydrographic data in the western BoB. He grouped the surface waters of BoB into three, viz., the Northern Dilute Watermass (NDW), Transition Watermass (TW) and Southern Bay of Bengal Watermass (SBBW). Later, studies regarding watermass were carried out in the BoB but based on specific region and periods. Rao and Jayaraman (1968a) based on their observations in the southwestern BoB during northeast monsoon noticed BoB watermass (S < 34; σ_t < 22) in the surface layers. Rao and Jayaraman (1968b) named the low salinity water in the upper 50 m of the eastern Bay and Andaman Sea (S < 33, σ_t < 21) as Eastern Dilute Water of Indo-Pacific origin. Their study also revealed another watermass in the upper 100 m of the southern Bay and the western and middle parts of the central Bay (S: 33-34, σ_t: 21-22) which resembles the SBBW. Emery and Meincke (1986) characterized BoB water as that having salinity in the range 28 to 35 and temperature 25-29°C. In the northwestern BoB, low density water (σ_t < 14) with strong horizontal gradients in the surface layer and σ_t more than 21 at 50 m depth were reported by Sasamal (1989). He observed, low density to be associated with low salinity water which lead to surface density distribution similar to that of salinity. Shetye et al. (1993) observed variations in T-S due to freshwater influx during summer monsoon. Varkey et al. (1996) documented the characteristics of the Bay of Bengal Low Salinity Water in the northern Bay and Andaman Sea as T = 27°C, S = 33 and σ_t ~ 21.2.

Studies subsequent to La Fond (1958) considered the surface watermasses of BoB as a single entity without classifying, despite the fact that surface water exhibit wide variations from one region to another due to differences in freshwater inflow and

heat exchange. Also, information regarding the spatio-temporal variation of watermasses and their generation mechanisms are very much limited. Hence this chapter focuses to describe and document the evolution and spreading of the three watermasses in the upper layers of BoB as reported by La Fond (1958). The study is confined to upper 200 m as changes in the hydrographic properties are rapid up to this depth with marginal variation below. The availability of temperature and salinity data from SODA with higher spatial resolution is utilized in this chapter to address the spatio-temporal variation of the watermasses. In addition, the generation mechanism and mixing regimes associated with these watermasses are also investigated.

4.2   Classification of watermasses

The T-S diagrams presented in Figure 4.1 shows the presence of three distinct watermasses in the upper layers of the BoB viz., the NDW, the TW and the SBBW similar to that reported by La Fond (1958). During the period May to January, the NDW is conspicuous below the σ_t level 19 in the temperature and salinity ranges of 25-30°C and 17-31 respectively. This watermass exhibits considerable variation in the 3-D domain, i.e. with space, time and depth. NDW attain its maximum temperature (~30°C) during June-July and saltier (~31) in May-June. On the other hand, this water has minimum temperature (25°C) and maximum freshening (17) in January and September - October respectively. One noticeable observation regarding the NDW is the drastic variation in temperature and salinity characteristics between summer monsoon and winter. During the summer monsoon season, the northern BoB received large amount of freshwater and its subsequent lateral spread results in large variation in the salinity (16 to 32). However, the trend changes in November as the winter sets in. As a result, the northern Bay experiences significant heat loss (Fig. 4.5) resulting in considerable cooling of the water column leading to large spread in the temperatures. In other words, the NDW shows large spread in salinity during the monsoon season when significant freshening occurs, while the temperature spread is more during winter when there is significant cooling of the water column.

It is evident from Fig. 4.1 that both the TW and SBBW are present throughout the year. The TW has the characteristics $19 < \sigma_t < 21$, temperature 25-30°C and salinity 31-33. The SBBW is the denser with $21 < \sigma_t < 22$, temperature 25-29°C and salinity 33-35. In the case of TW and SBBW, the temperature variation is more compared to salinity, because these watermasses are mostly confined to the

thermocline. In general, the least scatter during pre-monsoon season suggests near homogeneous distribution of watermass characteristics while wide scatter during summer monsoon indicate heterogeneous nature of the watermass in the BoB.
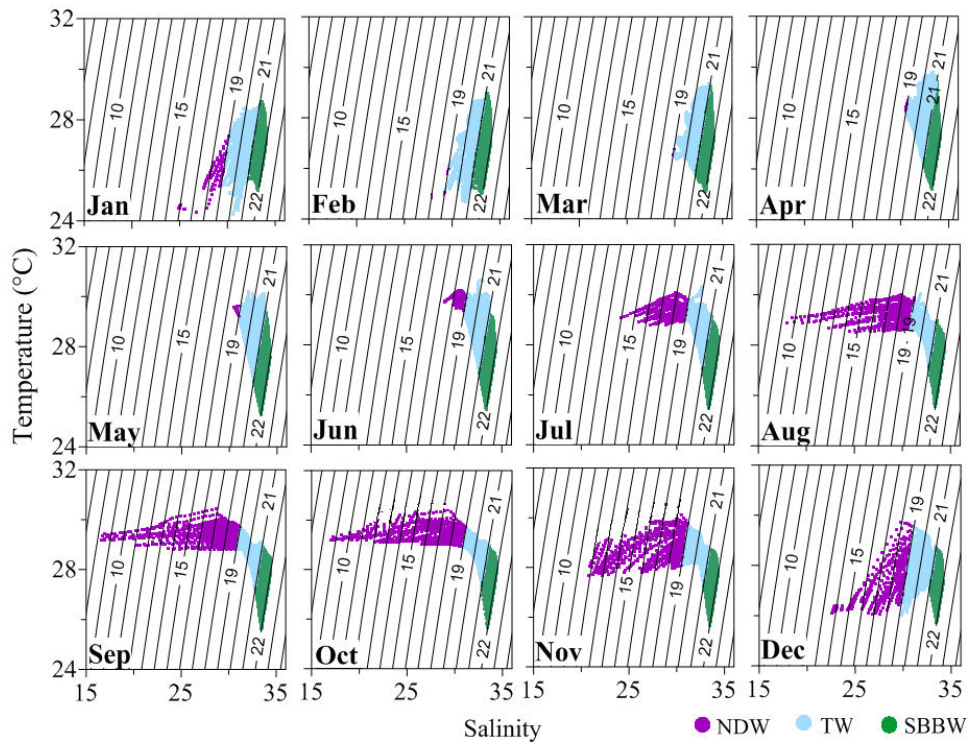
Fig. 4.1 T-S diagram for the Bay of Bengal. NDW indicated by violet, TW by blue and SBBW by green colour. The contour lines represent the σ_t levels.

4.3   Environmental conditions in the Bay of Bengal

In order to understand the evolution of watermass, it is essential to address the physical processes in response to the atmospheric forcing. Therefore, a brief description of the climatology of freshwater flux, river runoff, wind stress curl, net heat flux and remote forcing in the form of propagating waves in the BoB is provided in the subsequent sections.

4.3.1 Freshwater flux (Evaporation minus Precipitation and River runoff)

The freshwater flux shows distinct pattern (Fig. 4.2) with regions of negative values coinciding with maximum precipitation. The intense precipitation and the subsequent river discharge (Fig. 4.3) increases the freshwater input into the northeastern BoB. The bay receives large amount of river runoff from the Ganga and the Brahmaputra, Mahanadi, Godavari, Krishna and Cauvery; along with several minor rivers. Sengupta et al. (2006) suggested that river runoff accounts for about 60% of the total freshwater received by the BoB of which 40% is supplied by the Ganga- Brahmaputra river system.

46
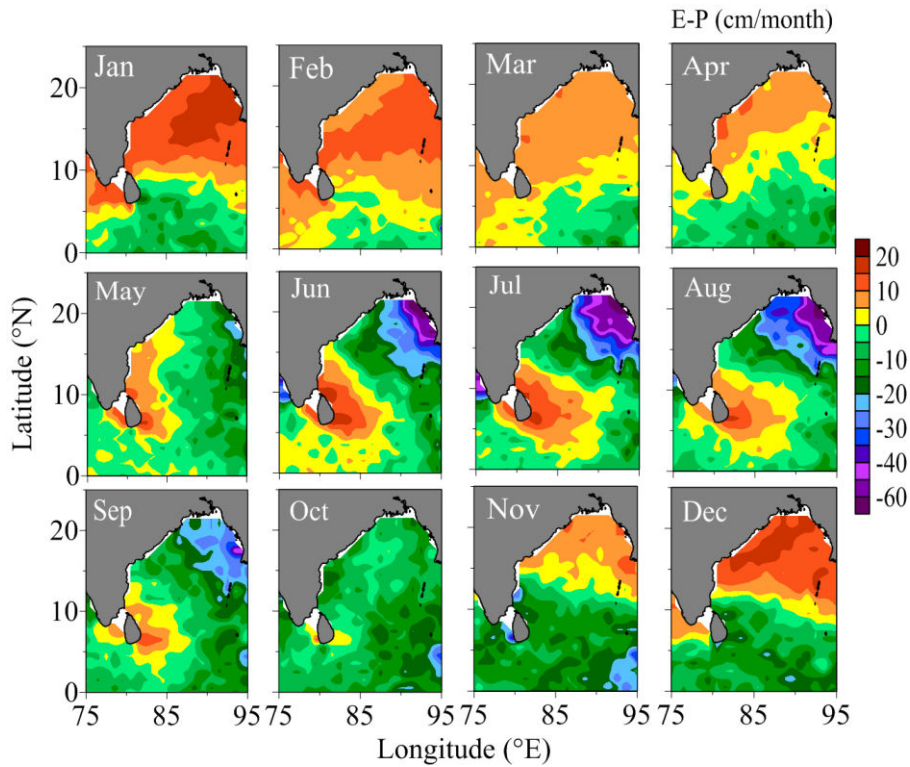
Fig. 4.2 Monthly distribution of evaporation minus precipitation (E-P)
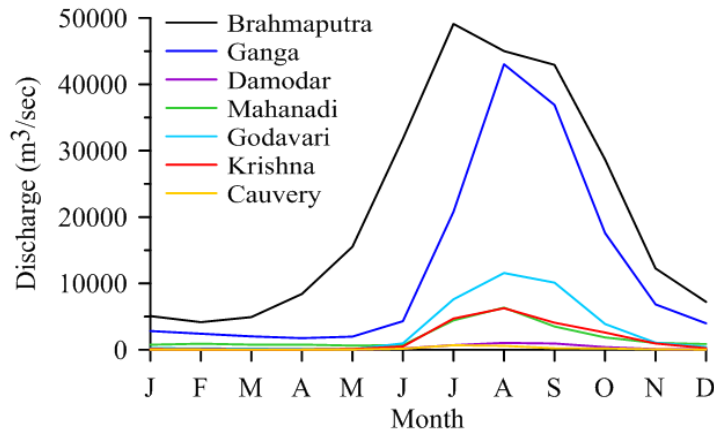
Fig. 4.3 Monthly distribution of river discharge

The eastern BoB starts gaining freshwater at a rate of 20 cm/month (Fig. 4.2) from May and it increases to ~60 cm/month (in July) as the monsoon strengthens. The positive E-P noticed in the southwestern BoB and off Sri Lanka coincides with comparatively low precipitation in those regions. Owing to the decrease in the evaporation due to weak winds in October (Fig. 4.4), the entire bay experiences freshwater gain. However, north of 10°N, there is a net increase in the evaporation (16 cm/month) over precipitation (~1 cm/month) during November to February while freshwater gain (-10 cm/month) continues south of this latitude. The weak winds (Fig. 4.4) during the pre-monsoon season reduce the evaporation (8 cm/month) in the

northern BoB, thereby reducing E-P to 5 cm/month. Earlier studies (Prasad, 1997; Sengupta et al., 2006) have shown higher precipitation than the evaporation in the BoB during summer monsoon.

4.3.2 Wind stress curl

The wind stress over the BoB is highly seasonal (Fig. 4.4). There are significant differences in the wind stress curl between the northern and southern BoB, which divides the BoB zonally, leading to downwelling in the northern part and upwelling in southern part. The wind stress curl is negative during October to April in the regions north of 10°N and positive south of this latitude. The strong negative wind curl (-10 x 10^{-8} Pa/m) north of 9°N is a major force in the formation of a prominent anti-cyclonic eddy in winter. From May till the withdrawal of summer monsoon, the divergence indicated by positive wind curl (15 x 10^{-8} Pa/m) leads to coastal upwelling and subsequent surface cooling in the western periphery of the BoB. At the same time negative values in the eastern BoB indicates downwelling. Another noticeable observation is the change in the wind stress curl in the equatorial from positive to negative in May. October is the transitional period from summer monsoon to winter conditions, as indicated by the changes in the wind stress curl form positive to negative values in the northern BoB.
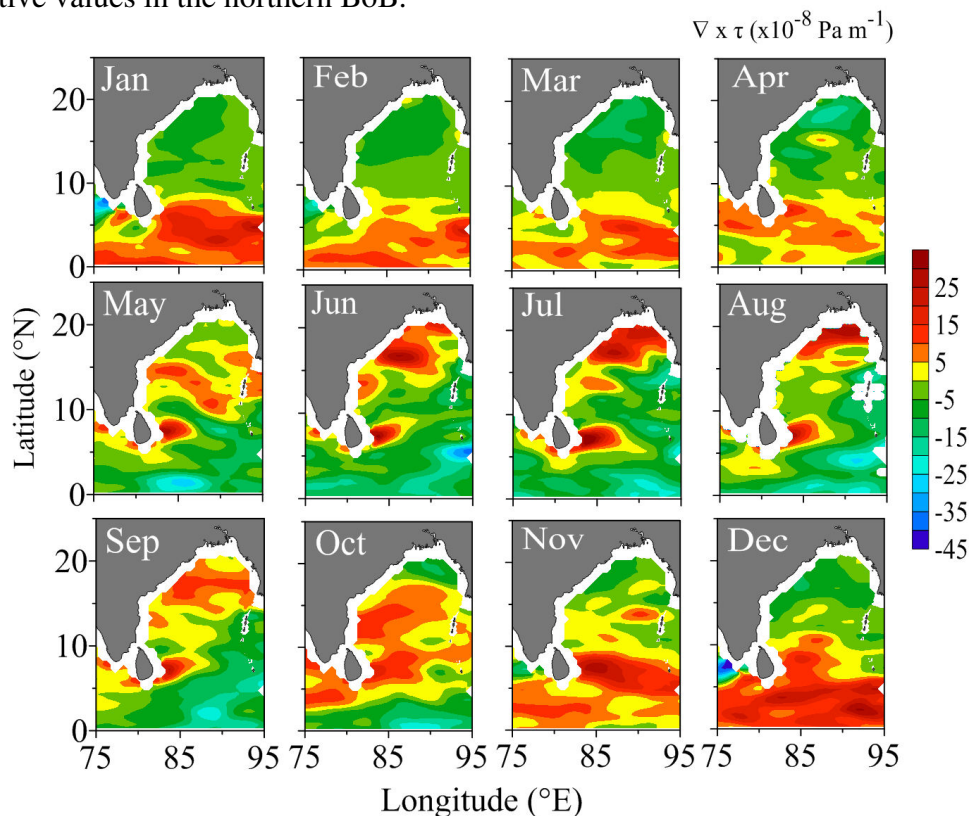
Fig. 4.4 Monthly distribution of wind stress curl (∇x τ)

4.3.3 Net Heat Flux

In general, the net heat flux is positive in the entire Bay during most of the period expect during winter (Fig. 4.5). The maximum gain of heat into the Bay occurs in April, when values in excess of 120 W/m^2 are observed north of 5°N and it drops to 20-40 W/m^2 with the commencement of summer monsoon. It is interesting to note that even during the summer monsoon, the net heat flux is positive in the entire basin. The secondary period of heating initiates in the BoB from August. The winter is characterized by significant heat loss from the northern Bay, i.e. north of 10°N. Here, the loss exceeds 120 W/m^2 in December, while the regions south of 10°N continue to gain heat.
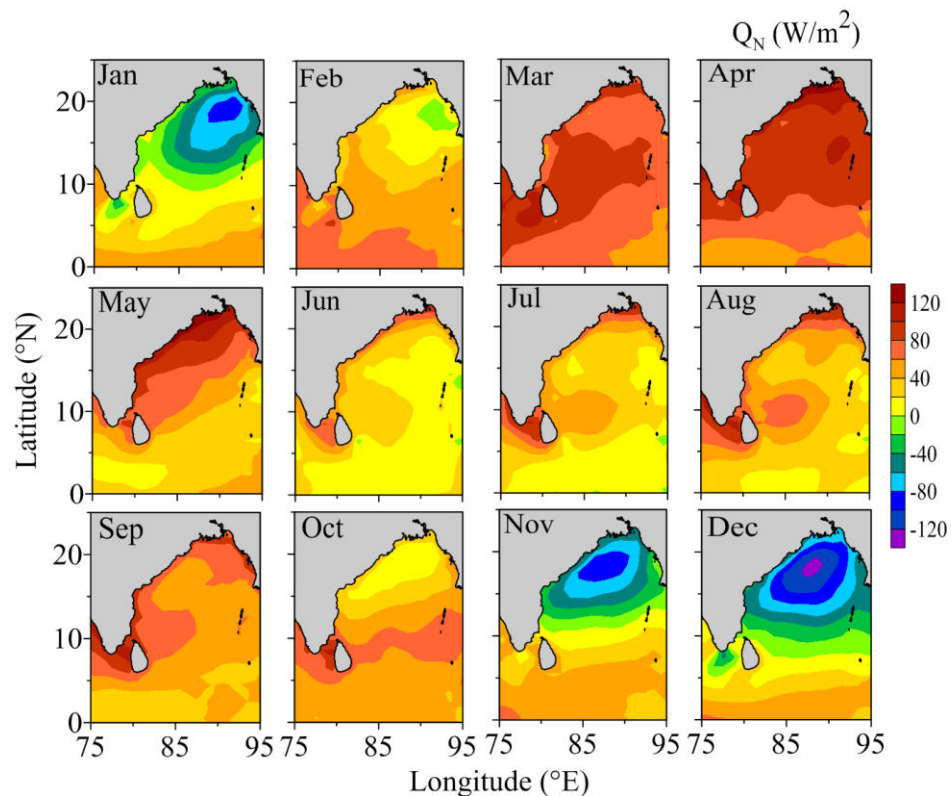
Fig. 4.5 Monthly distribution of net heat flux (Q$_N$)

4.3.4 Eddies and Propagating waves

The monthly averaged SLA shows negative values along the coastal boundaries of the BoB from January to April (Fig. 4.6), indicating the arrival of the first upwelling Kelvin wave formed in the equatorial belt in January (Yu et al., 1991; Rao et al., 2010; Hareesh Kumar et al., 2013). At the head of the Bay, the Kelvin wave attains its maximum amplitude during February-March (SLA of -16 cm). As this Kelvin wave propagate along the eastern coastal boundary of the BoB, it radiates

Rossby wave offshore causing negative sea level in the interior Bay. The Kelvin waves reach 10°N along the east coast of India in February and disappear in April. The formation of the two anti-cyclonic eddies in the western BoB; one off Visakhapatnam and another off the Sri Lanka (closed cells marked in Orange-Red) might inhibit the advance of this Kelvin wave further southward. In April, the positive SLA in the vicinity of equator indicates the generation of downwelling Kelvin waves which propagate eastward and subsequently along the coastal periphery of the BoB. The SLA in the western BoB show signature of a cyclonic circulation from May centered at 18°N with SLA of -6 cm. The southward advance of this Kelvin wave along the east coast of India is curtailed by the cyclonic eddy around 18°N and later due to negative SLA associated with the coastal upwelling.
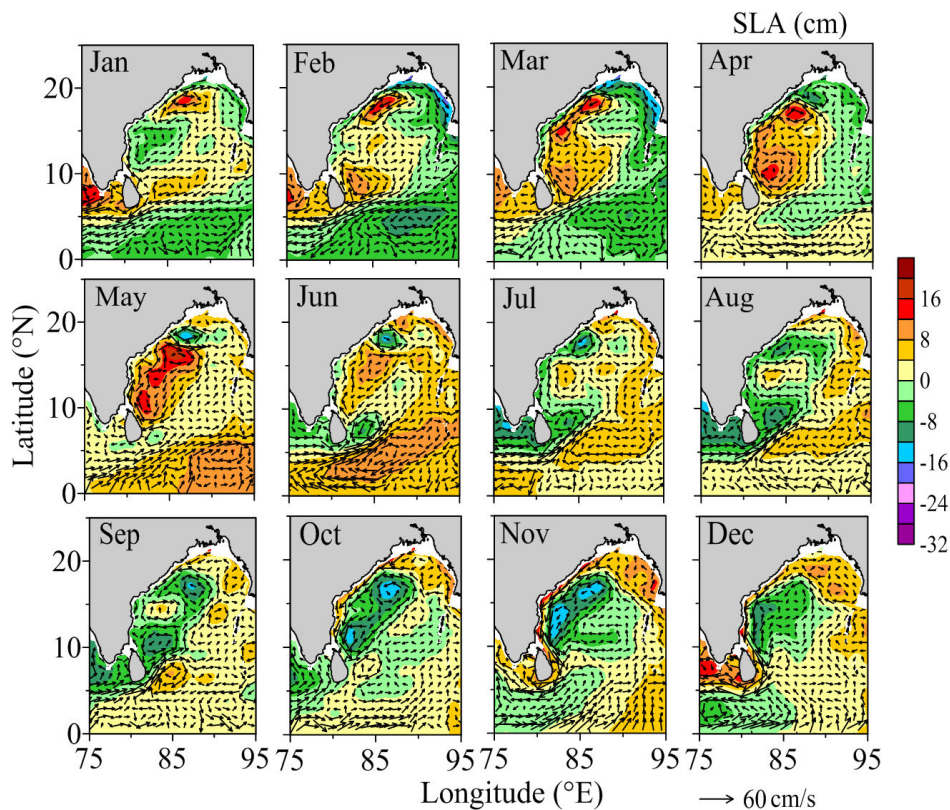
Fig. 4.6 Monthly distribution of sea level anomaly (SLA) overlaid with geostrophic current.

During the summer monsoon season, the freshwater discharges from various rivers (Shetye et al., 1993; Han and Webster, 2002) can raise the sea level at the head Bay by few centimetres. The second downwelling Kelvin wave formed in the equatorial region during the post-monsoon season propagate around the coastal boundaries of BoB and enters the SEAS in November/December. During the

northeast monsoon period, the north-easterly winds produce downwelling along the east coast of India, which also raise the sea level a few centimetres

4.4 Evolution of surface watermasses

As discussed in the previous section, there are three distinct watermasses in the upper layers of the BoB viz., NDW, TW and SBBW. The evolutions of these watermasses are discussed utilizing SODA data in the subsequent sections.

4.4.1 Northern Dilute Watermass (NDW)

The commencement of summer monsoon increases the precipitation and river discharge into the head Bay (Martin et al., 1981, Figs. 4.2 and 4.3) thereby freshening the surface layers of the northern periphery of the BoB (S ~15) and leading to the formation of a watermass which is typically low saline, i.e. the NDW (Fig. 4.7). This implies that the source of this watermass is primarily the continental river runoff. The coastal periphery of the northern BoB is unique by the presence of very low salinity NDW (σ_t < 19) between June and January.
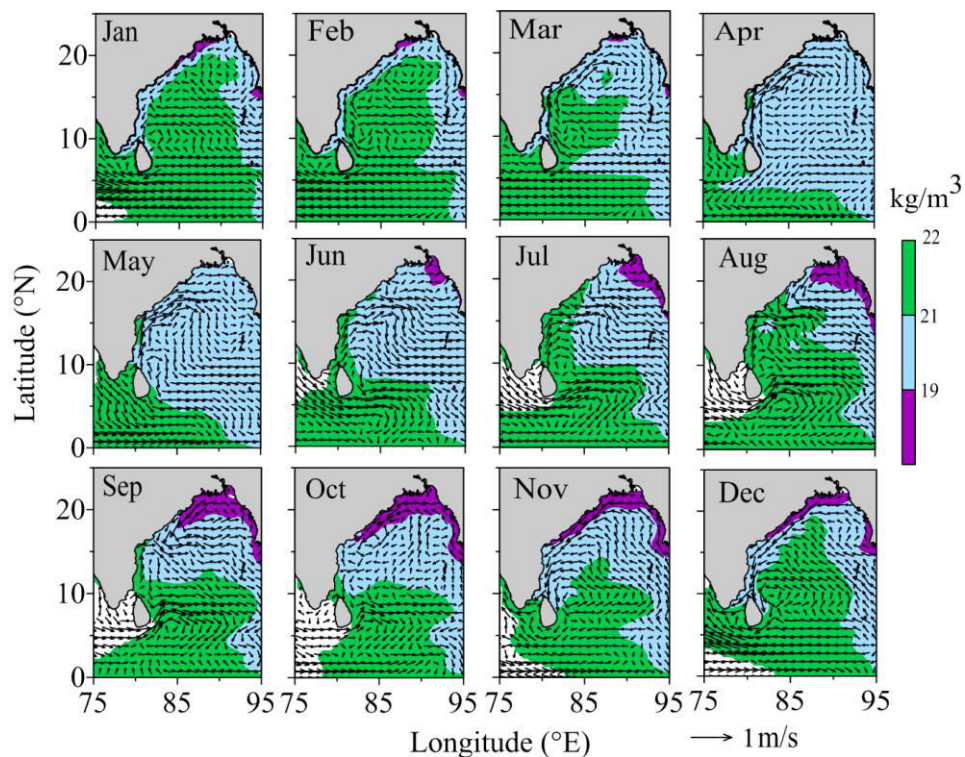
Fig. 4.7 Monthly evolution of surface density estimated from SODA data for the three watermasses in the Bay of Bengal overlaid with surface currents. NDW indicated by violet, TW by blue and SBBW by green colour.

During the initial phase of its formation, this watermass is visible in the northeastern BoB and occupies a thin shallow layer, i.e. upto 10 m (Fig. 4.8). A

substantial amount of this low salinity water then advects along the eastern periphery of the BoB by the prevailing south eastward currents (Fig. 4.7). The thickness of this watermass exceeds 40 m near the coast, but its thickness reduces to less than 20 m farther offshore. This could be attributed to paucity of freshwater. The low salinity NDW in a shallow layer above the comparatively saltier subsurface water leads to very strong near surface stratification. On the other hand, NDW is noticed in the coastal periphery of the western BoB only after September. Along the east coast of India, its maximum southward extension, i.e. upto 15°N, is observed during November-December.
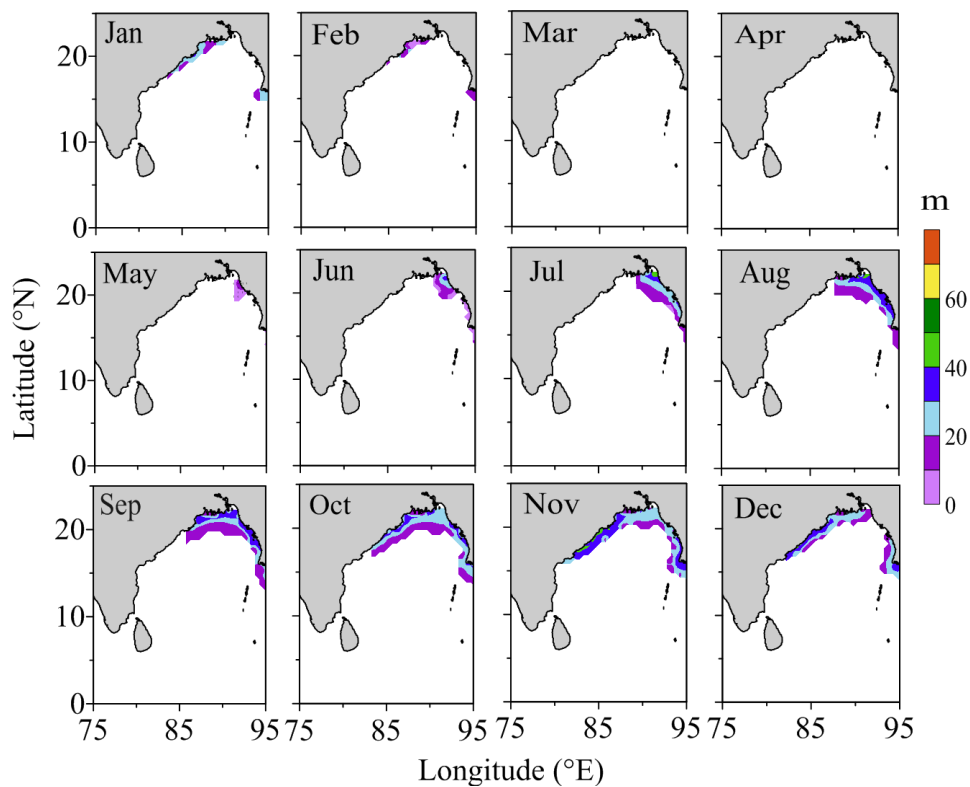
Fig. 4.8 Monthly distribution of the thickness of Northern Dilute Watermass

Turner angle (Fig. 4.9) indicates doubly stable (-45° < Tu < 45°) condition in the region of NDW (Fig. 4.7) during the initial stages of its formation, i.e. in June. As the monsoon strengthens, increase in the freshwater from continental runoff freshens the surface layers resulting in an increase in the salinity with depth (0.5 to 0.8). In additon, thermal inversion (upto 1.2°C) is another feature in the regions of NDW. This together leads to diffusive convection (-90° < Tu < -45°). During the withdrawal phase of summer monsoon, i.e. September-October, diffusive convection prevailed very close to the coast and doubly stable condition in the offshore. During winter, diffusive convection reign in the whole region of NDW.
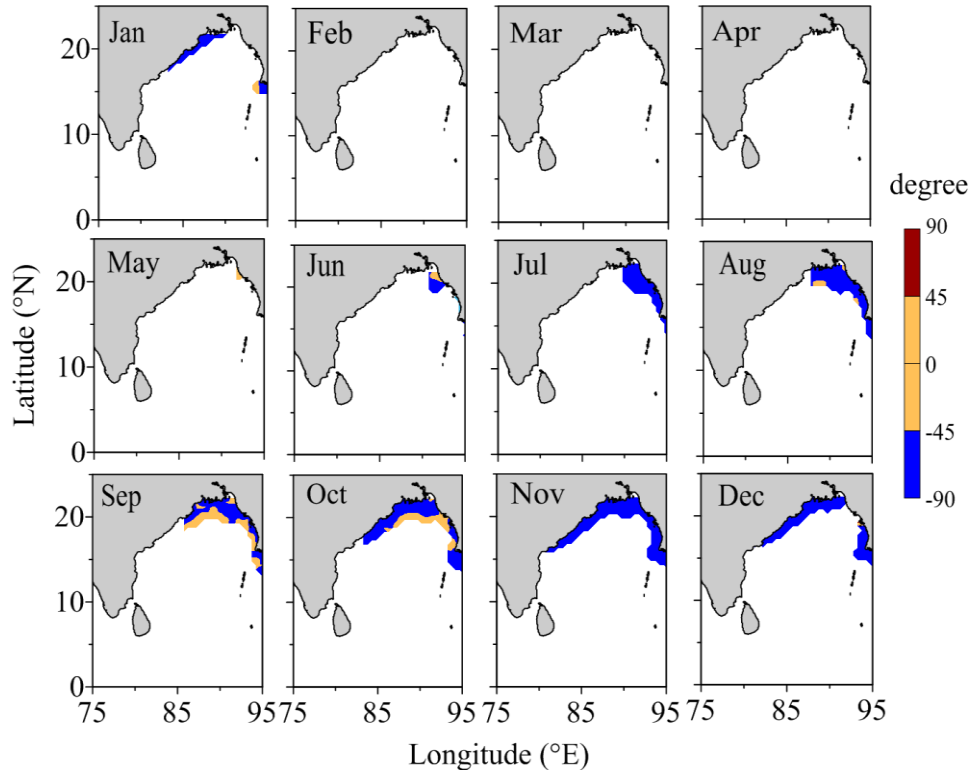
Fig. 4.9 Monthly distribution of Turner angle (Tu) in the region of NDW

4.4.2 Transition Watermass (TW)

The TW ($19 < \sigma_t < 21$) is observed in the BoB throughout the year (Fig. 4.7) but at different depths (Fig. 4.10). It has maximum spatial coverage at the surface during April-May (Fig. 4.7) and could be traced upto depths of 30 - 40 m in the northeastern coastal periphery (Fig. 4.10); and at shallower depth in the interior of the basin. During summer monsoon, TW is noticed below the NDW in the coastal regions of the northern BoB. However, it disappears from the coastal regions of the western BoB. In order to probe into the mechanisms leading to disappearance of TW, the circulation pattern (Fig. 4.7) and wind stress curl (Fig. 4.4) are examined. During this period, the northward flowing EICC (Fig. 4.7) along with positive wind stress curl (Fig. 4.4) favours offshore Ekman transport. As a result, the subsurface saltier SBBW is lifted towards the surface replacing the existing TW thereby increasing the salinity in those regions. In the western BoB, the presence of cyclonic and anti-cyclonic eddies during May-June (Fig. 4.6) significantly influences the vertical extent and thickness of TW. For example, the divergence at the core of a cyclonic eddy (~18°N, 87°E) shoals the TW to ~20 m from ~ 30 m whereas the convergence associated with an anti-cyclonic eddy (16°N, 86°E) increases the thickness to more than 40 m. After the withdrawal of summer monsoon, the TW regains the condition similar to that in

the pre-monsoon scenario, but is confined to north of 10°N. Even during winter, TW lies below the NDW (below 30 m) in the coastal regions of the northern BoB (Fig. 4.10). In the central bay formation of cyclonic eddy (Fig. 4.6) leads to the disappearance of TW from November as divergence at the core of this cyclonic eddy uplift the subsurface SBBW to the surface thereby replacing the TW from its surroundings. In December, the TW is confined mostly to the coastal periphery of BoB with a uniform thickness of 40-50 m (Fig. 4.10). Along the western boundary of BoB, the TW could be traced upto 8°N (Fig. 4.7) during winter.

Similar to NDW, thermal inversion (0.1 to 1.4°C) and increasing salinity (0.2 - 2) are prominent in the region of TW, especially during winter (December-February), which leads to the diffusive convection (-90° < Tu < -45°) in this region (Fig. 4.11). Otherwise, doubly stable condition pevailed in the region of TW.
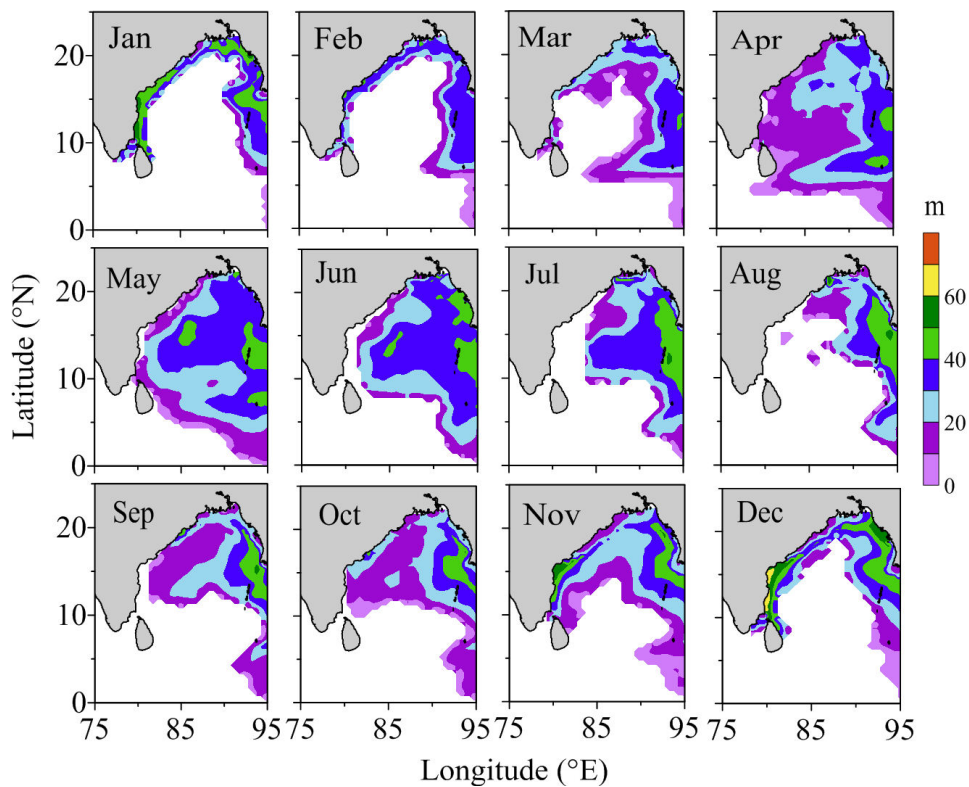
Fig. 4.10 Monthly distribution of the thickness of Transition Watermass
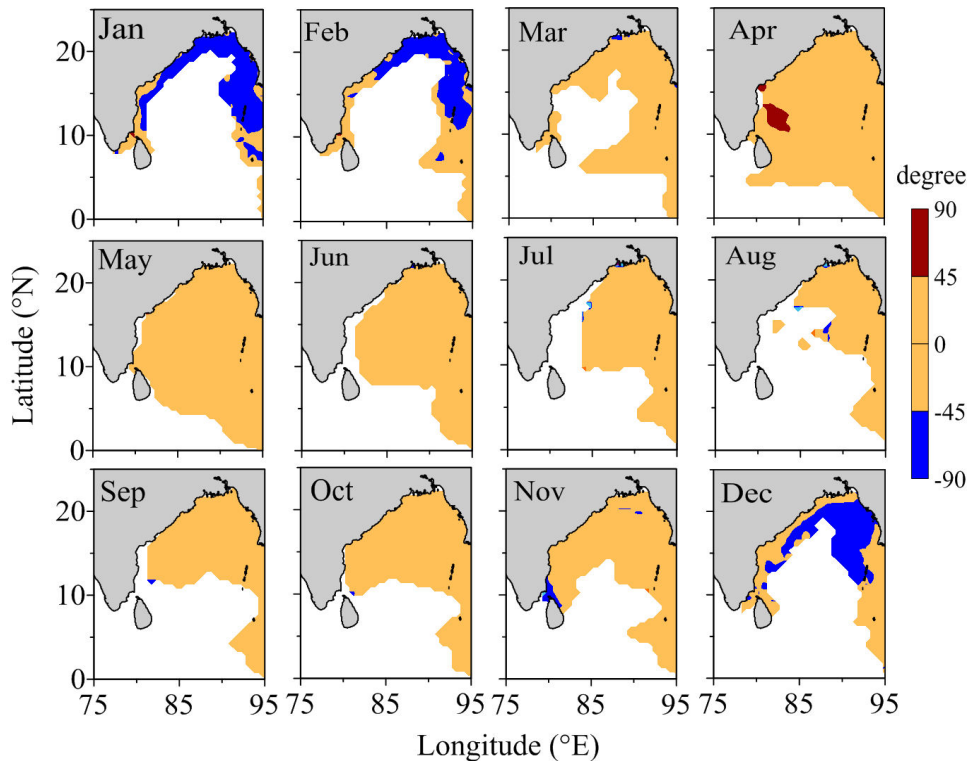
Fig. 4.11 Monthly distribution of Turner angle (Tu) in the region of Transition Watermass

4.4.3 Southern Bay of Bengal Watermass (SBBW)

The SBBW being more saline and denser fills the bulk of the surface layers of the southern BoB (south of 5°N) throughout the year between 21 and 22 σ_t levels (Fig. 4.7). In the northern and central BoB, this watermass could be traced below TW (Fig. 4.12). During the pre-monsoon period i.e., April-May, the SBBW has minimum horizontal extent in the BoB as it is confined to south of 5°N. Similar to TW, thickness of SBBW too gets affected by the meso-scale features. For example, in May, under the influence of an anti-cyclonic eddy present off the east coast of India north of 15°N (Fig. 4.6), the core of SBBW deepens to over 50 m depth (Fig. 4.12). In the coastal regions off the east coast of India, the prevailing positive wind stress curl during the summer monsoon cause offshore Ekman transport. As a result, SBBW from deeper depths is lifted towards the surface replacing the existing TW. As the monsoon withdraws and the EICC changes its direction southward, the SBBW gradually disappears from the surface layers of the southeast coast of India and TW replaces this watermass (Fig. 4.7). On the other hand, the formation of a cyclonic eddy in the western-central BoB in October (Fig. 4.6) induced by the wind stress curl (Fig. 4.4) causes divergence and uplifts the SBBW towards the surface, thereby increasing the salinity in those regions. By December, the SBBW has its maximum

55

spatial extent in the surface. In the region of SBBW, doubly stable condition (Fig. 4.13) prevails throughout the year.
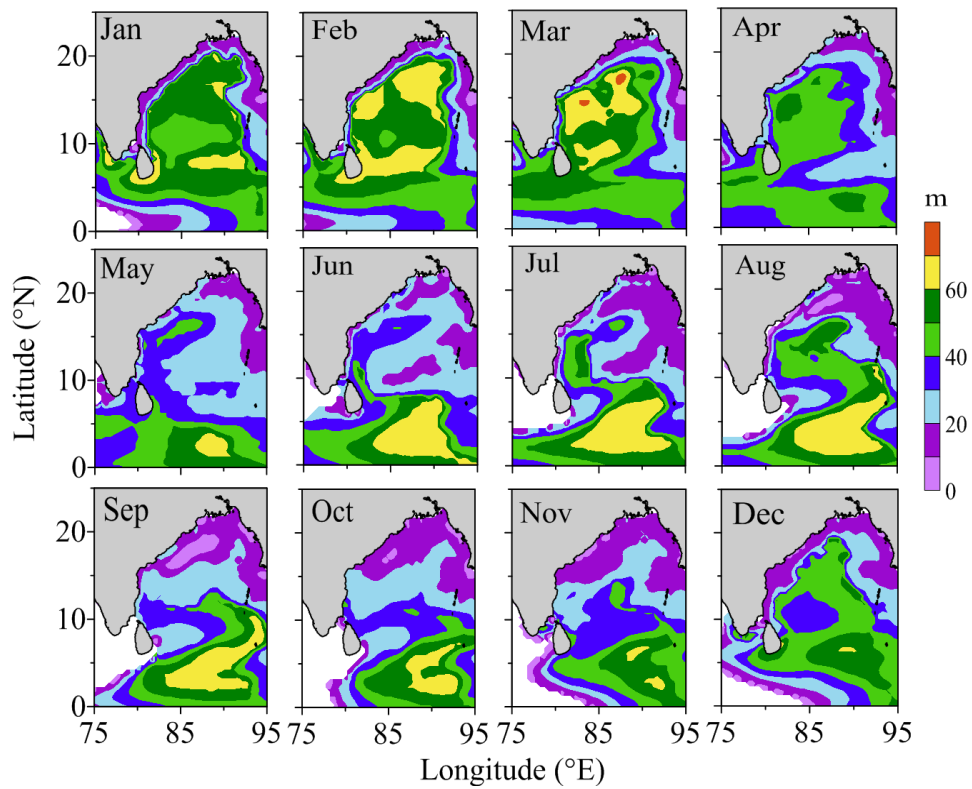
Fig. 4.12 Monthly distribution of the thickness of Southern Bay of Bengal Watermass
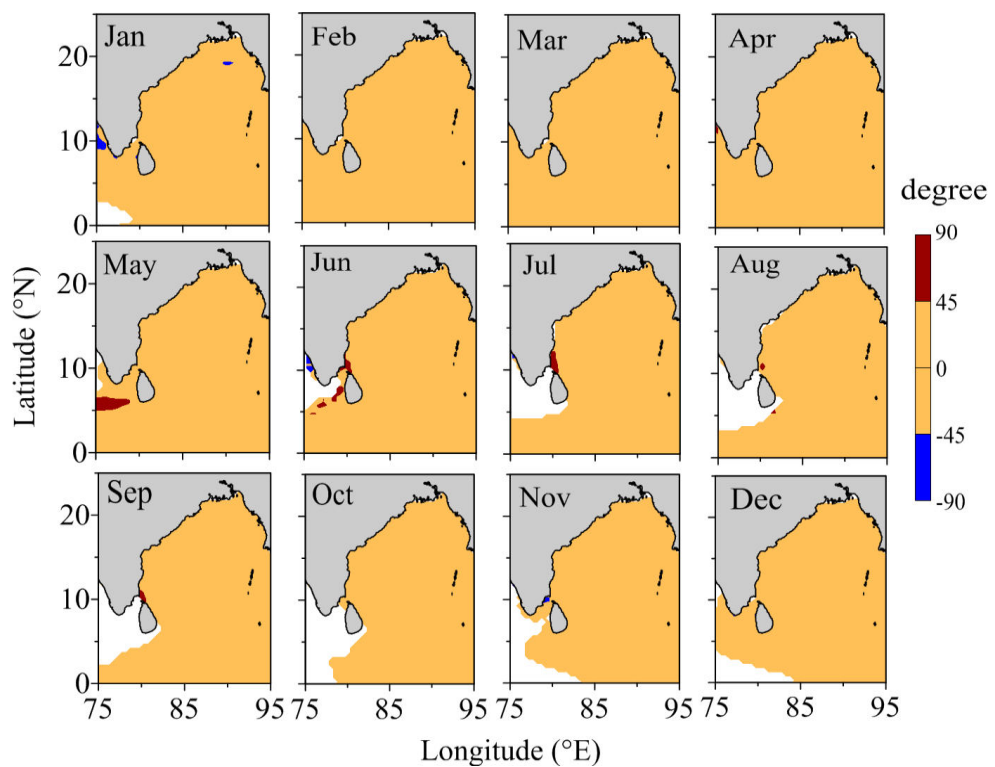
Fig. 4.13 Monthly distribution of Turner angle (Tu) in the region of Southern Bay of Bengal Watermass

4.4.4 Volume of watermasses

In addition to temperature, salinity and σ_t, volume being a physical characteristic of the watermass was estimated by multiplying respective thickness (falling within the pre-defined bounds of the watermasses based on T-S-σ_t ranges) and area (0.5°x0.5° grid). The individual volume were then added together to determine the total volume of each watermass for each month (Fig.4.14). The Figure shows that the NDW has its maximum volume in November (7.4 x 10^{12} m^3) during which the watermass occupy larger areas and maximum vertical extend (Fig. 4.8). In January, the volume of NDW is a meager value (2 x 10^{12} m^3) and hence not visible in the figure. On the other hand, the TW cover larger area and deeper depths in May (Fig. 4.10) resulting in a volume of 93.4 x 10^{12} m^3. The volume of this watermass is approximately 14 times that of NDW. It has its minimum volume in February (31 x 10^{12} m^3) as the SBBW occupies major portion of the BoB. The SBBW has volume in excess of 214.9 x 10^{12} m^3 in March due to deeper vertical extend and large coverage (Fig. 4.12). The reduced vertical extends in November leads to a reduction in the volume (117.5 x 10^{12} m^3). The volume of SBBW is almost twice the combined volume of TW and NDW. In nutshell, the analysis shows that the SBBW is the dominant component of watermass in the upper layers of the BoB, followed by the TW and finally the NDW.
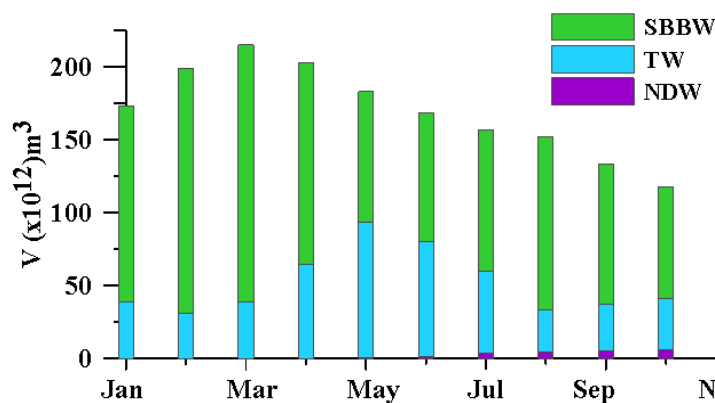
Fig. 4.14 Monthly distribution of the volume of NDW, TW and SBBW

4.5 Role of the BoB water in the Southeastern Arabian Sea

Several studies (Thadathil and Ramaraju 1987; Shetye, 1993; Hareesh Kumar and Mathew 1997; Jensen, 2001, 2003; Prasanna Kumar et al., 2004; Shenoi et al., 2005; Vinayachandran and Kurian, 2007; Benshila et al., 2014) have shown the presence of BoB water in the SEAS during the northeast monsoon. To document the

evolution of lowering salinity in the SEAS during winter, the monthly distribution of surface density, thickness and the Turner angle of SBBW are presented in Figure 4.15. The Figure 4.15a shows indication of the low salinity waters transported from the BoB by the southward flowing EICC and entering the SEAS from November. From the σt distribution (Fig. 4.15a), it is found that this water is having the characteristics of SBBW. Subsequently, this water is transported toward north along the west coast of India by the WICC and the propagating Kelvin waves and could be traced up to upto 12°N in January. Beyond this latitude, there is no evidence of SBBW. As the Kelvin wave propagates northward, they radiate Rossby wave offshore and transport of SBBW into the interior AS, which is also reported by Shankar and Shetye (1997). The depth occupied by this water increases from November and reaches maximum of 60 m in February (Fig. 4.15b). After January, as the EICC reverses its direction to northerly, this water starts fading from the coastal regions of the SEAS; but its signatures continue to exist in interior basin till May (upper 40-50 m). Throughout the period of its existence in the SEAS, the entire thickness of this watermass show a doubly stable condition (Fig. 4.15c).
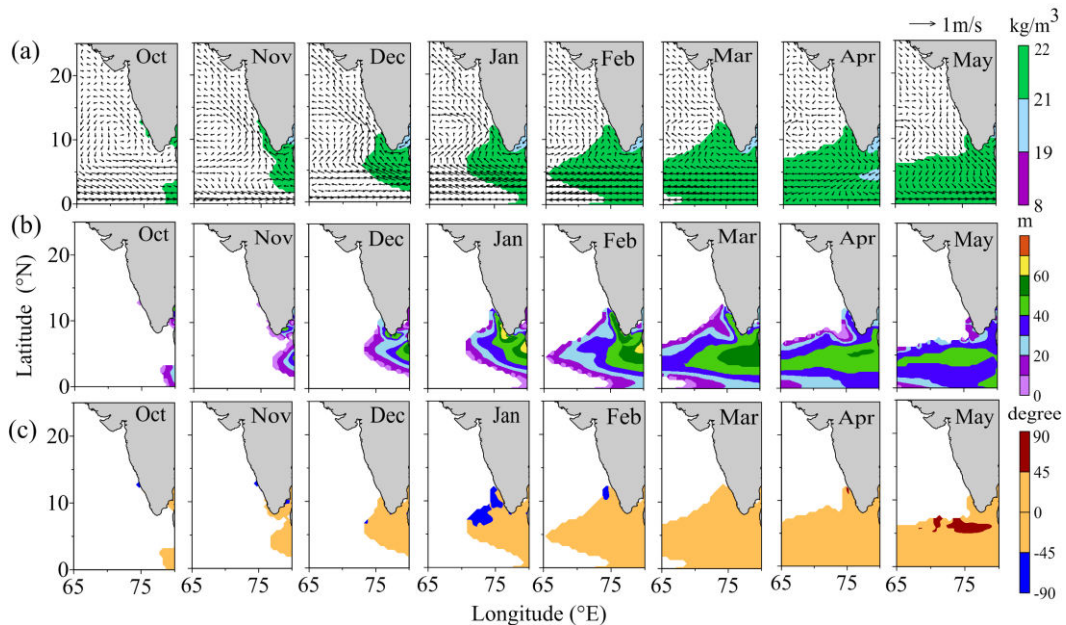
Fig. 4.15 Monthly distribution of (a) surface density (b) thickness and (c) Turner angle of Southern Bay of Bengal Watermass in the southeastern Arabian Sea

It is very difficult to provide a satisfactory pattern of salinity distribution from the climatology where combination of data from different sources is utilized. In the SEAS, INS Sagardhwani carried out dedicated oceanography surveys within a 2°x2° grid between 30 m and ~2000 m depth contours in October 2007, November 2007,

December 2010, January 2008, February 2009, March 2008, April 2009, and May 2008 (Fig. 4.16). The surveys were carried out along five zonal transects perpendicular to the coast (along 8.5°N, 9°N, 9.5°N, 10°N, 10.5°N) with stations at 5 NM intervals between 30 m and 200 m depth contours and at 15 NM intervals offshore beyond 200 m depth contour. Temperature and salinity data from these experimental programs are utilized to investigate presence of BoB water in the SEAS.
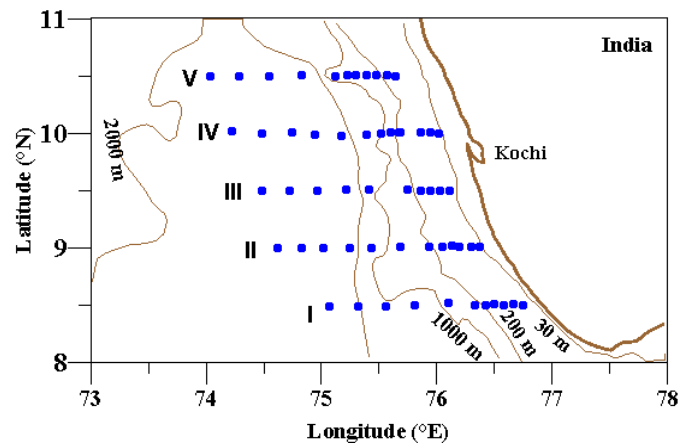
Fig. 4.16 Blue dots indicate the station location. Stations separations are 5NM between 30 and 200m depth contours, while it is 15 NM beyond the 200 m depth contours. Hydrography data sets are collected using Mini CTD systems (accuracy: temperature ±0.01°C, salinity ±0.02, pressure ±0.02% of 1000 m).

To understand the temperature-salinity characteristics in the SEAS, T-S diagrams are prepared separately for coastal (<100 m depth contour, Fig. 4.17) and deep waters (>100 m depth contour, Fig. 4.18) from October to May. Figure 4.17 shows the presence of three watermasses, viz. Arabian Sea Watermass, Indian Equatorial Watermass and Bay of Bengal Watermass in this region. Anoopa et al. (2013) also observed the presence of these waters in SEAS during this period. Since the objective of this chapter is to document the changes in the advection of water from BoB, the discussion is confined to the Bay of Bengal Watermass.

The T-S diagrams show significant modification in the watermass structure in the SEAS between October and May at both the locations. Here, a low salinity plume appears in November in the coastal regions of the southern tip of India which is in contact with the BoB (Fig. 4.19), which is having large variations in salinity and homogeneous temperature (28-29°C). This result in minimum scatter in T-S diagram and freshening of the surface layers by ~1 unit compared to October (Fig. 4.17-4.19). This water is noticed in the T-S diagram (Figs. 4.17 and 4.18) around 22 σ_t levels (<

59

34.5, ~28 to 29°C) and resembles to that of SBBW. As the SBBW enters SEAS from south, there is a gradual increase in salinity with depth.
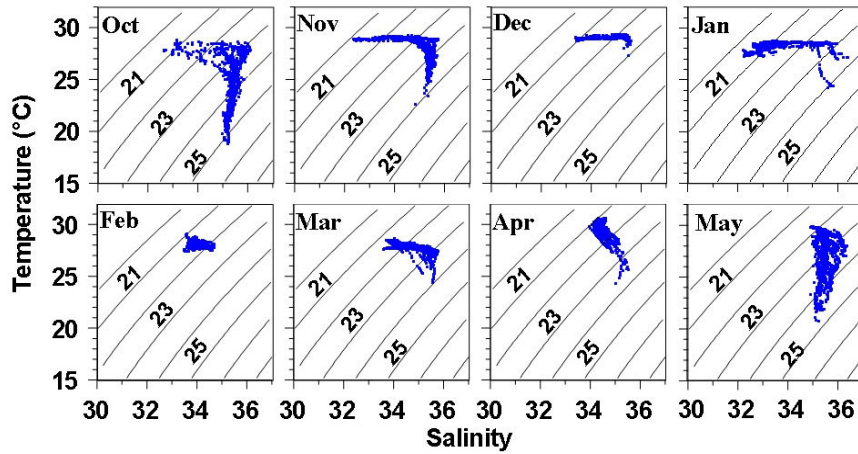
Fig. 4.17 Monthly T-S diagrams in the shallow waters (<100 m depth contour)
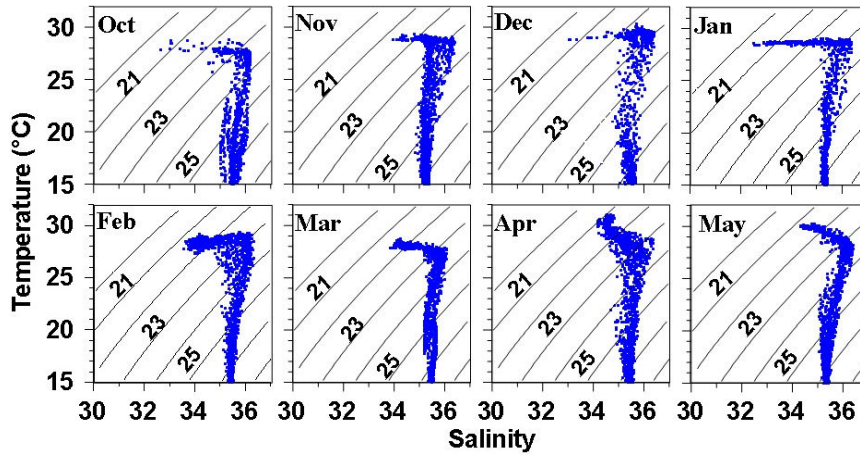
Fig. 4.18 Monthly T-S diagrams in the deep waters (>100 m depth contour)
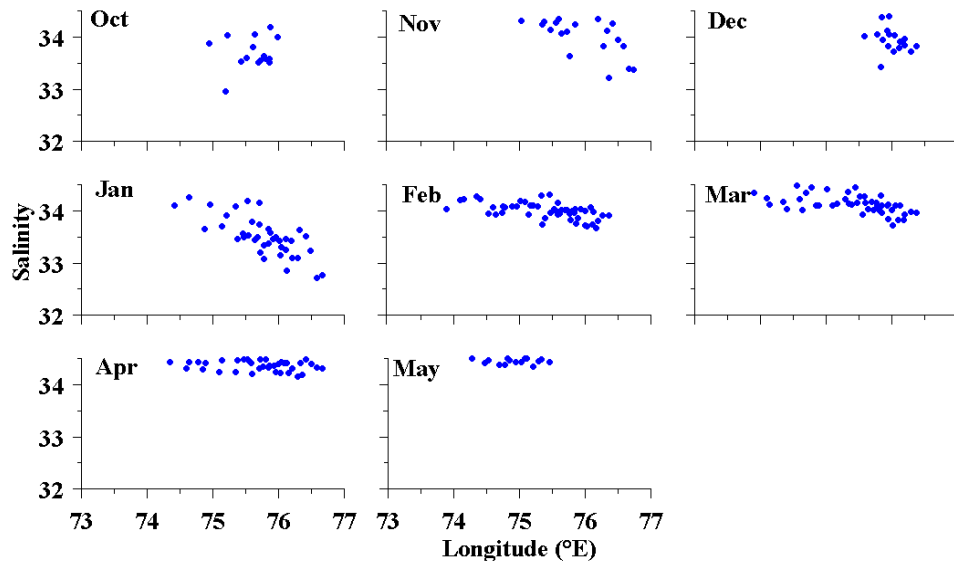
Fig. 4.19 Monthly evolution of salinity of the SBBW in the SEAS

60
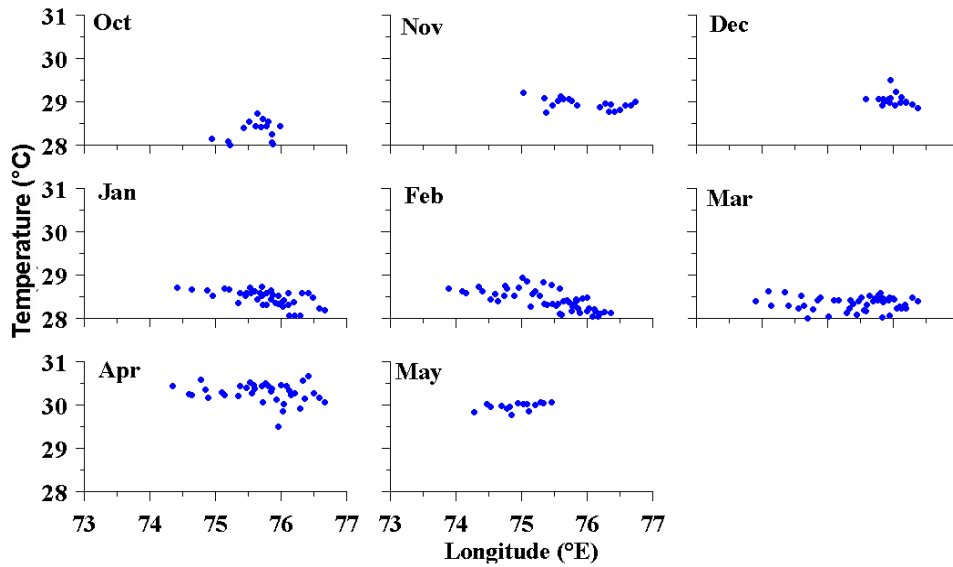
Fig. 4.20 Monthly evolution of temperature of the SBBW in the SEAS
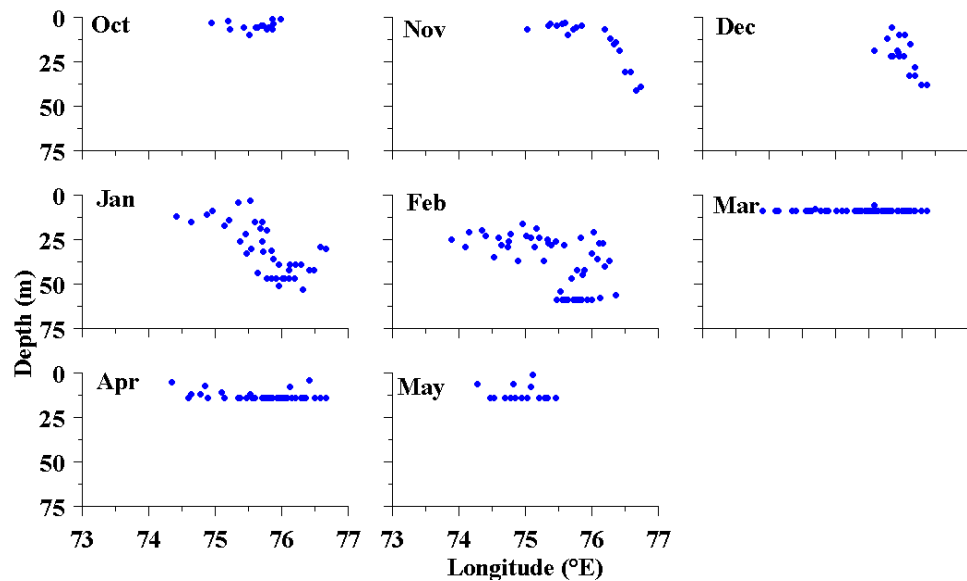
Fig. 4.21 Annual cycle of the vertical extent of SBBW

In January, the SBBW could be traced upto 75°E and minimum salinity (~32.5) is noticed very close to the coast. Here, this water is evident upto a depth of 50 m (Fig. 4.21), whereas in the offshore region, its vertical limit is the upper 10 m. After January, as the EICC reverse its direction to northward, the core salinity increases. This watermass is having minimum spread in February, indicating a highly homogeneous structure in the entire coastal regions of the SEAS (Fig. 4.18). But from March, salinity in the water column starts increasing and by May it becomes more or less homogeneous in salinity but its temperature vary from nearly 23°C to 30°C. In the deep water also similar features are observed. West of 75.5°E, this watermass

continue to exist until May, even though currents are southward. However, its temperature and salinity gets slightly modified (>30°C, ~34.5; Fig. 4.19, 4.20), but still maintain the same σ_t level. Hareesh Kumar et al. (2009) also reported the watermass in May at the core of Arabian Sea Mini Warmpool.

Figs. 4.17-4.19 clearly show the evolution of SBBW in the SEAS, as evident from the appearance of low salinity water from November, well established in January, retreat from February, and transport to interior basin due to the offshore radiation of Rossby wave. The lowering of salinity in this region is marked by an increase in the sea level to 5 cm (Fig. 4.22a). The transition of sea level from negative to positive in November coincides with the arrival of coastally trapped downwelling Kelvin wave (Fig. 4.22b). Studies (Bruce et al., 1994; Shetye et al.,1991) have indicated that the downwelling Kelvin wave force an equatorward EICC in the western BoB. There is evidence from climatology (Hastenrath and Lamb, 1979; Cutler and Swallow, 1984) that a circulation exists around the southern tip of India from BoB to the AS that brings SBBW into the SEAS.
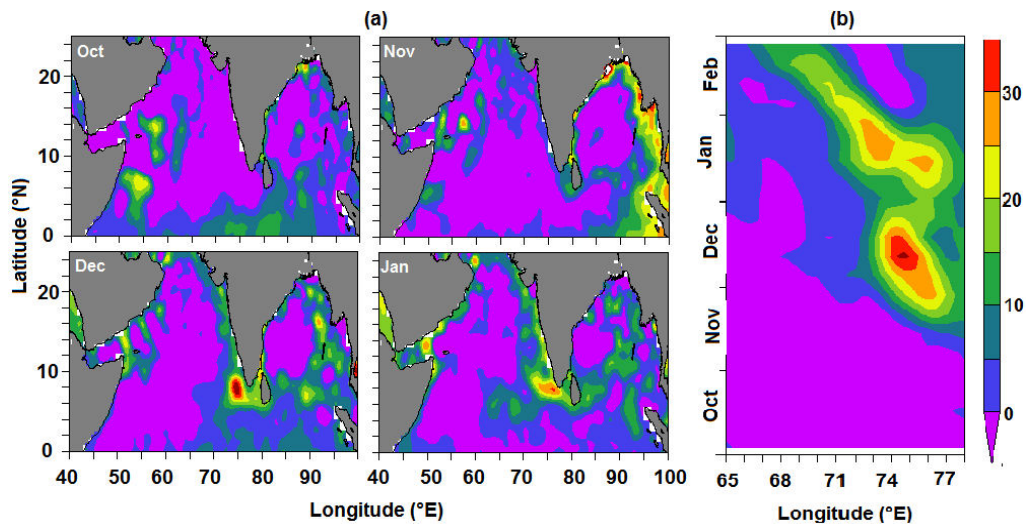
Fig. 4.22 Evolution of SLA (cm) in the north Indian Ocean during October-January and (b) Hovmullor diagram along 8.5°N

As the coastal Kelvin wave propagates along the west coast of India (Fig. 4.22), the SBBW also spread northward and dilutes the surface layers of the coastal regions by ~1.5 during winter (34 in October to 32.5 in January). At the bottom, the corresponding values are ~1.5 to 2. In January, SBBW (< 32.5) could be traced upto 10.5°N along the west coast of India. The westward shifting of positive sea level (Fig. 4.22) supports the offshore radiation of Rossby wave (Bruce et al., 1994), which

carries SBBW along with it. The westward transport of SBBW freshen the surface layers of those regions by nearly 2 units (35.75 in December to 33.75 in January at 75°E). The EICC reverses its direction to northward in January and impedes transport of SBBW into the SEAS resulting in an increase in the surface salinity. In the SEAS, the signature of SBBW is evident upto May, but slightly in the offshore. This cycle of salinity variability in the entire water column of the southwest coast of India during winter is typical in the SEAS.

To investigate the source of the low saline water that enters the SEAS during winter, a correlation analysis is carried out. The correlation between surface salinity in a 2° x 2° grid in the SEAS (8-10°N, 74-76°E) and rest of the BoB from October to March is estimated (Fig. 4.23). The figure shows a very strong positive correlation (~0.8) between the surface salinity in the SEAS and around Sri Lanka, whereas a strong negative correlation exists between the SEAS and southern BoB. The region of maximum correlation approximately coincides with the path of advection of low salinity water advect from BoB. Therefore, it can be inferred that the water that enters the SEAS during winter is off the east coast of Sri Lanka.
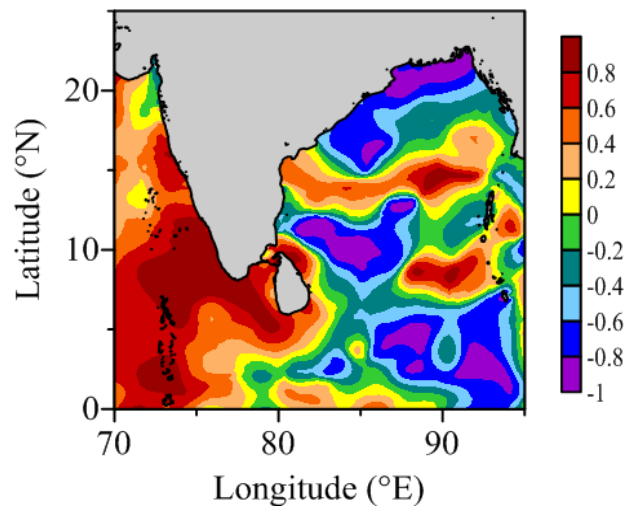
Fig. 4.23 Correlation coefficient (R) between sea surface salinity in the southeastern Arabian Sea (8-10°N, 74-76°E) and rest of the basin for the period October to March

In this chapter, three watermasses are identified in the surface layers of BoB viz., Northern Dilute Watermass (NDW), Transition Watermass (TW) and Southern Bay of Bengal Watermass (SBBW). The NDW ($\sigma_t < 19$) is present during May to January and forms as a result of large quantities of fresh water influx. The TW ($19<\sigma_t<21$) and SBBW ($21<\sigma_t<22$) are present in the BoB throughout the year but at varying depth levels depending on the locations. In the coastal periphery of the

northern BoB, TW is observed below NDW and has maximum spatial coverage at the surface during April-May. During summer monsoon, the prevailing coastal upwelling off the western boundary of BoB uplift the comparatively saline SBBW towards the surface resulting in the disappearance of TW. Later in September in the central BoB, the existing TW at the surface is replaced by SBBW due to the formation of a cyclonic eddy. As a result, the SBBW is noticed below the TW north of 5°N and at the surface south of 5°N throughout the year. Finally the transport of SBBW water into the SEAS and its evolution is documented.

Chapter 5

Saltwater pumping in the Bay of Bengal

5.1   Introduction

In the BoB, salinity is highly heterogeneous both in the vertical and horizontal domain due to the massive fresh water influx from precipitation and four major river systems viz. Ganges-Padma, Brahmaputra-Jamuna, Surma-Meghana and the Chittagong river systems. Among them, the Ganges, Brahmaputra, and the upper Meghana rivers are the prime contributors of the surface dilution in the northern BoB. In addition, rivers like Irrawaddy, Mahanadi and Godavari also contribute significantly to the freshwater budget of the BoB. Subramanian (1993) reported that the BoB receives excess precipitation (~2 m) and freshwater influx ($1.6 \times 10^{12} m^3 yr^{-1}$) from these major rivers. Since most of these freshwater sources are located north of 15°N, the surface layer of the northern BoB is always fresher than other regions of the Indian Ocean, especially during and after the monsoon (Chamarti and Sri Ram, 2009; Satya Prakash et al., 2012; Akhil et al., 2014; Benshila et al., 2014). The low salinity values are in phase with the seasonal cycle of runoff of rivers in and around the BoB (Yaremchuk et al. 2005).

The freshwater occupies upper few meters (~10 to 20 m thick) of the northern and north-eastern part of the basin, and invades into the northern half of the bay (Vinayachandran and Kurian, 2007). An outcome of the freshwater influx is the increase in the upper layer stratification at the head Bay (Varkey et al., 1996, Rao and Sastry, 1981; Gopalakrishna et al, 2002; Prasanna Kumar, 2002; Agarwal et al., 2012; Narvekar and Prasanna Kumar, 2014) and the formation of barrier layers (Vinayachandran et al., 2002; Rao and Sivakumar, 2003; Vinayachandran and Kurien, 2007; Thadathil et al., 2007). The enhanced vertical stratification usually results in a shallow mixed layer (Mignot et al., 2007; Thadathil et al., 2007; Girishkumar et al., 2013) and affects the surface layer circulation of the BoB (Shetye et al., 1991; Chamarthi et al., 2008) and biological productivity (Prasanna Kumar et al., 2002, 2004; Nuncio, 2007; Vidya and Prasanna Kumar, 2013). The warm and shallow layer over the highly stratified thermocline also affects storm-induced surface cooling in the BoB, which may in turn favour the intensification of tropical cyclones (Sengupta et al., 2008; Neetu et al., 2012; Vincent et al., 2012). Moreover, the increase in salinity with depth is sufficiently large to support thermal inversions in the northern BoB.

This chapter mainly focuses on how the excess of freshwater is replaced with saltier water in order to prevent the bay from continuous freshening. In the bay, the

temperature decreases rapidly with depth just below the mixed layer whereas salinity increases rapidly with depth from the surface. Temperature and salinity are forced or modified either in the upper ocean or at the air-sea interface by processes such as air-sea exchanges or the vertical exchanges between the upper ocean and the interior, but their vertical exchanges with the deep interior occur at much lower rates. One process by which saltier water enters the bay is through the SMC from the AS (Murthy et al., 1992; Vinayachandran et al., 1999; Schott and McCreary, 2001). Because of the density contrast, this water slides under the prevailing low salinity waters of BoB (Vinayachandran et al., 2013). The modelling study of Akhil et al. (2014) shows that vertical mixing of surface fresh waters with underlying saltier waters is the primary mechanism for the salinity increase. Their study also implies that erosion of the freshwater tongue along the east coast of India is due to vertical processes rather than horizontal advection. Chowdary et al. (2016) emphasizes the significance of accurate representation of vertical processes in general circulation models so that they simulate realistic surface and subsurface salinity structure in the BoB. Therefore, to maintain the salt balance of the BoB, the entrainment of this saltier subsurface water towards the surface plays a crucial role. During May 2015 (pre-monsoon) and February 2016 (winter), two physical oceanography surveys were carried out in the northern BoB to address the pumping of saltwater into the surface layers of the northern BoB. In the present chapter, the role of coastal upwelling, divergence induced by eddies and their interaction, tropical cyclones, etc. on the saltwater pumping of the BoB is discussed.

5.2   Observations

The *in situ* hydrographic data used in this study were acquired onboard *INS Sagardhwani* cruises during (i) 5-9 May 2015 and 9-14 February 2016 (from the coast up to 88°E in May and up to 91°E in February) along 17°N (TR1) and 17.5°N (TR2) in the northern BoB (Fig. 5.1a). Hydrographic profiles were collected along these two tracks with a SeaBird CTD system from a maximum depth of 500 m at 15 nautical mile intervals. The bottom topography (Fig. 5.1b) indicates narrow shelf width (< 50 km) with steep slope extending from 83°E along 17°N and 83.75°E along 17.5°N. Figure 5.1b also indicates that there is a slight decrease in the depth of water column towards north. The evolution of eddies and their spatial structure was examined using 7-day snap-shots of the merged SLA for the period October 2014 to March 2016 obtained from AVISO product having a spatial resolution of 25 km (Le Traon et al.,

1998). To study the meso-scale variability from SLA data, high-pass filter was used for each grid point so that any variability with periods longer than 30 days is essentially removed to obtain a non-seasonal anomaly. After that, a boxcar filter was applied to the SLA data to remove any spatial in-homogeneity in the data. The wind stress curl is estimated from the weekly wind data acquired by the Scatterometer aboard the ERS-1/2 satellites for the same period as the SLA data: from October 2014 to March 2016.
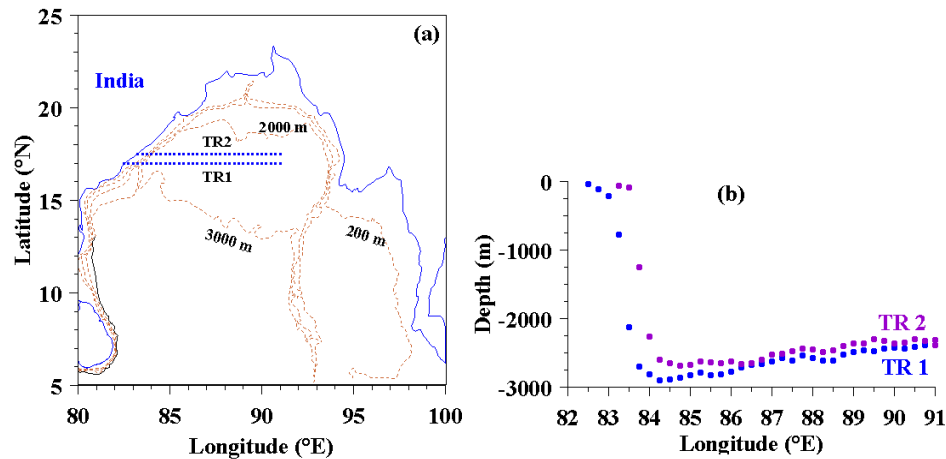
Fig. 5.1 (a) Station locations (Blue dots) in the Bay of Bengal and (b) bottom depth along the two transect (violet dots along 17.5°N and blue dots along 17°N). During May 2015, the experiment was planned only up to 88°E. For the same period, due to the winch failure, data could be collected only up to 50 m depth along 17°N. The bathymetry data were collected using the multi-beam echo-sounder onboard the ship.

The saltwater pumping is further investigated using the Argo floats at the northern (Float nos. 2901336, 2901292), central (Float no. 6901558) and southern BoB (Float nos. 2902365). These are supplemented with data from RAMA buoy (15ºN, 90ºE), BOBMEX-99 (along 13ºN, 81º-87ºE) and World Ocean Circulation Experiment (WOCE) during February 1995 to further investigate the observed increase in salinity due to meso-scale eddies. To document the influence of cyclone on the saltwater pumping, data from nearby Argo float 2902114 during the passage of cyclone Hudhud in October 2014 and Argo float 290133 during the passage of cyclone Viyaru in May 2013 are utilized. The snap-shots of the merged SLA for the corresponding periods are presented to demarcate eddies.

5.3   Thermohaline Structure

The vertical sections of temperature and salinity (Fig. 5.2a) indicates that the coastal waters of the western periphery of the BoB (at 17.5°N, 83.25°E) are cooler

and fresher (27.9°C, 31.9) in February and warmer and saltier (28.8°C and 34.1) in May (Fig. 5.2b). Interestingly, in February, a pool of freshwater (<31.5) that extends up to a depth of 20 m is observed between 88.25°E and 90.5°E. Within the freshwater pool, cold (<26.5°C) and very low saline water (<30.2) caps the upper 10 m between 88.5°E and 89.5°E thereby increasing the vertical stratification. Figure 5.2a also shows that further eastern BoB (at 17.5°N, 91°E) is cooler by 2°C and fresher by 0.4 units than its western periphery, whereas in May, the surface layers centred at 17.5°N; 88°E is warm by nearly a degree and fresher by 1.4 units. In May, even though there is an overall increase in the salinity of the water column, still the freshwater cap is present east of 85.25°E but extends to deeper depths (around 60 m), while comparatively saltier water (>33) replaces the freshwater in the western Bay. The very low salinity present in this region can be attributed to the river runoff and monsoonal precipitation during the previous year as the northern BoB receive minimum river discharge (Fig. 4.3) during the period February-May (Sengupta et al., 2006). The fresher water over a thick layer (up to 60 m) in the central BoB enhances the near surface haline stratification and leads to a barrier layer (Fig. 5.2), which facilitates the trapping of net heat flux in the near surface layers during the pre-monsoon season. The salinity stratified layer above the thermocline is very crucial for the development of warm pool, formation of cyclones, onset of summer monsoon (Maneesha et al., 2012) and also affect the vertical transport of heat. The eastern Bay is both cooler and fresher in February compared to the western Bay; but the pre-monsoon heating causes the eastern Bay to be warmer which may be due to the presence of low salinity surface waters. This large-scale gradient exists throughout the year, but is modulated seasonally suggesting the seasonal spread of net freshwater input. In February, the vertical section of temperature shows inversions in the coastal as well as offshore regions (Fig. 5.2). The inversion intensity is large at time when surface temperature decreases; the largest inversion (1.75°C) occurs in the eastern Bay adjacent to the Irrawaddy river system. The inversion layer is evident from the surface up to a maximum depth of 25 m in the shelf of the western Bay and up to a depth of 50 m further offshore, while it is present mostly at the subsurface depths in the eastern Bay. In contrast, in May, the thermal inversions (up to 0.55°C) are confined to the subsurface levels between 60 and 100 m depths east of 84.75°E and the relationship between the surface layer temperature and the inversion is very weak. The possibility of the lateral advection of cold water (around 26.75°C) around 65 m

for the subsurface thermal inversion cannot be ruled out. The magnitude of inversion increases at times when temperature at 65 m decreases and temperature from 85-100 m is uniform. In the inversion layer, the vertical stability is maintained by the increase in salinity during February and May (0.25 to 0.96). Since this increase in salinity compensates for the increase in temperature, the inversion layers are vertically stable.
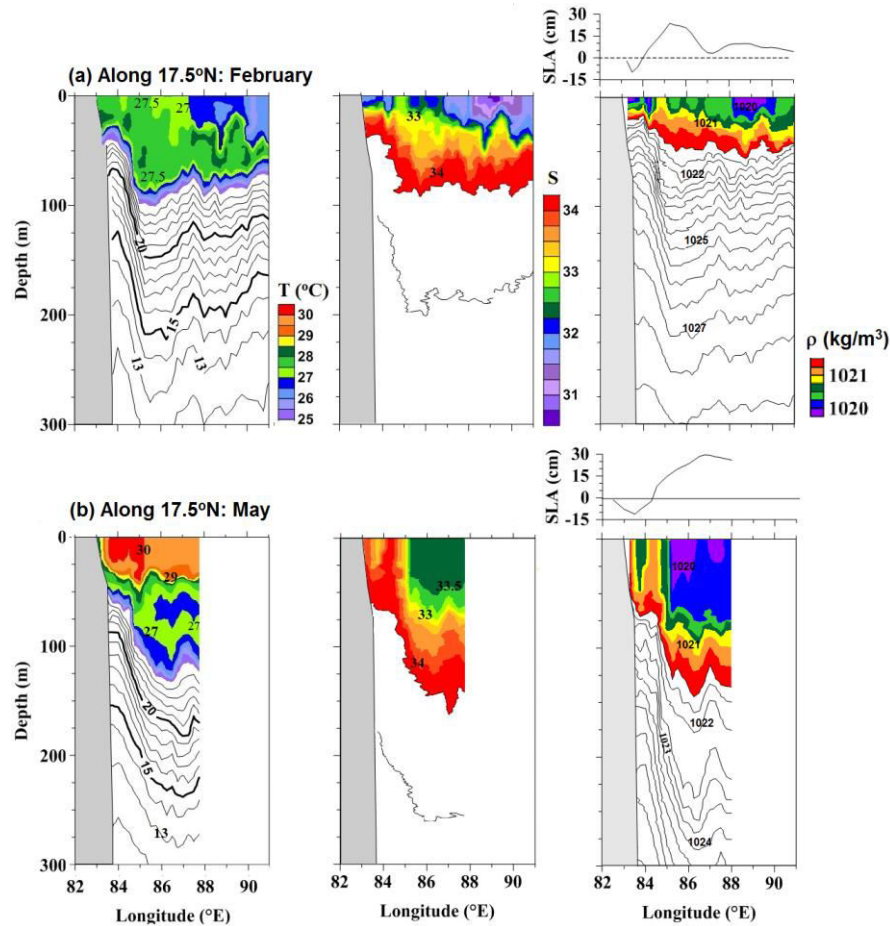
Fig. 5.2 Vertical section of temperature, salinity and density along 17.5°N (TR2) during (a) February 2016 and (b) May 2015

Figure 5.2c shows pockets of saltier water west of 86.5°E, which signify uplifting of saltwater from the subsurface towards the surface. In February (Figs. 5.2a, c), the uplift to the surface is observed at two regions along TR1 and TR2, centered at 84°E and 86°E. It is interesting to observe another region of uplift of saltier water centered at 89°E, but confined to depths below 10 m. In May (Figs. 5.2b, d), the nearshore saltwater pocket disappears while the offshore pocket shifts closer to the coast, i.e. to 84.5°E (about 110 km away from the coast). The uplift of saltier water cause abrupt changes in the vertical and lateral distribution of salinity, resulting in the formation of a salinity front, especially between the shelf and deep water (between 30 m and 3000 m isobaths). The westward limit of the offshore salinity front, defined as

the region up to which large horizontal gradients in salinity exist, is 84°E in February and 83.75°E in May.
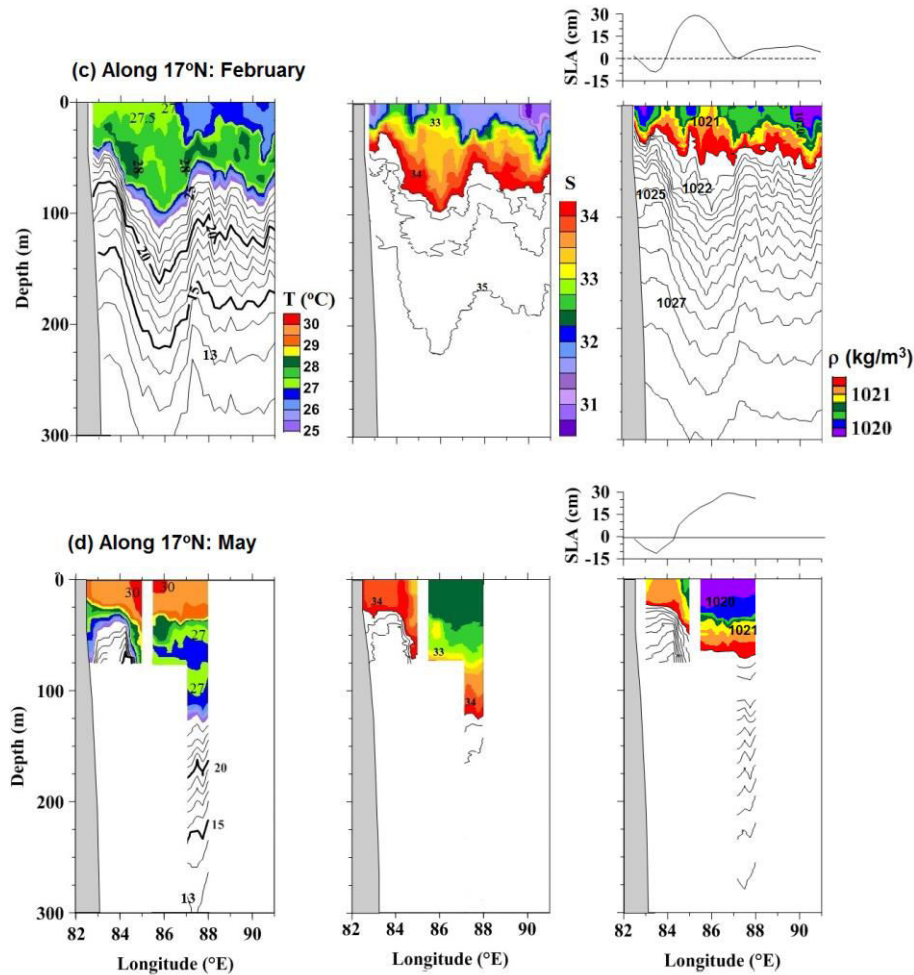
Fig. 5.2 Vertical section of temperature, salinity and density along 17°N (TR1) during (c) February 2016 and (d) May 2015

The variability in temperature, salinity and density across the offshore front are 0.85°C, 1.56, 0.4 kg/m^3 along TR2 and 0.15°C, 1.40 and 1.0 kg/m^3 along TR1, with its eastern side having comparatively cold and fresher water. The lateral salinity gradient across the front is very weak in May (0.02 km^{-1}) compared to February (0.16 km^{-1}). To add, a zone of moderately warm (27.25°C) and relatively saline water (32.97) separates the nearshore and offshore fronts. This region, referred to as transition zone, has very weak lateral and vertical stratification and nearly uniform temperature or thermal inversion up to 80 m in February and 25 m in May. Width of the offshore transition zone increases from 130 km in February to 165 km in May. As a result of strong near-surface stratification near the coast (Fig. 5.2), the thickness of the surface mixed layer based on density gradient is much shallower than that based on temperature (1°C drop from SST). Here, the entire water column is found to be

isothermal in February, whereas it is limited to 25 m in May. Similar features are observed along TR1 also, but with an enlarged magnitude.

T-S analysis indicates that surface layers (< 50 m depths) of the study region during the northern winter are influenced by two different types of watermasses (Fig. 5.3). Based on the classification of LaFond (1958), these watermasses are identified as the TW ($19 < \sigma_t < 21$) and SBBW ($21 < \sigma_t < 22$). In February, the TW is characterized by a heterogeneous salinity structure (31 to 32.75) with temperature in the ranges of 26° - 28°C and occupies the upper 50 m water column. The seasonal heating in May increases the temperature by 1.5°C (28.5°C in February to 30°C in May) in the upper 30 m (Fig. 5.2), resulting in the formation of a modified TW with a near homogeneous salinity (32.25 to 32.75). The SBBW with salinity 32.75 to 34.5 and temperature around 27° to 28°C is traced below the TW. However, west of 84.5°E, SBBW is traced at the surface but with a modified temperature (up to 30°C) and salinity (around 34.5). As a consequence of the pre-monsoon heating in May and the uplift of saltwater from subsurface level, the watermasses manifest as two distinct "salinity pockets" in the T-S diagram with salinity less than 32.5 in the eastern bay and more than 33.75 in the western BoB (Fig. 5.2).
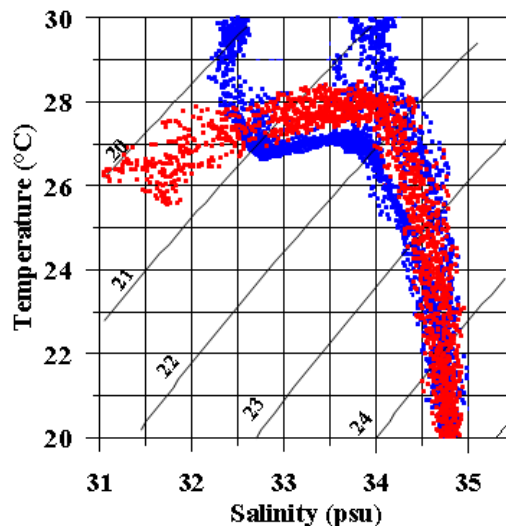
Fig. 5.3 T-S characteristics: February 2016 (red dots) and May 2015 (blue dots).

5.4   Impact of eddies on the thermohaline structure

To elucidate the spatial structure of meso-scale features in the BoB, typical snap shots of SLA corresponding to the observational period (February 2016 and May 2015) is presented in figure 5.4. The figure depicts several large-sized (R > 50 km) strongly interacting cyclonic and anti-cyclonic circulation patterns, which are

indicative of the prevailing cyclonic and anti-cyclonic eddies respectively. From the figure, it is obvious that the comparatively small size eddies are cyclonic; while the large-size eddies are more likely anti-cyclonic. In both February and May, the observational track 17°N and 17.5°N cut across both cyclonic and anti-cyclonic eddies, and hence the impact of both these eddies on the thermohaline fields were captured (Fig. 5.2). Compared to other regions of the BoB, the areas of high meso-scale eddy activities are confined to the western BoB, as seen from the bands of relatively large eddy kinetic energy (EKE) in Figure 5.5. Here, the SLA shows four regions of high eddy variability during winter: coastal cyclonic eddy (CCE), offshore cyclonic eddy (OCE), offshore anti-cyclonic eddy (OAE), and southern coastal anti-cyclonic eddy.
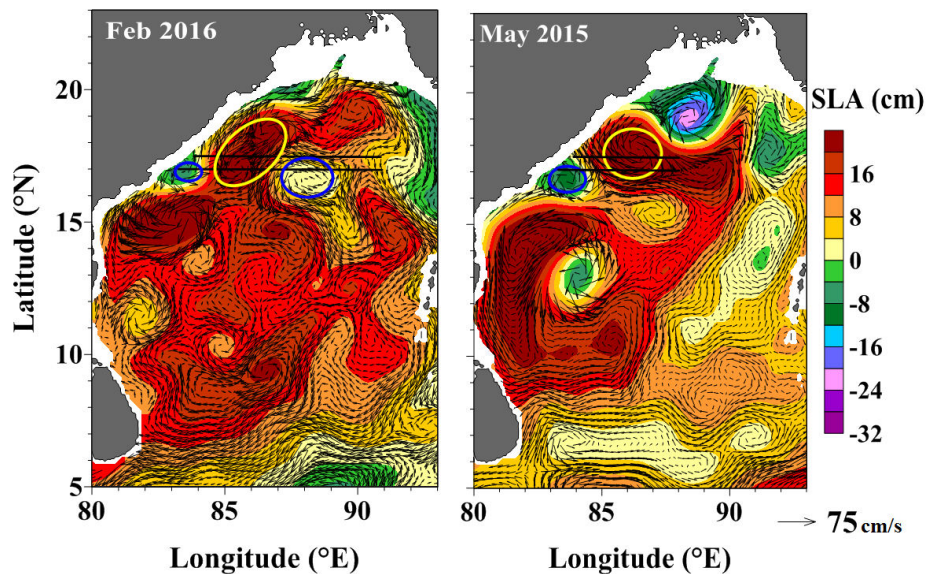
Fig. 5.4 Monthly snap shots of sea level anomaly (SLA) overlaid with the geostrophic currents in Bay of Bengal in February 2016 and May 2015. Black lines represent the observational track along 17°N and 17.5°N in February 2016. The blue encircled region shows cyclonic eddy and yellow encircled region shows anti-cyclonic eddy.

As a prelude, the moving speed of the eddy is estimated based on the Rossby wave theory (Pond and Pickard, 1983). Here it is assumed that the eddy is forced just in barotropic mode and its moving speed is estimated by β/k^2. Here $\beta = \delta f/\delta y$; f is the coriolis parameter ($2\omega\sin\varphi$); ω is angular velocity of earth's rotation (7.29 x 10^{-5} rad/s); y is the meridional distance (m); k wave number ($2\pi/L$); L is the wave length (eddy radius*2). In February, the gyre, which was earlier centred at 19°N, 90.5°E, intensifies and forms a large anti-cyclonic gyre, hereinafter referred to as offshore anti-cyclonic eddy (OAE), whose centre is shifted south-westward to 18°N, 87°E with

a translation speed of ~3.1 km/day; but this moving speed is very slow compared to its size (~235 km).
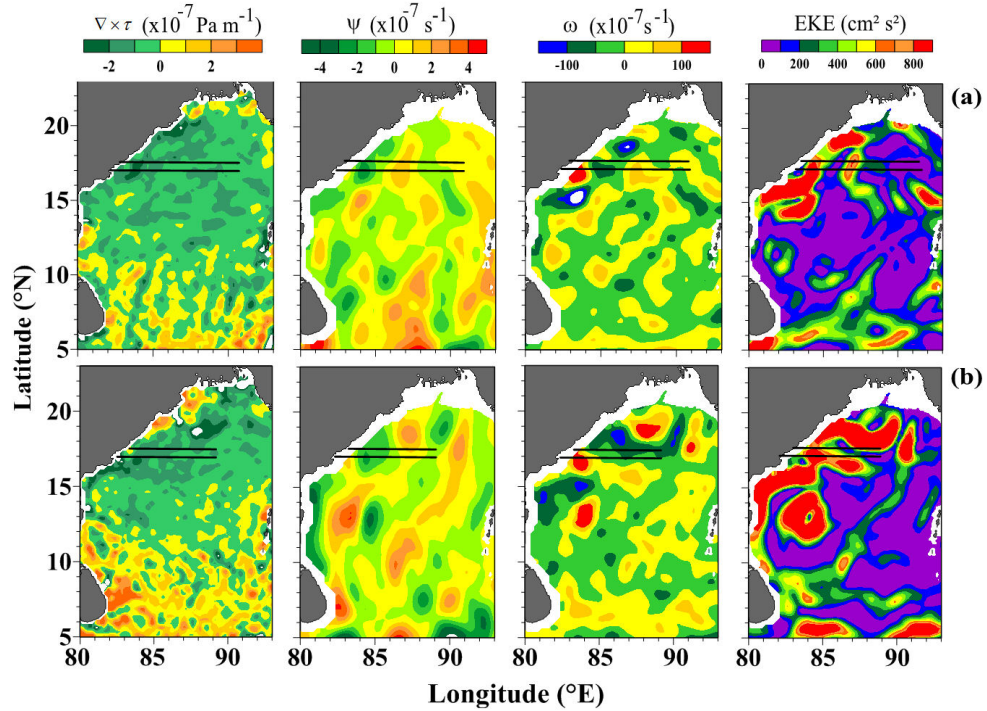
Fig. 5.5 Wind stress curl ($\nabla \times \tau$), divergence (ψ), vorticity (ω) and eddy kinetic energy (EKE) in the Bay of Bengal for the period (a) February 2016 and (b) May 2015.

At the latitude where the anti-cyclonic circulation is observed (centered at 17.5°N and 86.5°E), a negative sea level (west of 85°E) co-exists with a positive sea level anomaly to its east. In the northern Bay, the negative curl ($\nabla \times \tau$ in Fig.5.5) prevailing from November through March/May (wind curl for February and May are presented in Fig. 5.5) favours Ekman convergence (ω in Fig.5.5) in the upper ocean and spins up anti-cyclonic eddies that lead to intense open ocean downwelling at the base of the mixed layer. Therefore, deepening of the isolines in the central Bay in February and May (centered at 86°E along TR1 and TR2 in Figs. 5.2) signifies the large scale impact of wind induced convergence in this region. The intensification of the wind driven anti-cyclonic circulation in a closed basin like BoB gives rise to a strong northward flowing western boundary current. As these current flows against the local winds, these boundary currents can become unstable. Besides the wind forcing, the thermal forcing can also influence the fluctuation in eddy activity. Local heating/cooling alters the density structure in the upper layers of the ocean and, hence, affects the stability properties. The cooling-induced convection and wind-induced vertical mixing enhance the available potential energy in February causing the thermocline to become steeper and further deeper (in excess of 100 m) (Fig. 5.2). The

westward tilt of the upper thermocline reaches its maximum in May resulting in strong baroclinic instability.

At the centre of OAE (Figs. 5.2 a-d), low salinity and warm waters stretch to deeper depths (>80 m). The converse occurs at the core of cyclonic eddies. This suggests that the isothermal layer (ILD) is warmer and deeper in OAE compared to CCE. Therefore to quantify the influence of eddies on the thermohaline structure, the composite temperature and salinity maps over two cyclonic and one anti-cyclonic eddies are presented (Fig. 5.6). The anomaly (Δ) for a field at a given time and depth level is found by removing the horizontal average of the field along the two transects. By examining the vertical salinity profiles corresponding to CCE and OAE mentioned above, it was found that the OAE also deepens the isohaline contours towards its center; but reducing salinity at the centre compared to its edge. For example, in May, the 34.0 isoline deepens from the surface at the eddy periphery to nearly 125 m at the eddy centre (Fig. 5.2b). The depression of isolines, at the centre of this eddy brings fresher water towards deeper depths thereby decreasing salinity at those levels. Also the halocline intensity is weaker at the eddy centre (-0.025/m) than at the eddy edge (-0.05/m). The situation at the CCE is just the reverse. The impact of these two eddies on the halocline illustrate weaker intensities at the eddy edge than at its center. At the center of CCE, the intensity varies between -0.07 to -0.1/m whereas at the edge, the corresponding value is ~0.05/m.

In general, OAE result in positive temperature anomalies (ΔT) and raise the temperature by 1 to 4°C; but results in negative anomaly in salinity (ΔS). The peak corresponds to 4°C and 0.5 units respectively. In contrast, the CCE lower the temperature up to 5.5°C and increases salinity up to 0.75 units. Both types of eddies have weaker effects on the temperature distribution in the surface layer. As the depth increases, there is a clear discrepancy in the anomaly. The ΔT due to OAE sharply increases until 100 m well within the isothermal layer at this latitude, and then gradually weakens in the subsequent layers. The maximum ΔS (-0.5 units) associated with the OAE occurs at around 75 m, which corresponds to the depth of the halocline. However, the ΔT due to CCE is positive in the upper 35 m and a sharp increase up to 75 m, which is well within the thermocline. Similarly, the cyclonic eddy increases ΔS up to 0.75 units, as the associated divergence brings comparatively saltier subsurface waters towards the surface replacing the fresher water. The effect of CCE is not significant below 250 m in the temperature and below 100 m in the salinity

distribution (Fig. 5.6). These results indicate that the subsurface temperature reflects the existence of eddies better than at the surface layer. The depth of the maximum ΔT associated with anti-cyclonic eddy in the western BoB (approximately 100 m) is shallower than in the other regions (approximately 400 m); while the depths are comparable with other regions in the case of cyclonic eddies (Kurian et al., 2011). In nutshell, the OAE cause larger positive temperature anomaly in the upper 600 m and the most significantly affected depth is between 50-200 m (in excess of 2°C), whereas the CCE affects the temperature structure in the upper 250 m and the most affected depth is between 50-200 m (in excess of -0.2°C). The SLA corresponding to the observational periods (Fig. 5.4) indicates weak negative amplitude in the case of CCE and comparatively large positive values for OAE. Also, the anti-cyclonic eddies are stronger and its effects penetrate to deeper depths than in cyclonic eddies.
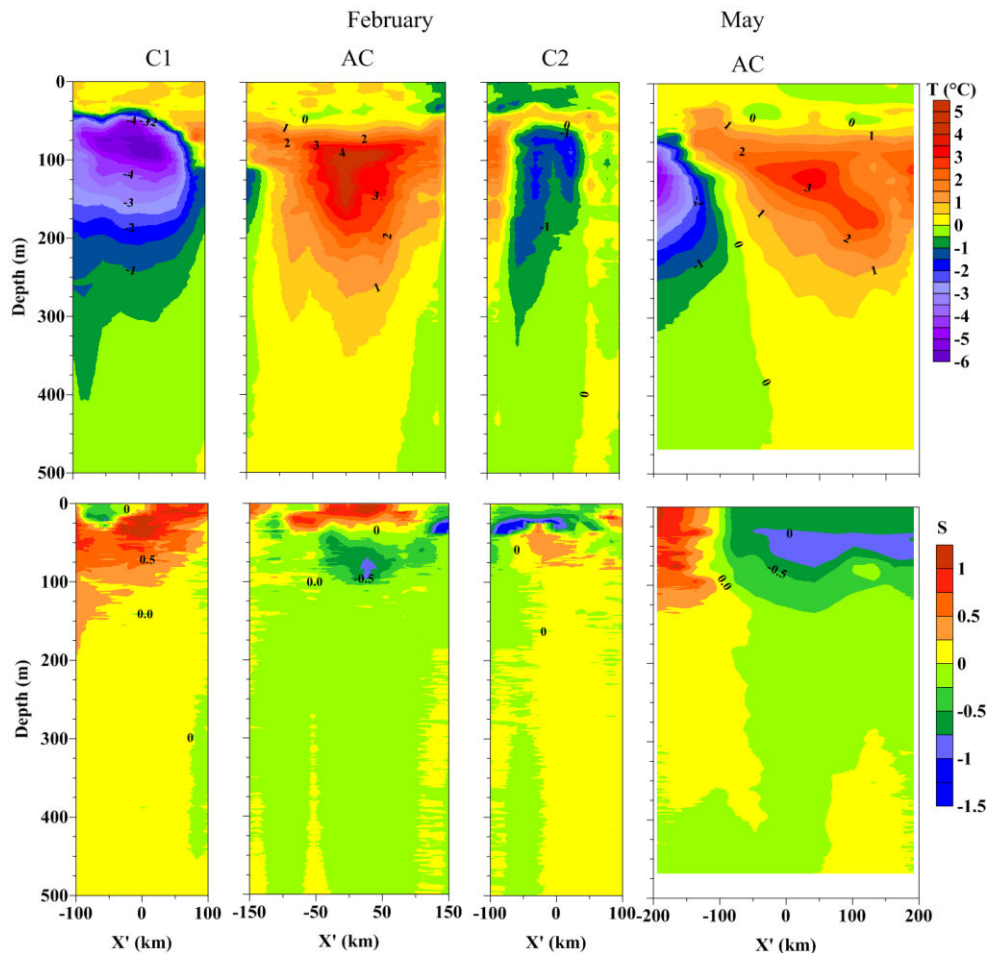
Fig. 5.6 Composite anomaly (relative to the horizontal mean along 17°N and 17.5°N from the first station up to the last station relative to the eddy center) of temperature (top panel) and salinity (bottom panel) for cyclonic and anti-cyclonic eddies during February 2016 and May 2015. Yellow to Red indicates positive values and Green to Violet indicates negative values.

5.5   Dynamics of saltwater pumping

In the BoB, except in the cases of thermal inversions observed during winter, the temperature decreases with depth, but the salinity always increases with depth. Therefore, any processes that lead to the uplift of subsurface water towards the surfaces increase the salinity in those regions and are a vital source for maintaining the overall saltwater budget in the BoB. Now the question to be answered is which are the mechanisms responsible for the pumping of saltier water into the surface mixed layer and thereby resulting in a salinity front? The mechanisms that lead to the pumping of saltier water from subsurface levels includes passage of cyclones, coastal and open ocean upwelling, presence of cyclonic/anti-cyclonic eddies and their interaction, lateral advection of saltier water from the AS into the southern BoB through the SMC etc. In the present case, the first cause can be ruled out as there was no atmospheric system formed during the observational period.

Near the coast, the upwelling is one process that causes uplift of subsurface waters towards the surface. The upwelling variability involves many factors such as wind stress, the sharp bathymetry along the east coast of India (Fig. 5.1), large-scale circulation and eddies. The upsloping of isolines towards the shore along 17°N and 17.5°N in the vertical sections of temperature and salinity in May (Fig. 5.2) clearly indicate coastal upwelling in the western BoB, confining to the nearshore zone up to ~30 km wide, i.e. to west of 83.5°E (Shetye et al. 1991; Chamarthi 1995; Rao 2002). The low sea level (Fig. 5.4) in this region centered at 17°N in May (-10 cm) also shows signatures of coastal upwelling in those regions. Here, the 29°C isotherm representing the top of the thermocline surface at 83.75°E from a depth of 35 m suggesting weak intensity of upwelling. As a result of upwelling, the coastal waters cool by 1.2°C (30°C to 28.8°C) and saltier by 0.3 units (33.75 to 34.05). Therefore, in the present case, the contribution of upwelling in increasing salinity in the western periphery of the BoB is around 0.3 units.

The vertical exchanges of subsurface waters between the surface layers and the interior of the ocean can be linked to processes occurring (i) at the interior of meso-scale eddies and (ii) at the interface between two strongly interacting meso-scale eddies. The first case considers the vertical exchange as purely a linear relationship which include eddy pumping concept whereas the second one deals with the vertical exchange produced by the eddy to eddy interaction. In the BoB, both these processes play a significant role in the vertical exchange of properties. Since the

77

observational track along 17°N cut across the cyclonic and anti-cyclonic eddies (Fig. 5.1), the changes in the temperature and salinity field due to these eddies were captured. To probe into the role of eddies in increasing the surface salinity of the BoB; they are compared with the vertical sections of temperature, salinity and density (Fig. 5.2).

The SLA presented in Fig. 5.4 indicates a cyclonic eddy, CCE in the western BoB centered at 83.5°E in February and in May with a slight southwards displacement. The observational track along 17°N cut across the core of CCE in February whereas in May the track lies on the northern arm of CCE. The lateral dimension of the CCE is less than 120 km in February and it exceeds 220 km in May. In the BoB, a cyclonic eddy is capable of pumping cold and saltier water from below to the surface in the vicinity of its center. Figure 5.2 shows that in February there is an overall increase in the surface salinity by 0.5 units from the periphery to the core of CCE (31.5 to 35.2) and the water that reaches the surface came from a depth of 10 m. This fresher water overlies subsurface saltier water (>32.5) thereby creating a strong vertical haline stratification below 5 m. In contrast, deep (~25 m) and warm (around 27.5°C) isothermal layer along with subsurface thermal inversions make the upper layers weakly stratified in temperature. As the strong uplift at the core of CCE triggers comparatively saltier but not colder water in the surrounding region, the signatures of temperature are not necessarily seen in the surface layers of the core of a cyclonic eddy. Thus the expected thermohaline changes in the surface layers within the cyclonic eddy can likely be biased toward a higher estimate. However, due to the divergence induced by the cyclonic eddy, there is an overall increase of salinity by 0.5 units in the upper 10 m of the western BoB.

Figure 5.5 indicates strong divergence at the transition zone between CCE and the offshore anti-cyclonic circulation, i.e. between 84.25°E and 84.5°E, (as indicated by negative values of ψ marked in green colour). Here, the 1020.5 kg/m^3 isopleths surfaces in February from a depth of 20 m thereby increasing the density by nearly 1 kg/m^3. In the surface layers of the northern bay, the progressive cooling till February is replaced by warming from March. Between February and May, the surface layers warm by 2.5°C and the salinity increases due to the reduction in the freshwater discharge resulting in an increase of 0.5 kg/m^3 in the surface density. Hence in May, surfacing of the 1021 kg/m^3 isopleths from a depth of 30 m is evident in the transition zone compared to the 1020.5 kg/m^3 in February. In other words, the vertical extent of

the frontal zone deepens from a depth of ~20 m in February to depths in excess of 30 m in May. Here also, because of the possible surface overprints of warm and subsurface saltier waters along with deep isothermal layer and strong surface stratification, the signature in temperature due to the strong uplift is not evident at the surface.

As a consequence of strong divergence saltier water lifts upward from its sub-surface domain towards the surface. Here, comparatively saltier water (32.75 in February and ~34 in May) sandwiched between low salinity waters are observed. Owing to the entrainment of sub-surface saltier water into the surface mixed layer and subsequent mixing with the existing fresher water, surface salinity increases by approximately 0.5 to 1.25 units (32.25 to nearly 32.75 in February and 33.5 to 34.05 in May) at the interface between these two opposing eddies (Fig. 5.2). The phenomena of saltwater pumping further results in strong thermal and salinity gradients between the nearshore region and the transition zone thereby forming a "salinity front" in this region. The vertical extent of the frontal zone deepens from a depth of ~20 m in February to depths in excess of 30 m in May. The region of saltwater uplift centered at 84.75°E in February shifts westward in May is centered at 84.25°E (westward shift of ~55 km) and also associated with an increase in the surface salinity by 1.25 units. Interestingly, from the core of saltwater uplift, there is rapid drop in salinity towards east as the fresh water (<31.5 in February and ~32.25 in May) caps the upper layers east of 85.25°E. Hareesh Kumar et al. (2013) also reported an offshore front in January, which appears to be the result of a meso-scale re-circulation around an eddy, bringing cold and freshwater from the northern BoB further away from the shore. The strong uplifting at the periphery between the cyclonic eddy and the anti-cyclonic eddy explains why comparatively high salinity in the surface layers of the upwelling areas compared to the surrounding regions are observed.

In February, the SLA (Fig. 5.4) shows a cyclonic eddy between 87° and 89°E centered at 16.5°N and an anti-cyclonic circulation pattern west of 89.5°E and south 17°N. In the transition zone (centered at 89.5°E) between these two opposing eddies, i.e. cyclonic eddy on the west and the anti-cyclonic eddy on its east, strong divergence is noticed (indicated by negative values of ψ in Fig. 5.5, marked in green colour). This leads to the uplift of subsurface saltier water towards the surface (Fig. 5.2), but their signatures are confined below 10 m depth. As a result of divergence in the transition

zone, the subsurface saltier water erupts upwards and the column becomes saltier (by ~0.5 units at 10 m and ~0.9 units at 40 m) leading to an overall increase in the density by~0.3 kg/m^3. Figure 5.2 shows that the water column is homogenous with fresh water (around 30.8) up to 10 m and with uniform temperature up to 75 m. This situation leads to the formation of a strong barrier layer around 10 m depth (Fig. 5.2), which might have prevented the subsurface saltier waters reaching the surface.

In nutshell, the analysis revealed that the possible mechanisms for the observed saltwater pumping in the BoB are coastal upwelling, open-ocean upwelling due to divergence induced by cyclonic eddy and eddy to eddy interaction, i.e. between a coastal cyclonic eddy and an offshore anti-cyclonic eddy. This aspect is further investigated using the Argo floats covering northern (Float nos. 2901336, 2901292), central (Float no. 6901558), southern BoB (Float nos. 2902365); data from RAMA buoy (15ºN, 90ºE), Field experiments like BOBMEX-99 (along 13ºN, 81º-87ºE) and World Ocean Circulation Experiment (WOCE). In addition, the data from Argo floats 2902114 and 290133 are also utilized to document the influence of cyclone on the saltwater pumping

5.5.1   Case study 1: Saltwater pumping in the northern Bay of Bengal

In the northern BoB, data from the Argo floats 2901336 and 2901292 are utilized to document the salt water pumping.

(a)   Meso-scale eddies (Argo floats 2901336, 2901292)

The Argo float 2901336 located at 17.25ºN, 88.6ºE in January drifted westward and reached 16.4ºN, 87.6ºE in October 2012 (Fig. 5.7a). The SLA along its track indicates substantial lowering (up to -30 cm) during the period March-May (Fig. 5.7c), which is found to be associated with a cyclonic eddy centered at 17ºN, 87ºE (Fig. 5.7b). This eddy is substantiated by the Okubo–Weiss parameter (Fig. 5.8e), negative divergence (Fig 5.8c), and positive vorticity (Fig 5.8d). Its influence on the thermohaline fields are presented (Figs. 5.7d, e) when the Argo float is located in the vicinity of the core of this cyclonic eddy during March-April. The figure shows that the prevailing low salinity water (< 33) in the upper 50 m is replaced by water having salinity in excess of ~34 by end March, resulting in an increase of 1 unit in the surface salinity. The water surfaces from a depth of 90 m and continue to exist till mid June. The uplifting of saltier water from the subsurface depths leads to a salinity front resulting lateral salinity gradient. But, there is no visible evidence of a thermal front in

Figure 5.7a. However, at subsurface depth levels i.e. below 30 m, upward lifting of isotherms are noticed.
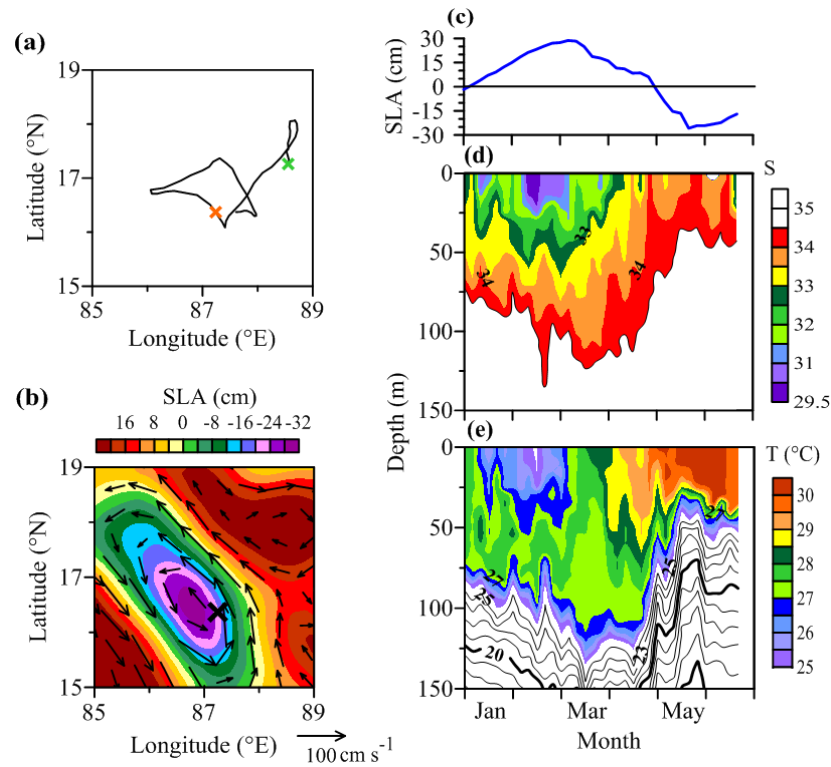
Fig. 5.7 (a) Track of Argo float 2901336 (black line) in the northern BoB during January-October 2012. Green cross: Initial float position, Orange cross: Region of saltwater pumping, (b) Sea level anomaly (SLA) overlaid with geostrophic current on 15 May 2012; black cross: float position, (c) SLA along the track of Argo float, vertical section of (d) salinity and (e) temperature.

Fig. 5.8 (a) Divergence (ψ), (b) vorticity (ω) and (c) Okubo-Weiss parameter (W) on 15 May 2012. Positive values: yellow to red, negative values: blue to yellow. Black cross represent position of float on this day.

The surface waters undergo warming during March-May and its effect are visible upto a depth of 30 m. The upper layer stratification due to the accumulation of heat may have opposing effect on the uplifting of subsurface waters towards the surface. Another possibility is that the marginal reduction in temperature due to uplift

might have been offset due to the significant warming occur during this period. The figure (Fig. 5.7d, e) further indicates that the period of uplift is associated with the divergence induced by a cyclonic eddy that is centered at 17°N, 87°E (Fig. 5.7b). Therefore, it is concluded that the pumping of saltier water towards the surface is due to the divergence induced by the cyclonic eddy.
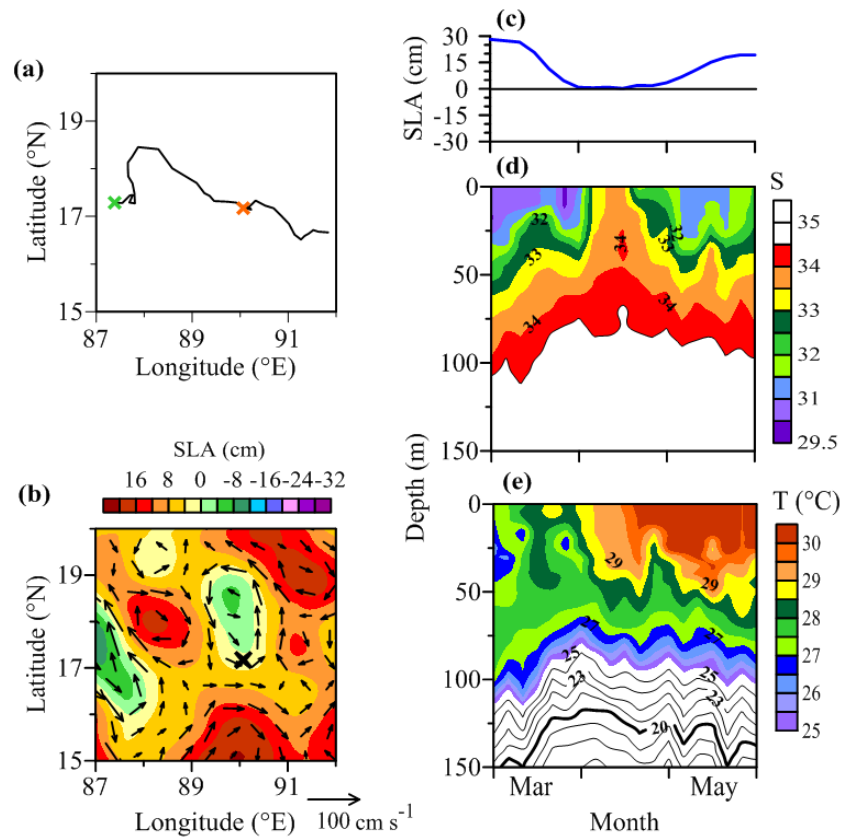
Fig. 5.9 (a) Track of Argo Float 2901292 (black line) in the northern BoB during January-May 2012. Green cross: Initial float position, Orange cross: Region of saltwater pumping, (b) sea level anomaly (SLA) overlaid with geostrophic current for the period 23 April 2012; black cross: float position, (c) SLA along the track of Argo float, vertical section of (d) salinity and (e) temperature.

Similarly, the Argo float 2901292 after its initial northward displacement, drifted southeastward during March to May 2012 (Fig. 5.9a). In April, as the float entered the vicinity of a cyclonic eddy centered at 18°N, 90°E (Fig. 5.9b), SLA dropped by nearly 30 cm along the track (Fig. 5.9c). This cyclonic eddy is corroborated by negative values of Okubo-Weiss parameter (Fig. 5.10c) and positive vorticity (Fig. 5.10b). At the same time, salinity (Fig. 5.9d) increases by ~2 units up to a depth of 50 m (>33.5) compared to its surrounding. The zone of saltier water is found sandwiched between fresher waters (<31.5), thereby creating a salinity front with lateral variation in excess of 2.5 units. Figure 5.10a show that the increase in

salinity is closely related to divergence induced by the cyclonic eddy. In temperature (Fig. 5.9e) the eddy effect is perceptible below 15 m only, while the signal at the surface might have been masked by the opposing effect of stratification due to pre-monsoon warming.
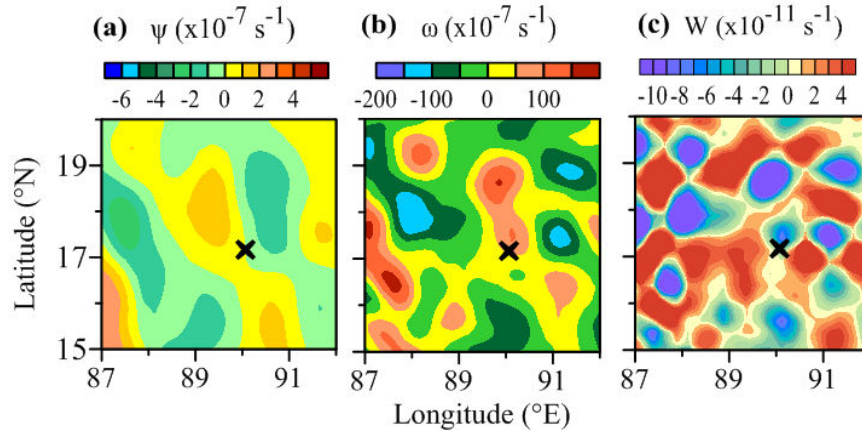
Fig. 5.10 (a) Divergence (ψ), (b) vorticity (ω) and (c) Okubo-Weiss parameter (W) on 23 April 2012. Positive values: yellow to red, negative values: blue to yellow. Black cross represent position of float on this day.

5.5.2 Case study 2: Saltwater pumping in the central Bay of Bengal

In the central BoB, the data collected along 11°N between 81°-90°E during 11-15 July 1993 is utilized to document the influence of coastal upwelling on the saltwater pumping. Data from the Argo float 6901558, RAMA buoy (15ºN, 90ºE) and BOBMEX-99 (along 13°N, 81°-87°E) are utilized to document the observed change in salinity due to meso-scale eddies. Further, data from the Argo float 2902114 is utilized to explain the saltwater pumping due to the cyclone Hudhud.

(i) Coastal upwelling

The data collected onboard Sagar Kanya along 11°N, 81-82°E during 11-15 July 1993 (www.nodc.noaa.gov) shows upsloping of isolines in the upper 60 m towards the east coast of India signifying the coastal upwelling (Fig. 5.11b, c). Sil and Chakraborty (2016) also reported upwelling in the western BoB during May-September. Here, the wind stress curl (Fig. 4.4) shows positive values which are conducive for the occurrence of coastal upwelling through Ekman divergence. The water that upwells and reaches the surface comes from a depth of ~50 m and having the characteristics of SBBW. As mentioned in Chapter 4 (Fig. 4.7), during summer monsoon, SBBW (Fig. 5.11d) occupies the upper 50 m in the western coastal regions of BoB. This also corroborates with the observation by Anoopa and Hareesh Kumar

(2015). As a result of the uplifting, cooler and saltier subsurface water are brought towards the surface thereby cooling the surface layers (upper 75 m) by 0.5°C (28.5°C to 28°C) and saltening by 0.5 (33.5 to 34). This analysis suggests that the upward movement of subsurface SBBW towards the surface due to the prevailing coastal upwelling is responsible for the increase in surface salinity by 0.5 units.
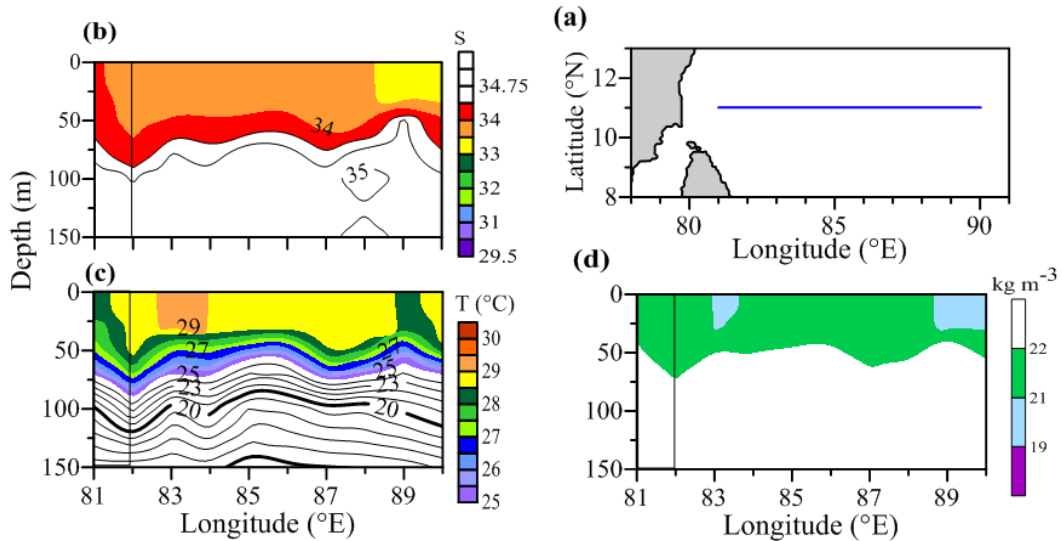
Fig. 5.11 (a) Track along 11°N from 81° to 90°E during 11-15 July 1993, vertical section of (b) salinity, (c) temperature and (d) sigma-t. Vertical bar: upwelling zone.

(ii)   Meso-scale eddies (from Argo float 6901558)

In the central BoB, a cyclonic circulation is observed at 15°N, 88.5°E during November-December 2015 (SLA for November is presented in Fig. 5.12b). The Argo float 6901558 (Fig. 5.12a) drifted westward from its initial position in the eastern Bay and cut across the cyclonic eddy in November.

The SLA corresponding to the track of Argo float changes its sign from positive to negative in November (Fig. 5.12c) and reaches its minimum (-5 cm) by mid November. During this period, the float is located within the vicinity of the core of the cyclonic eddy (Fig. 5.12b), where the circulation is cyclonic and normally upwelling occurs. However, the doming of isolines is more visible in the temperature and salinity fields below 50 m depth. Negative values of W surrounded by positive values, negative divergence, and positive vorticity (Fig. 5.13a-c) confirm the occurrence of cyclonic eddy during this period. Corresponding to the SLA minimum, the vertical sections of salinity (Fig. 5.12d) indicates increase in the surface salinity. In the vertical, the salinity increase is noticed up to a depth of around 50m. The uplift of saltier water from a depth of 50 m creates a salinity front during this period. The

uplift of saltier subsurface water towards the surface centered at 15.2°N, 88.6°E increases the surface salinity by ~0.5 units (32.5 to ~33.3) and cools the surface layers by 0.5°C (Fig. 5.12e).
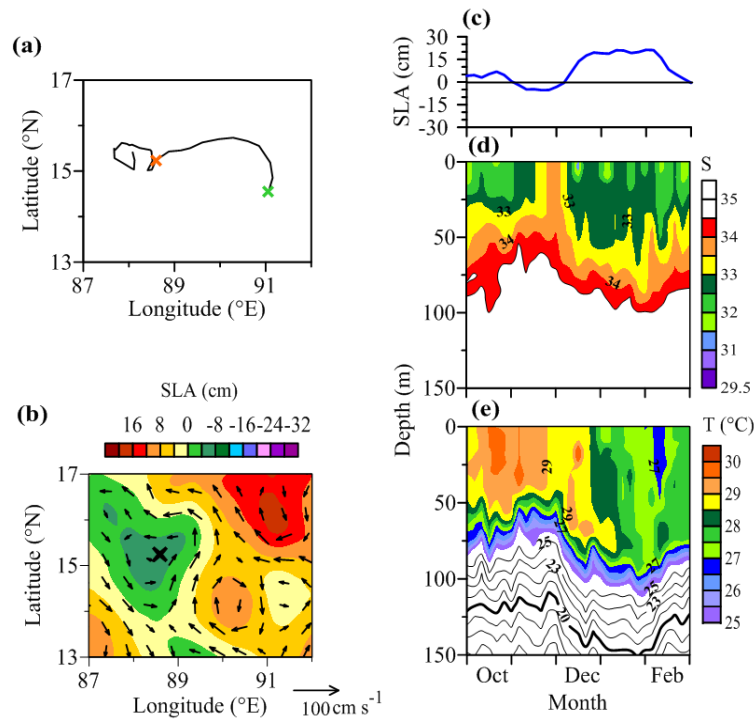
Fig. 5.12 (a) Track of Argo float 6901558 (black line) in the central BoB during October 2015 to February 2016. Green cross: Initial float position, Orange cross: Region of saltwater pumping, (b) SLA overlaid with geostrophic current for the period 28 November 2015; black cross: float position, (d) SLA along the track of Argo float, vertical section of (d) salinity and (e) temperature.
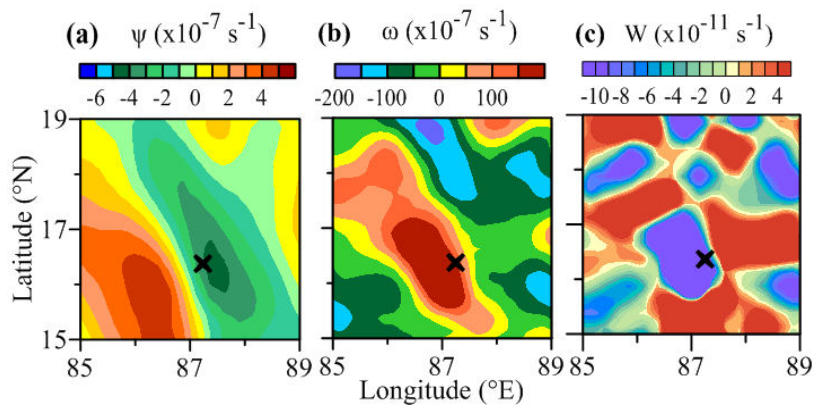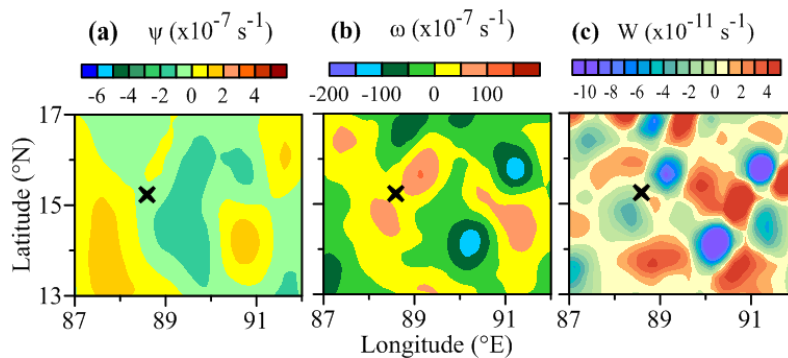

Fig. 5.13 (a) Divergence (ψ), (b) vorticity (ω) and (c) Okubo-Weiss parameter (W) on 28 November 2015. Positive values: yellow to red, negative values: blue to yellow. Black cross represent float position on this day.

(iii) **Meso-scale eddies** (from RAMA buoy)

RAMA is a network of buoys deployed in the BoB to obtain long time series measurements of atmospheric and oceanic parameters. The data from one of the RAMA buoy network, located at 15ºN, 90ºE over a period of seven months, i.e.

December 2014 to July 2014 is utilized to probe into the uplift of saltier waters in the central BoB. In general, surface salinity is less than 33 in the region (Fig. 5.14).
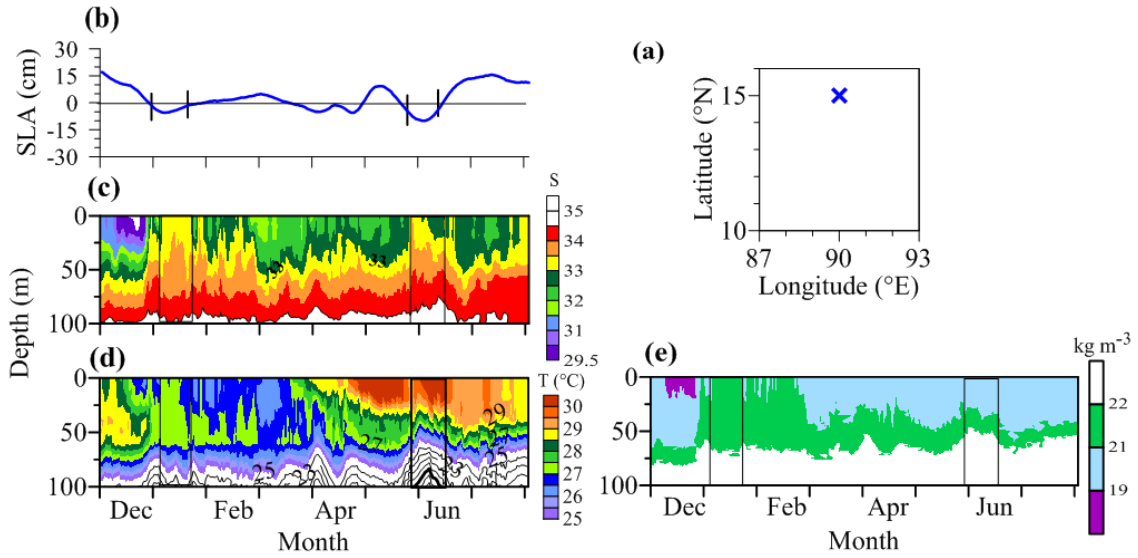
Fig. 5.14 (a) RAMA buoy location (15°N, 90°E, Blue cross) (b) sea level anomaly at buoy location, vertical sections of (c) salinity, (d) temperature and (e) sigma-t during December 2013 to July 2014. The duration of uplift is indicated between vertical bars.
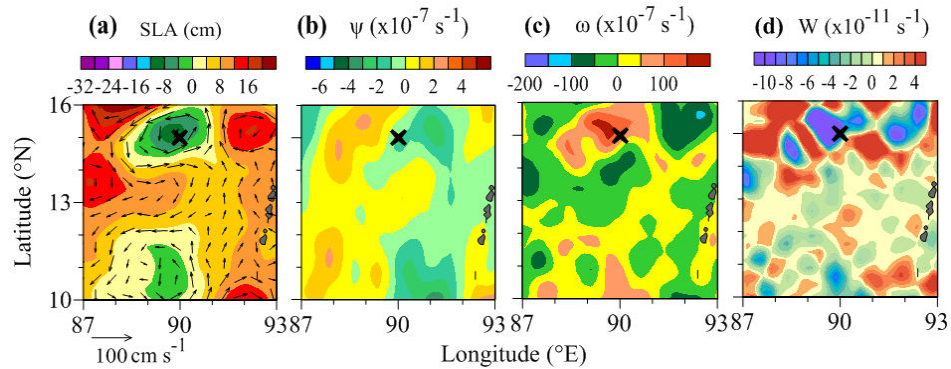
Fig. 5.15 (a) SLA overlaid with geostrophic current, (b) divergence (ψ), (c) vorticity (ω) and (d) Okubo-Weiss parameter (W) on 6 June 2014. Positive values: yellow to red, negative values: blue to yellow. Black cross represent RAMA buoy location.

One conspicuous observation in the figure is the two events of saltwater pumping, one in January and another in June of which the first event lasted longer. The saltier water is found to surface from a depth of around 40 m. From the figure, it can be seen that the existing water become more salty (by 1.25 units, i.e. 32 to 33.25) and cooler (1.5°C, i.e. 28.5° to 27°C) due to the uplift, as the BoB is characterized by increase in salinity with depth. During rest of the period, salinity is less than 33 in the surface layers. From the sigma-t it is found that the existing TW (sigma-t: 19-21) is replaced by SBBW (sigma-t: 21-22) (Fig. 5.14e). Figure 5.14c indicates that the SLA changes its sign positive to negative and drop by more than 15 cm during both the events. The Figure 5.15a indicates a cyclonic circulation in the vicinity of the float on

6 June (marked as black cross). The negative divergence, positive vorticity and Okubo-Weiss parameter substantiate the presence of cyclonic eddy in June at this location (Figs. 5.15 a-c). Therefore, the uplift of the subsurface waters towards the surface observed in this region can be attributed to divergence at the core of this cyclonic eddy.

(iv)   Meso-scale eddies (BOBMEX-99)

In the BoB, the cooling of the water column and increase in the salinity are possible when there is divergence at subsurface levels. The regions of the doming of isotherms coincide with the drop in SLA (Fig. 5.16.a) and also a cyclonic circulation in its vicinity. Hareesh Kumar et al. (2013) also reported strong eddy activity in this region during the summer monsoon of 1999. The negative divergence, positive vorticity and Okubo-Weiss parameter substantiate the presence of cyclonic eddy resulting in divergence at this location (Figs. 5.16 a-d). Therefore, the 0.5 unit increase in salinity in the surface layer results from the divergence in presence of a cyclonic circulation (Fig. 5.17d).
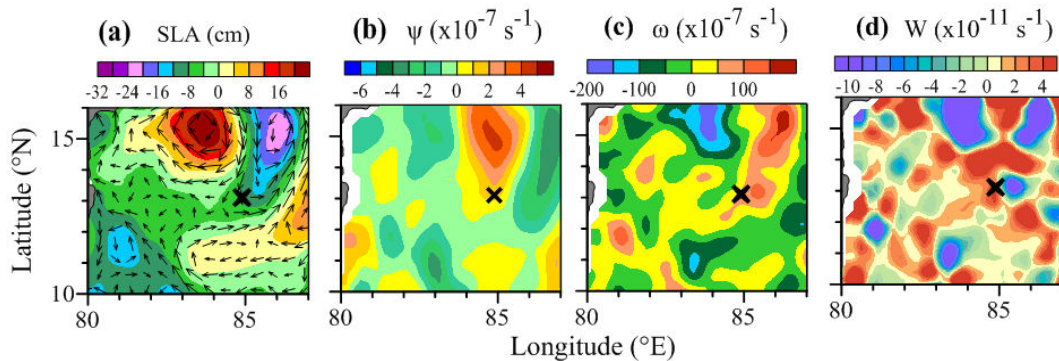
Fig. 5.16 (a) Sea level anomaly (SLA) overlaid with geostrophic current, (b) divergence (ψ), (c) vorticity (ω), and (d) Okubo-Weiss parameter (W) on 29 July1999. Positive values: yellow to red, negative values: blue to yellow. Black cross represent station location.

The impact of cyclonic eddy (Fig. 5.17c, d) on thermohaline field is further examined utilizing the data collected along 13°N transect during the BOBMEX-99 experimental program. In the BoB, during the monsoon season, temperature decreases and salinity increases with depth. The figure (Fig. 5.17c, d) shows doming of isopleths between 84° and 85ºE causing uplifting of saltier and cold water from a depth of around 60 m. Consequently, the surface layers cools 0.5°C (>28.75°C to 27.75°C) and surface salinity increases by 0.5 units. Hareesh Kumar et al. (2013) attributed the cooling of the water column in the western BoB to the southward elongation of a cyclonic eddy formed due to the baroclinic instability caused by the

two opposing currents along the coastal periphery of the western BoB along with the wind stress curl. The uplifting also leads to the formation of a salinity front with saltier water sandwiched between comparatively warm and low salinity (<34.25) water on either side.
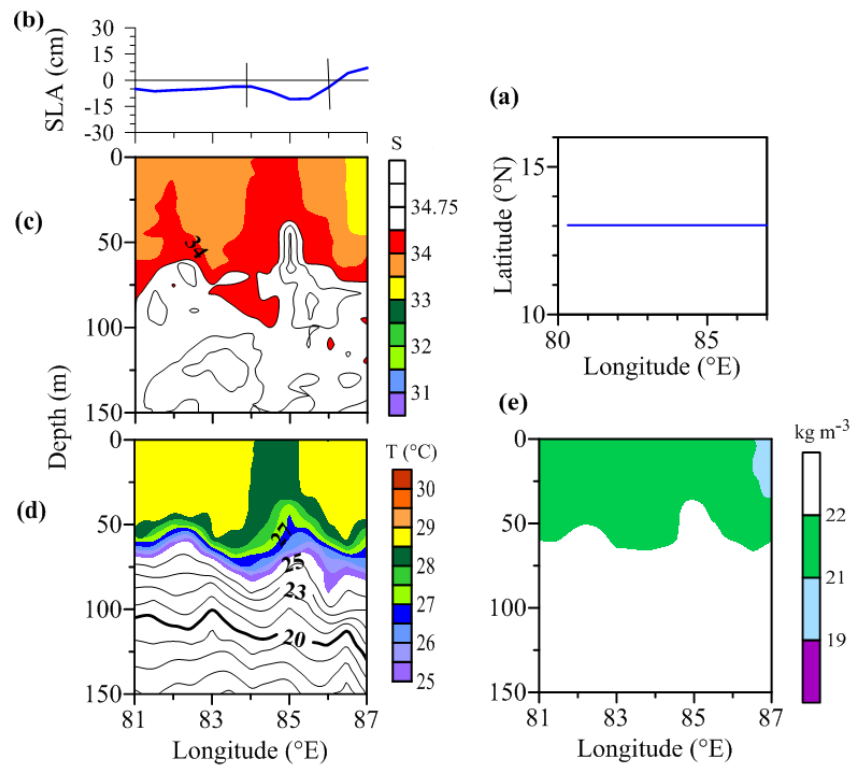
Fig. 5.17 (a) BOBMEX track (Blue line) along 13°N,81-87°E during 28-30 July 1999, (b) sea level anomaly, vertical section of (c) salinity, (d) temperature and (e) sigma-t.

(v)   Meso-scale eddy and Tropical cyclone (Argo float 2902114)

Over the Andaman Sea, a low pressure system was formed on 7th October 2014. Later this low pressure was upgraded as "very severe cyclonic storm" on 10th October, when it was centered near 15ºN and 86.8ºE around 470 km east-southeast of Visakhapatnam (Fig. 5.18a). This cyclone was termed as Hudhud, (means Hoopoe bird in Arabic). Thereafter the system moved in a north-westward direction. The availability of Argo float 2902114 in the vicinity of Hudhud track helps to understand its impact on the thermohaline variability. The passage of the cyclone is denoted by a drop of -15 cm in the sea level (Fig. 5.18c). Figures 5.18b, c also shows cyclonic circulation in the vicinity of the Hudhud and its gradual evolution as it moves. The vertical sections (Figs. 5.18d, e) corresponding to the period of this cyclone is associated with cooling and saltening of the surface layers.
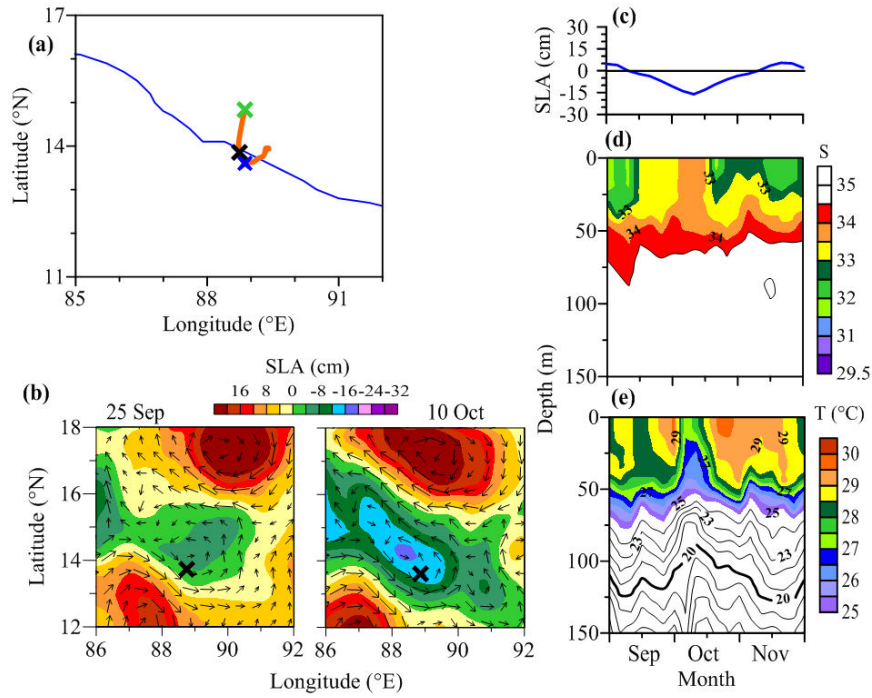
Fig. 5.18 (a) Track of Argo float 2902114 (Orange line) during September to November 2014 and cyclone Hudhud (Blue line) formed in the BoB during October 2014; Green cross: Initial float position, Black and blue cross: Regions of saltwater pumping, (b) Sea level anomaly (SLA) overlaid with geostrophic current on 30 September and 10 October 2014; black cross: float position, (c) SLA along the track of Argo float, vertical section of (d) salinity and (e) temperature.
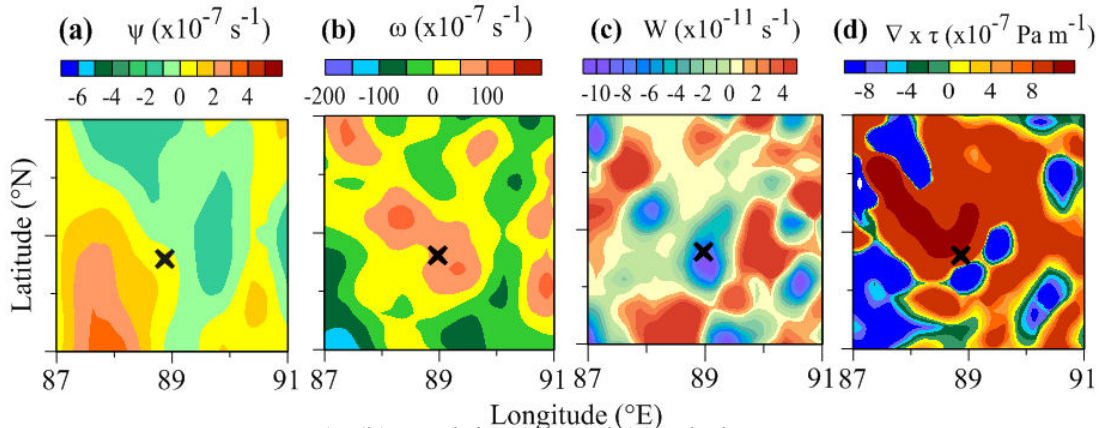
Fig. 5.19 (a) Divergence (ψ), (b) vorticity (ω) and (c) Okubo-Weiss parameter (W) for the uplift on 10 October 2014 and (d) Wind stress curl ($\nabla \times \tau$). Positive values: yellow to red, negative values: blue to yellow. Black cross represent float position on this day.

The estimated geostrophic currents shows a cyclonic circulation in September 2014 in the central BoB centered at 14°N, 89°E, and associated with a SLA lowering by -10 cm (Fig. 5.18b, c). The vertical sections of temperature and salinity show cooling of the surface waters by more than 2°C and increase in salinity by more than 0.5 units as water from a depth of 40 m reach the surface when Hudhud was at its

maximum intensity. This leads to the formation of a thermohaline front in this region. The cyclone Hudhud not only caused the saltwater pumping in the upper 40 m but significant cooling in the water column and a thermohaline front.

5.5.3 Case study 3: Saltwater pumping in the southern Bay of Bengal

In the southern BoB, data from Argo float 2902365 and WOCE in 1995 are utilized to document the observed increase in salinity due to meso-scale eddies. The Argo float 2901331 is utilized to document the change in salinity due to cyclone Viyaru.

(i) Meso-scale eddies (Argo float 2902365)

The tracks of Argo float 2902365 (Fig. 5.20a) covers the southern BoB (around 7°N) during May to September 2013. During its traverse, it encountered a cyclonic eddy centered at 8°N, 85°E in June and an anti-cyclonic eddy at 6.5°N, 86.5°E in August. The most striking observation is that, under the influence of these opposing cyclonic and anti-cyclonic eddies, presence of saltwater is noticed in the upper layers; but the mechanisms are found to be different.
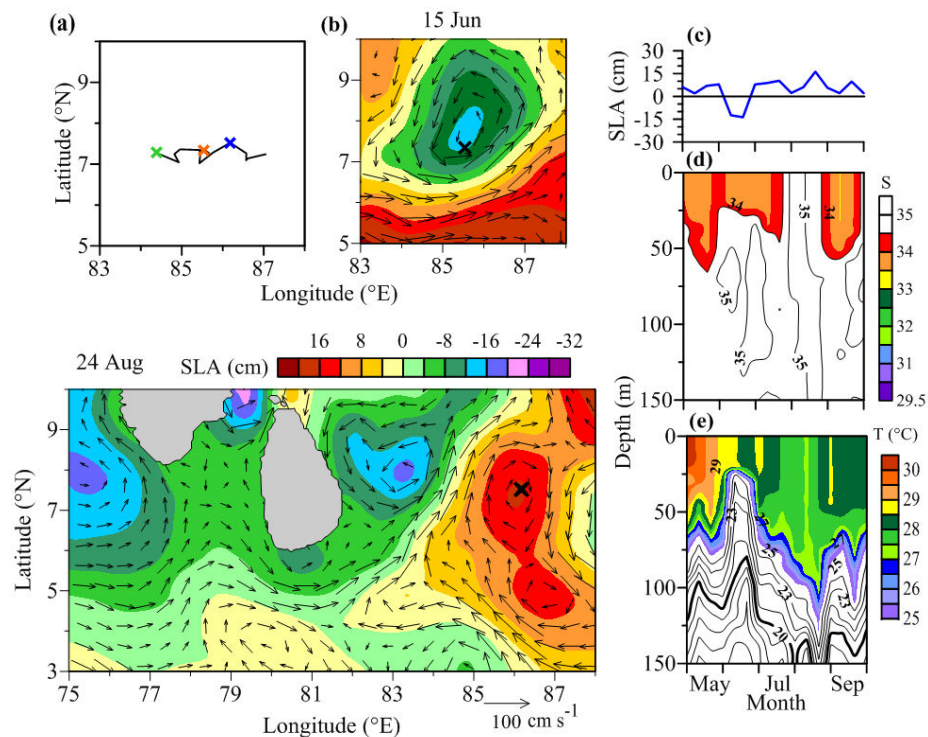
Fig. 5.20 (a) Track of Argo float 2902365 (black line) in the southern BoB during May-September 2013. Green cross: Initial float position, Blue and Orange cross: Regions of saltwater pumping, (b) sea level anomaly (SLA) overlaid with geostrophic current on 15 June and 24 August 2013; black cross: float position, (d) SLA along the track of Argo float, vertical section of (d) salinity and (e) temperature.

As discussed in the previous sections, the presence of cyclonic eddy in June (Fig. 5.20b) uplift comparatively saltier water from subsurface levels towards the surface, thereby increasing the salinity in the upper 50 m water column by 0.5 units (Fig. 5.20d). On the other hand, in presence of an anti-cyclonic eddy, the upper 150 m water column becomes homogenous in salinity (around 35). However, in the temperature field, the homogeneous condition is noticed only up to 100 m. The estimated geostrophic currents show the pathway of saltier water from the AS into the BoB (Fig. 5.20b). Vinayachandran et al. (2013) also reported the same. Moreover, the subsurface layer of the BoB is having salinity of the order of ~35. In the present case, the advection of saltier water (~35) from the AS in presence of the convergence induced by the anti-cyclonic eddy might have distributed the saltier water to deeper depths where already comparatively saltier water exists. Probably this may be the reason for the deeper isohaline layer compared to the isothermal layer. The role of lateral advection from the Arabian Sea as observed in the southern BoB is totally different compared to the saltening in the central and northern part of the BoB.
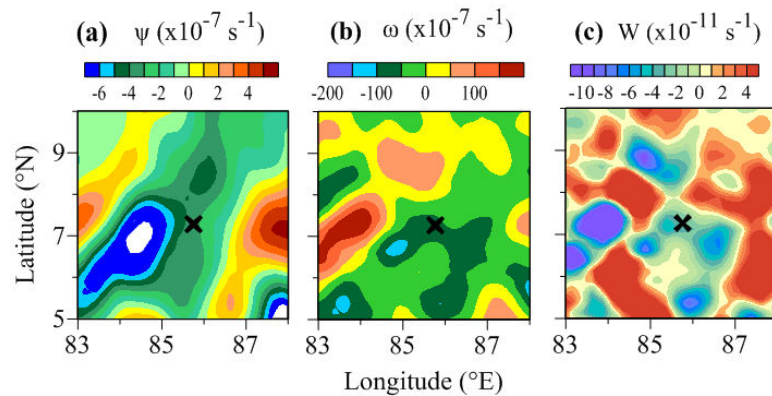
Fig. 5.21 (a) Divergence (ψ), (b) vorticity (ω) and (c) Okubo-Weiss parameter (W) for the uplift on 15 June 2015. Positive values: yellow to red, negative values: blue to yellow. Black cross represent float position on this day.

(ii)   Meso-scale eddies (WOCE)

As observed in the Argo float, the temperature and salinity section shows doming of isopleths along the WOCE track during February 1995 (Fig. 5.22a, b). Here also the upsloping is attributed to cyclonic eddy and lowering of SLA (-20 cm) in Fig. 5.22b is apparent along the track. The location being south of 10°N makes the water saline (~33.75) and is upwelled from a depth of 50 m. The divergence (Fig. 5.23b) associated with the cyclonic eddy further increases salinity by 0.5 units (Fig. 5.22c). Fig. 5.22d show drop in temperature by 0.5°C (from 29° to 28.5°C) at the surface and is further lowered near the centre of the eddy (28°C). The sigma-t section

(21-22 kg/m^3) also reflects the presence of SBBW in the upper 60 m (Fig 5.22e) and agrees well with the watermass distribution discussed in Chapter 4 (Fig. 4.7). In addition, Anoopa and Hareesh Kumar (2015) observed maximum spatial extent of SBBW at the surface during December-February. The presence of cyclonic eddy centered at 6.3°N, 90.3°E leading to modification in thermohaline structure is evident from Figures 5.23 a-d.
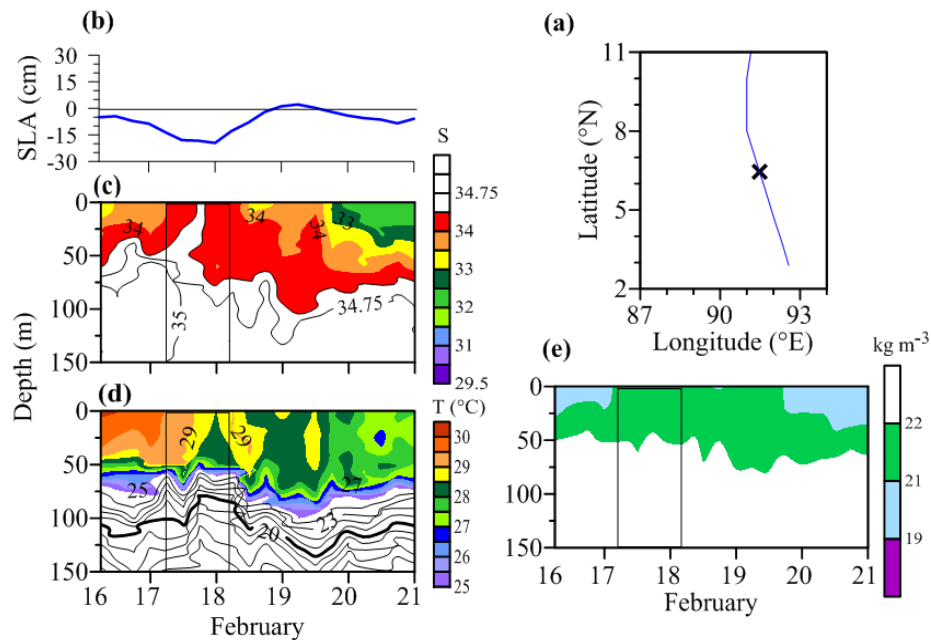
Fig. 5.22 (a) WOCE track (Blue line) during 16-21 February 1995 (Black cross: region of uplift), (b) sea level anomaly, vertical sections of (c) salinity, (d) temperature and (e) sigma-t along the WOCE track. The duration of uplift is indicated between vertical bars.
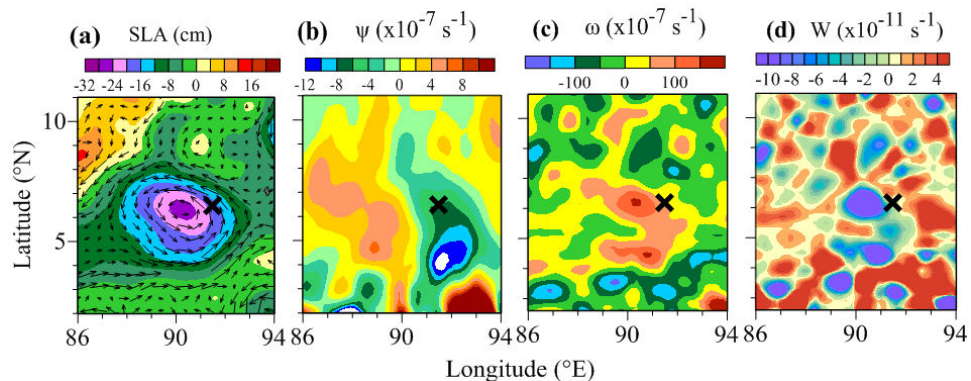
Fig. 5.23 (a) Sea level anomaly (SLA) overlaid with geostrophic current, (b) divergence (ψ), (c) vorticity (ω) and (d) Okubo-Weiss parameter (W) for the uplift on 18 February 1995. Positive values: yellow to red, negative values: blue to yellow. Black cross represent position of float on this day.

(iii)   Tropical cyclone (Argo float 2901331)

Cyclone Viyaru, formerly known as Mahasen, was a relatively weak tropical cyclone (Fig. 5.24a). It originated from an area of low pressure over the southern BoB

in early May 2013, slowly consolidated into a depression on 10th May. The Argo float 2901331 located at 9.5°N, 88.2°E in the vicinity of the cyclone track helped to understand the impact of Viyaru on the thermohaline variability. The SLA along the float lower by 3.7 cm associated with the passage of cyclone (Fig. 5.24c). Fig. 5.24b corroborates cyclonic circulation on 15 May 2013. Moreover, negative divergence, positive vorticity and negative values of W enclosed by positive values indicate cyclonic circulation (Fig 5.25 a-c).
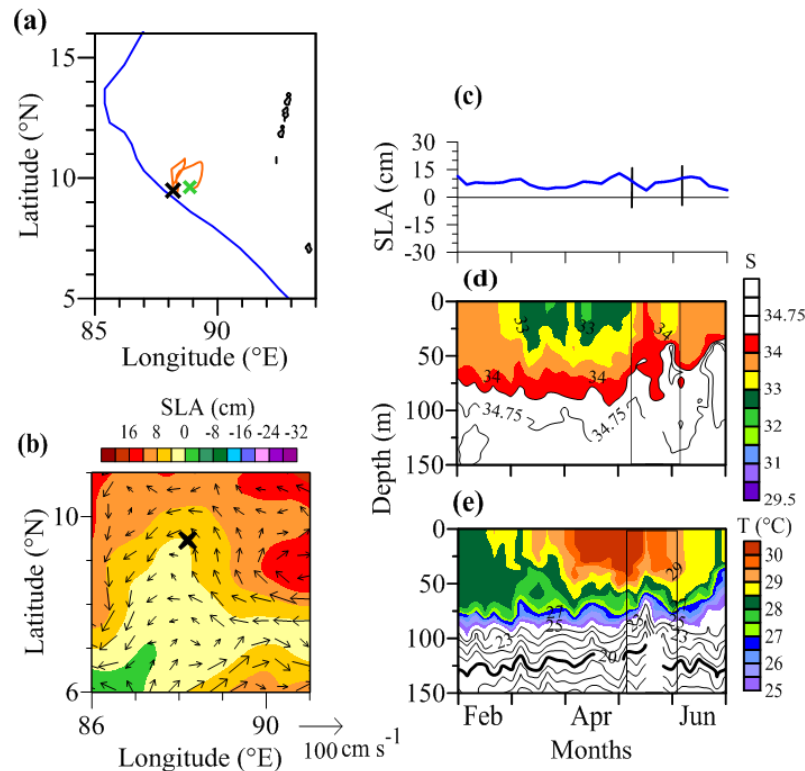
Fig.5.24 (a) Track of Argo float 2901331 (Orange line) during February-June 2013 and cyclone Viyaru (Blue line) formed in the BoB in May 2013, Green cross: Initial float position, Black cross: Regions of saltwater pumping, (b) Sea level anomaly (SLA) overlaid with geostrophic current on 15 May 2013, black cross: float position (c) SLA along the track of Argo float, vertical section of (d) salinity and (e) temperature. The duration of uplift is indicated between vertical bars

The vertical sections (Fig. 5.24 d, e) show increase in salinity by 0.75 and marginal drop in surface temperature when cyclone was at its maximum intensity. In this case the, the cyclone causes only the saltwater pumping in the upper 50 m without significant cooling in the water column leading to the formation of a haline front. The water uplifts from a depth of 60-75 m. In this case the, the cyclone causes only the saltwater pumping in the upper 50 m without significant cooling in the water column leading to the formation of a haline front. This could be possibly due to comparatively weaker strength of cyclone and the presence of deep isothermal depth upto 50 m.
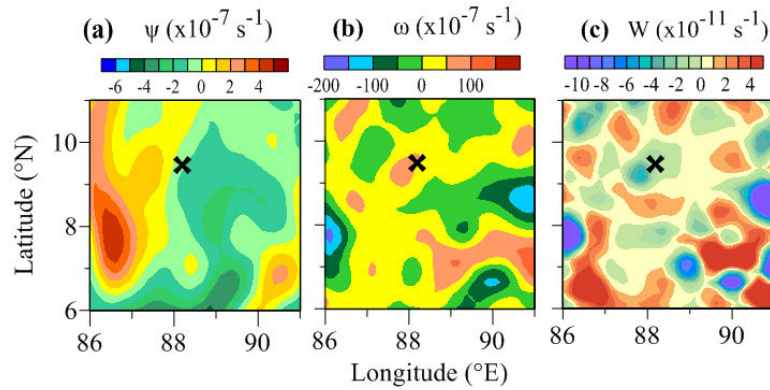
Fig. 5.25 (a) Divergence (ψ), (b) vorticity (ω) and (c) Okubo-Weiss parameter (W) for the uplift on 15 May 2013. Positive values: yellow to red, negative values: blue to yellow. Black cross represent position of float on this day.

In this chapter, the saltwater pumping in the BoB and various causative mechanisms are described. Primarily, saltwater pumping varies spatially and temporally. In the western boundary of the BoB, the prevailing southwesterly wind during summer monsoon causes coastal upwelling, which result in the uplifting of subsurface cooler and saltier waters towards the surface. However in the open ocean, saltwater pumping occurs owing to the presence of cyclonic eddy as water diverges at its centre. In addition, eddy to eddy interaction also leads to divergence and subsequent salt water pumping. The analysis indicated that the uplift of saltier water from subsurface levels increases the salinity in the surface layers thereby creating a salinity gradient, which varies from north to south. During the monsoon season, the advection of saltier water from the Arabian Sea also leads to an increase in the salinity in the surface layers. The formation of tropical cyclone during pre- or post-monsoon season also increases salinity in the surface layers of the BoB.

Chapter 6

Response of salinity variability in the
Bay of Bengal to major climatic events

6.1 Introduction

In the tropical Indian Ocean, researchers documented the seasonal cycle of sea surface salinity (SSS) based on climatology (Conkright et al., 2001) and insitu data collected along ships of opportunity (Donguy and Meyers, 1996; Rao and Sivakumar, 2003; Murty et al., 2004; Delcroix et al., 2005). The seasonal cycle in salinity is associated with the monsoonal rainfall, river runoff and upper ocean circulation (Benshila et al., 2014; Akhil et al., 2014). Also, salinity exhibits substantial inter-annual variations due to the occurrence of various climatic events. However, studies are extremely sparse linking salinity variability in the BoB and climatic events. This is probably due to the lack of sufficient ground truth observations.

Researchers have shown that the El Niño Southern Oscillation (ENSO) (Tziperman et al., 1998; Rao and Sivakumar, 2003) and the Indian Ocean Dipole (IOD) (Saji et al., 1999) influence the SSS variability on inter-annual timescales (Thompson et al., 2006; Grunseich et al., 2011; Chaitanya et al., 2015; Pant et al., 2015). Utilizing the ocean numerical models, Thompson et al. (2006) showed that the surface circulation is anomalously anti-cyclonic during a pIOD and affects the freshwater transport between the equatorial Indian Ocean and BoB in the absence of ENSO events. This anomalous circulation pattern cause freshwater anomalies in the eastern bay (Thompson et al., 2006; Jensen 2007). Conversely, during a nIOD event, the BoB circulation is anomalously cyclonic (Thompson et al., 2006) and induces salinity anomalies in the eastern bay. Jensen (2007) examined the watermass exchanges between the Arabian Sea and BoB during El Niño, La Niña, and IOD events using a numerical model and concluded that transport from the Arabian Sea (BoB) to BoB (Arabian Sea) is enhanced (decreased) during El Niño and IOD years. Vinayachandran and Nanjundiah (2009) studied the seasonal and inter-annual salinity variability in the Indian Ocean using coupled model. After considering IOD, non-IOD and El Niño years, large inter-annual SSS anomalies exist in the Indian Ocean only during IOD years. Pant et al., 2015, also corroborate that pIOD is the chief climatic event causing inter-annual variability of salinity. In addition their study shows that southward EICC weakens or absent during October-December of pIOD years. However, the outcome of these events occurring independently, combined and the quantification of salinity variability has not been addressed. In the present chapter, an attempt has been made to quantify the salinity variability in the BoB due to climatic

96

events like Indian Ocean Dipole (IOD), El Niño / La Niña and different regimes of summer monsoon, viz. normal, dry and wet monsoon years.

6.2 Inter-annual variability of salinity

To decipher the inter-annual variability of salinity in the BoB, six locations representing northern, central and southern BoB are considered (Fig. 6.1). For each location, time series of salinity data for a period of 61 years from 1950 to 2010 is extracted from the monthly database (732 values). The anomaly is computed as the difference between individual salinity values and climatic mean at each point. Wavelet transformation based on Morlet wavelet is utilized to understand and decompose the prominent harmonics embedded in the salinity.
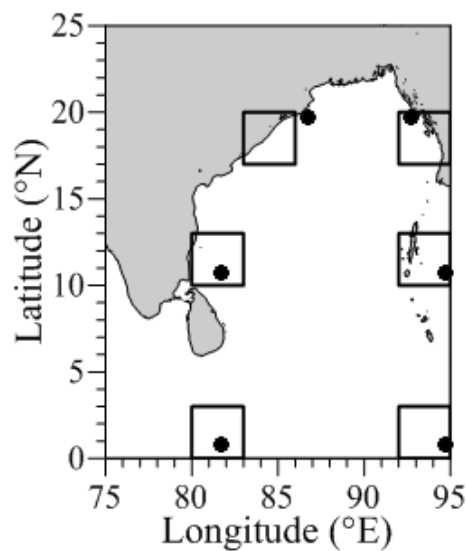
Fig. 6.1 Black dots represent stations at which inter-annual variability is analyzed. Regions in the BoB (boxes) where salinity in the western and eastern bay are considered for computing salinity difference.

In the northwestern BoB (19°N, 86°E), the monthly salinity anomaly (Fig. 6.2a) shows a variation similar to that of the basin averaged distribution (Fig. 3.7). The wavelet analysis of monthly time series of salinity indicate the dominance of annual harmonics, which is found significant at 95% confidence level and lies well within the cone of influence (Fig. 6.3a). The maximum salinity is observed in May/June and minimum in October throughout the 61 years. The figure shows that the magnitude of negative anomaly is higher (< 5 units) than positive anomaly (within 4 units). 62.5% (1951, 1963, 1982, 1998 and 1997, i.e., 5 out of 8 events as in Table 2.2) of the extreme low salinity events occur during combined pIOD and El Niño and 66.6% (1964, 1975, 1982, 1998 and 2010, 4 out of 6 events as in Table 2.2) is during

co-occurred nIOD and La Niña. Intense freshening is observed in October/November from 1994 to 2001 during the study period.
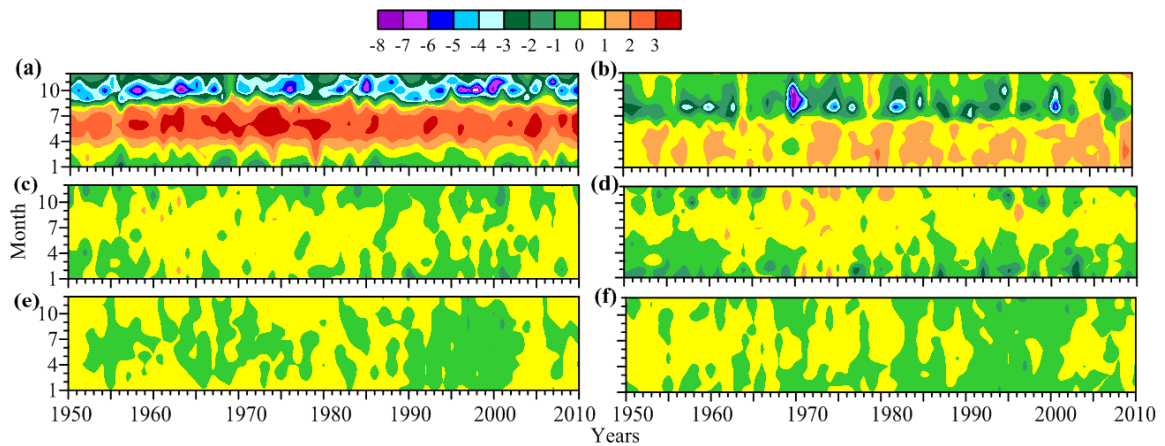
Fig. 6.2 (a) Monthly time series of salinity anomaly at (a) 19°N, 86°E, (b) 19°N, 92°E, (c) 10°N, 81°E, (d) 10°N, 94°E, (e) 0°, 81°E and (f) 0°N, 94°E.

In the northeastern BoB (19°N, 92°E), positive anomaly is within 2 units however, magnitude of negative anomaly is higher (Fig. 6.2b); the pattern being similar that in the eastern BoB. The main difference between northwestern and northeastern bay is in the phase of seasonal saltening and freshening. The positive anomaly (January-June) is observed in the first half of the annual cycle follows negative anomaly. Here, minimum salinity occurs in July/August and maximum in March-May. At 19°N, 92°E negative anomaly >5 is observed in fewer years than western bay. Significant lowering of salinity is noticed during July/August 1970 which is a flood year and in 2001, a normal year. On the contrary, in 1955, 1965-66, 1979-80 and 2004-06 exhibit only positive anomaly with the dominance of annual signal as revealed by the wavelet analysis (Fig. 6.3b), but the energy level is 1/4th of that in the western BoB. The annual harmonic contains less energy level during the years 1955, 1965-66, 1979-80 and 2004-06, majority of which are drought years (1965-66, 1979). Similarly, El Niño is observed during the years 2004-06. This shows that the events like droughts or El Niño years weaken the annual signal and thereby reducing its energy levels. On the other hand, high energy levels observed at 5-7 year band during 1969-82 coincide with the flood monsoon years of 1970, 1975 and 1983.

Fig. 6.2c shows that amplitude of negative salinity anomaly (upto 1.5) is higher than positive anomaly (upto 1) in the central western BoB (10°N, 81°E). The minimum anomaly is in November/December and maximum in July. The freshening

is associated with the advection of freshwater from northwestern BoB in the winter season. The influence of climatic events could be seen in the occurrence of positive anomaly during November/December of certain years instead of the usual freshening. For instance, saltening is observed during combined El Niño and pIOD years of 1951, 1963, 1994 and 1997. Similarly 1961, 1967, 1969, 1987, 2002, 2004, 2008 and 2009 were either El Niño or pIOD years during which positive anomaly exist. The wavelet analysis (Fig. 6.3c) indicates intermittent appearance of annual harmonics and it's the only significant frequency in the global wavelet power spectrum. Interestingly, the weak energy level in the annual frequency is confined to either pIOD, El Niño, their co-occurrences or drought. The higher energy levels in 1959-60, 1979, 1984-85, 1990-91 and 2000-01 are associated with comparatively negative anomaly (~-2). At 10°N, 94°E (Fig. 6.2d) positive anomaly persist during July-September and negative anomaly in November-February. The freshening corresponds to flood, pIOD and El Niño or its combined occurrence. This is reflected in the wavelet analysis (Fig. 6.3d) with presence of interrupted annual signal. The time series exhibit significant power in the 3-4 year harmonics between 1991 and 2004. In addition, during 1960-2000 a prominent 8 year harmonic is observed in the wavelet power spectrum but not within 95% confidence limit in global wavelet spectrum.

In the western equatorial BoB (0°, 81°E), continuous freshening is observed from 1990 to 2001 (Fig. 6.2e). The wavelet analysis also shows significant energy in the annual harmonics during this period (Fig. 6.3e). Also, peak in energy is observed at 2-4 years harmonics during the years 1965-1969 and 1990-2000 of which 1965 and 1968 are drought years whereas 1991, 1994 and 1997 are pIOD with El Niño years. However, the amplitude of saltening or freshening is less in the southern bay. The freshening during 1990-2000 is synchronous with that observed in basin averaged.

Similar to southwestern bay and whole basin, negative anomaly exist from 1982 to 2001 in the southeastern BoB, (0°, 94°E) (Fig. 6.2f). The annual periodicity is weak and significant at the 95% confidence level (Fig. 6.3f). In addition, in the 2-4 frequency bands, higher energy is observed during the years 1965-1969 and 1980-2000. However, it is not significant in the global power spectrum, only the annual periodicity is prominent.
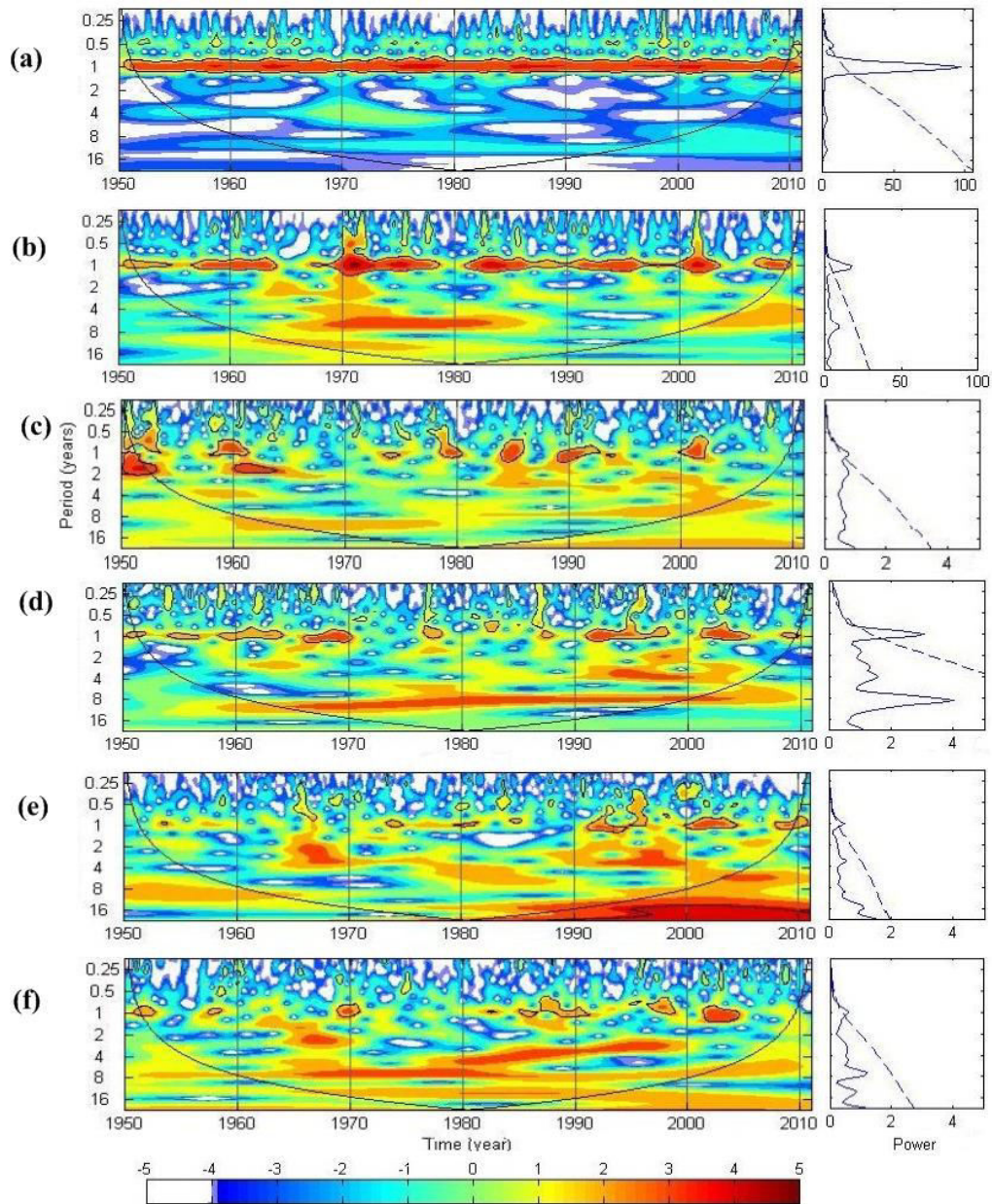
Fig. 6.3 Wavelet power spectra (left panels, black line indicates the cone of influence), and global wavelet spectra (right panels, dashed line indicates 95% confidence limit) at (a) 19°N, 86°E, (b) 19°N, 92°E, (c) 10°N, 81°E, (d) 10°N, 94°E, (e) 0°, 81°E and (f) 0°N, 94°E. X-axis: time (years) and Y-axis: frequency.

6.3   Response of salinity variability to major climatic events

As discussed in the previous chapters, variation in the continental runoff and its lateral advection associated with circulation are primarily responsible for the salinity variability in the BoB. The wavelet analysis reveals several harmonics in the salinity fields and its temporal variability. Recently, it is also established that the climatic events play a crucial role in the inter-annual variability of various parameters, especially in the upper layers of the BoB. In the present work, the role of three

climatic events viz. the IOD, El Niño/La Niña and different regimes of summer monsoon on the variability of salinity in the BoB is discussed.

6.3.1 Indian Ocean Dipole

The Indian Ocean Dipole (IOD) is a phenomena characterized by opposite sea surface temperature anomaly (SSTA) in the southeastern and western equatorial Indian Ocean. The two phases of IOD depending on the anomalies are positive IOD (pIOD) and negative IOD (nIOD). Over a period of 61 years between 1950 and 2010, 13 pIOD and 18 nIOD are identified (Table 2.2). Usually, IOD starts during May-June, matures by September-November and most of the anomalies disappear by January of the following year. However, the duration of this event is not same in all the years. During a pIOD year, positive SST anomaly exists in the western equatorial Indian Ocean (Saji et al., 1999), and negative anomaly in the southeastern equatorial Indian Ocean, as the SST in this region drops considerably compared to the western part. The vice versa occurs during a nIOD year. However, researches on salinity variability during the IOD events are comparatively meager.

(i) Indian Ocean Dipole index based on salinity

Understanding dipole events using the SST anomaly difference in the eastern equatorial Indian Ocean (EEIO) and western equatorial Indian Ocean (WEIO) was proposed by Saji et al. (1999). Thereafter most of the researchers considered temperature as the index for defining IOD in almost all the works. Salinity variation is an important factor of the IOD that contributes greatly to its formation through positive feedbacks that enhance temperature variations and drive IOD circulation across the tropical Indian Ocean. Although a signature for salinity cannot be directly observed in the atmosphere, feedbacks act indirectly on the atmospheric component of the dipole (Murtugudde and Busalacchi 1998).

The impacts of salinity on the dipole mode make it an important factor in understanding both the atmospheric and oceanic components of both phases of the IOD. This has motivated us to examine the IOD utilizing salinity. Some researchers used salinity while defining the IOD index, but they considered different regions for defining salinity index. Thompson et al. (2006) defined a Zonal Salinity Index, where they took the difference in SSS anomaly between two boxes (5°S-5°N, 80°E-90°E and 10°S-0°N, 90°E-105°E) in the eastern equatorial Indian Ocean. Later, Grunseich et al.

(2011) defined a Dipole Mode Index of Salinity utilizing the averaged SSS anomaly over the region off Sumatra (10°S-0°N, 95°E-105°E) to capture the different IOD phases. More recently, Li et al. (2016) identified dipole events based on SSS anomaly between the central equatorial Indian Ocean (70°E-90°E, 5°S-5°N) and off Sumatra-Java coast (100°E-110°E, 13°S-3°S) for the period September to November. They noticed a correlation coefficient of -0.7 between the DMI and SSS anomaly index. In the present study an attempt has been made to define a salinity index based on salinity anomaly for the same grids as in Saji et al. (1999), where the DMI based on SSTA is estimated. As a first step, the average difference between SST of the individual year and the climatology (ΔT) for all pIOD and nIOD years are estimated. Similarly ΔS of pIOD and nIOD years are also estimated. Then the bi-monthly composites of ΔT and ΔS from May to December are estimated separately for the pIOD (Fig. 6.4) and nIOD events (Fig. 6.5).
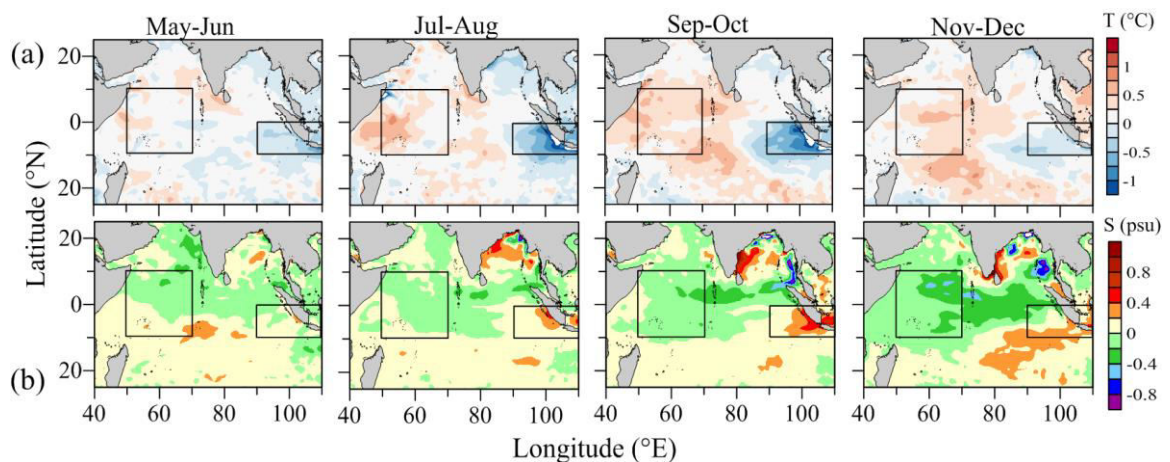
Fig. 6.4 Composite maps of (a) SST anomaly and (b) SSS anomaly during positive dipole years from May to December.

During the pIOD years, the figure (Fig. 6.4a) shows the commencement of negative ΔT (-0.25°C) in the EEIO from May-June. At the same time warming occurs in the western and central Indian Ocean. In the subsequent months, negative ΔT intensifies in the eastern and positive ΔT in the WEIO. In the salinity field, the pIOD periods are marked by positive ΔS in the EEIO while negative anomaly exists in the western counterpart (Fig. 6.4b). During its mature phase, i.e. during September-October, both ΔT and ΔS attains its peak in the eastern (-0.75°C, 0.4) and in the western Indian Ocean (0.5°C, -0.4). The values of salinity anomaly during September-October concur with that of Thompson et al. (2006). From December the anomalies show a decreasing trend. At the same time, positive ΔS continue to exist off the southern Sumatra in the EEIO while negative values covers the entire regions west of

this box. In conclusion, during pIOD events positive salinity anomalies are observed in the EEIO while negative anomaly exists in the western part.

The nIOD years (Fig. 6.5a) have a different pattern compared to pIOD events. Here, ΔT becomes positive (0.25°C) from May-June in the EEIO near the Sumatra coast and reaches its peak value (0.5°C) in September-October. On the other hand, negative values exist in the WEIO (peak value of -0.75°C). In the case of salinity, ΔS are negative in the EEIO and positive in WEIO (Fig. 6.5b). As in the case of temperature, peak values of negative ΔS (-0.4) occur in the EEIO during September-October. Also, the sign of ΔS reverses in the two defined boxes, but with weaker amplitudes compared to pIOD.
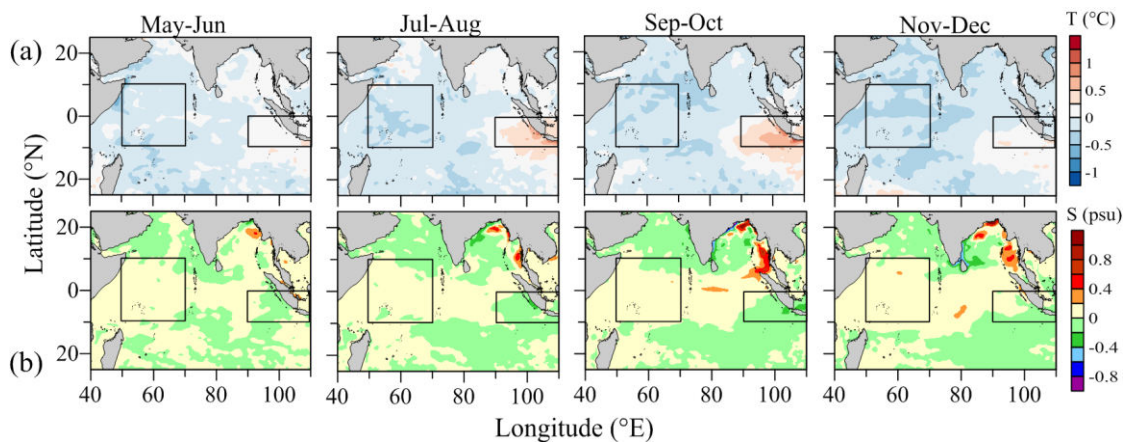
Fig. 6.5 Composite maps of (a) SST anomaly and (b) SSS anomaly during negative dipole years from May to December

During the positive phase of IOD, the SST decreases in the southeastern equatorial Indian Ocean relative to the western equatorial Indian Ocean (Saji et al., 1999), leading to positive SST differences between western and eastern equatorial regions. This SST difference is termed the dipole mode index (DMI). During the negative phase of the IOD, the DMI is negative.

In the present study, a new dipole mode index based on salinity anomaly is proposed. For this purpose, the difference in surface salinity (ΔS) between the individual year and the climatology is estimated from SODA for the period 1950-2010. Then the dipole mode index based on salinity anomaly (DMIS) is calculated as the difference in ΔS averaged over 10°N - 10°S, 50°E - 70°E in the WEIO Ocean and 0° - 10°S, 90°E - 110°E in the EEIO. The computed DMIS (Fig. 6.6) is smoothed by 3 month running mean and normalized by its standard deviation (σ). A year to be

considered as a dipole should have salinity anomaly index greater than 1σ and continue so for at least 3 to 4 months.
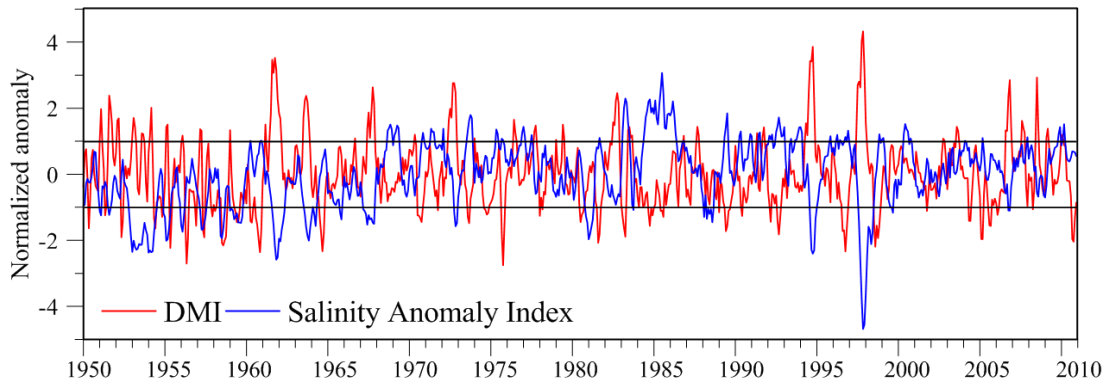
Fig. 6.6 Dipole Mode Index based on temperature anomaly (DMI, Red line) and salinity anomaly (DMIS, Blue line) for the period 1950-2010. Both indices are normalized by their respective standard deviations (σ). Positive dipole years corresponds to years with more than +1σ and negative dipole years with less than -1σ.

The DMIS captured all the major events (Blue line in Fig. 6.6) for the period 1950-2010. Also the variations in DMIS are in good agreement with DMI (Red line in Fig. 6.6), but with an inverse relation. Strong pIOD years 1961, 1963, 1967, 1972, 1982, 1994 and 1997 and the most intense negative mode occurred during 1996, 1998 and 2010 (Table 2.1) are also well represented in DMIS. The correlation analysis between DMIS and DMI during the mature phase of IOD (Fig. 6.7) showed a very good relation as indicated by the correlation coefficient of -0.7.
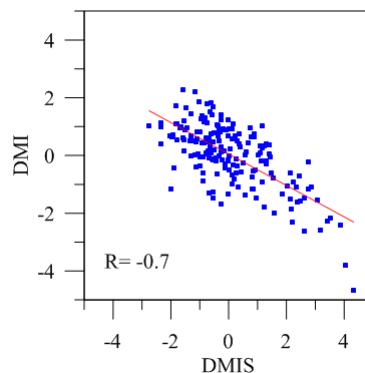
Fig. 6.7 Correlation (R) between DMI and DMIS during the mature phase of IOD, i.e. September-November for period 1950 to 2010.

(ii)   Salinity variability in the BoB associated with IOD events

(a)   Pure positive IOD events

The monthly composite of ΔS in the BoB during the five pure pIOD events (Table. 2.1) during May to December (as this period covers the beginning, maturation

and dissipation of the IOD) are presented in Fig 6.8 (a). Prior to the onset of summer monsoon, i.e. in May, ΔS is positive (0.2 to 0.4) in the regions south of 7°N and mostly negative north of this latitude. Off the east coast of India, the negative ΔS is replaced by positive ΔS with the commencement of summer monsoon. After June, positive anomaly (~0.6) intensifies along the entire east coast of India. Between 13°N and 18°N a tongue of positive anomaly extends offshore upto 92°E. Within this region the flow is found to be offshore and is sandwiched between a cyclonic circulation on the north and an anti-cyclonic circulation on the south. The lowering of salinity (negative ΔS >1) continues in the northeastern bay that reaches its maximum due to enhanced precipitation and runoff during this period. From October, the positive anomaly present in the western periphery of the BoB is replaced by negative values (-0.7) north of 15°N while positive (0.8) continue to exists in the regions south of this latitude. This is mainly due to the reversal of EICC which transport the remnants of the monsoonal freshwater from the northern bay into the western periphery of the BoB and limits its southward extend to 15°N. On the other hand, the flow is northward and brings comparatively saltier water from Arabian Sea thereby increasing the salinity in those regions. Jensen et al. (2007) also reported the advection of waters from Arabian Sea into the BoB during this period. This results in the occurrence of positive anomaly south of 15°N. These contrasting current patterns are typical during pIOD. On the hand negative anomaly continues through the period May-December in the eastern BoB.
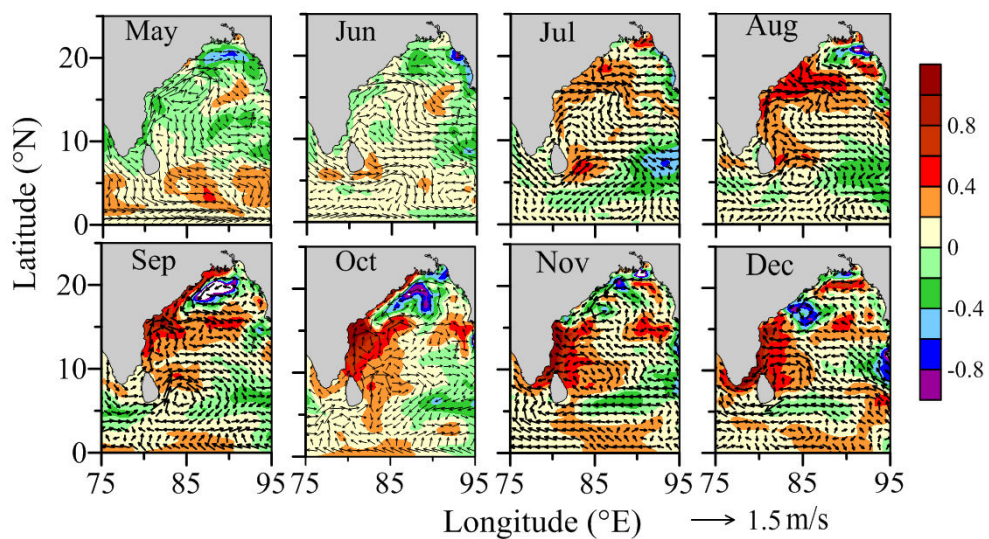
Fig. 6.8 (a) Composite maps of sea surface salinity anomaly (ΔS) overlaid with surface currents during positive IOD years.

(b)   Pure negative IOD events

The monthly composite of ΔS during eleven pure nIOD events (Table. 2.2) from May to December in the BoB are presented in Fig 6.8 (b). In May, salinity anomaly shows marginal variation (-0.2 to 0.2) in the entire BoB suggesting that variation in salinity during nIOD years are not large from the climatic mean. In general, negative anomaly prevails in the entire bay till the withdrawal of summer monsoon, i.e. in September, except in the northeastern Bay where small pockets of positive anomalies are noticed. The negative anomaly is mainly due to the influx of fresh water from various rivers into the BoB and its advection by the prevailing circulation pattern. The northward spreading of the zones of positive ΔS is found to be associated with the propagation of downwelling Kelvin waves along the coastal periphery of the BoB. The maximum southward extends of this positive anomaly along the east coast of India is found to be 16°N. The trend in the salinity anomaly and circulation pattern during the nIOD years is found to be similar to that of the normal years. While comparing the nIOD and pIOD years, a shift in the initial location of freshening is noticed. In the nIOD years, it occurs in the northwestern BoB whereas in the pIOD years, the freshening triggers in the northeastern BoB..
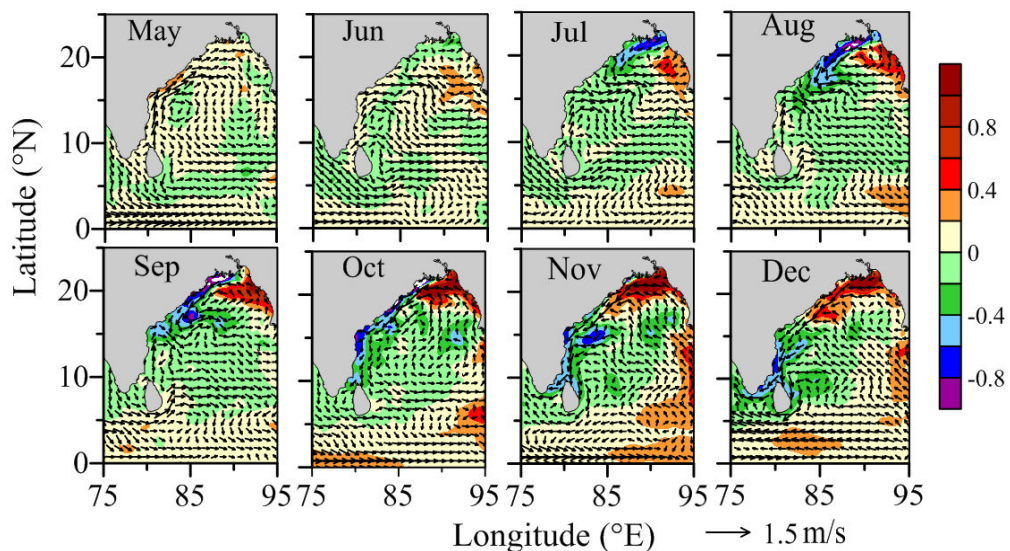
Fig. 6.8 (b) Composite maps of sea surface salinity anomaly (ΔS) overlaid with surface currents during negative IOD years.

The strong monsoon during pIOD makes northern bay less saline than that in nIOD. Another noticeable observation on comparison between the two phases is the occurrence of comparatively saltier water in the western periphery of the BoB south of 15°N. This is mainly due to the abnormal changes in the circulation pattern in the

pIOD years, which brings comparatively saltier water from the Arabian Sea into the western BoB
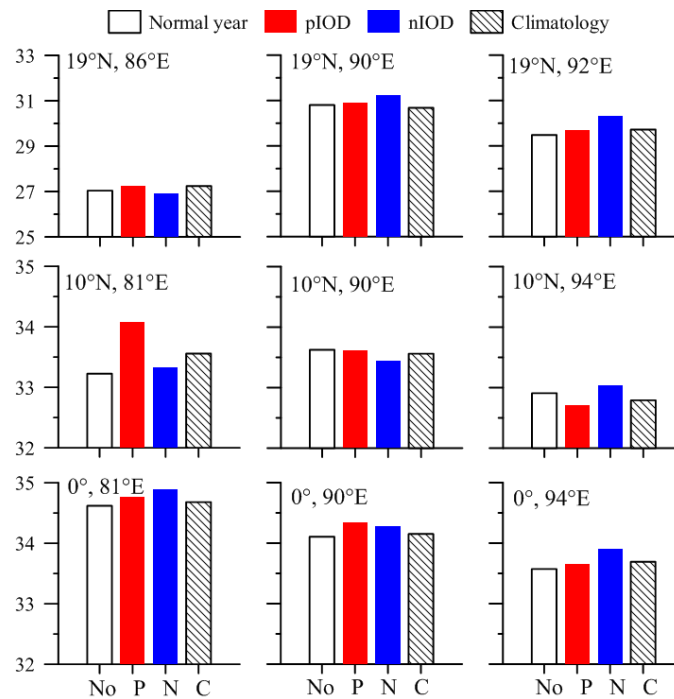
Fig. 6.9 Salinity in the northern, central and southern BoB during normal, pIOD, nIOD years and climatology averaged for September-November.

To understand the variability of salinity during positive and negative phase of dipole events covering the entire BoB, nine locations representing northern, central and southern BoB are selected. For each location, average salinity for the normal year, pIOD, nIOD and climatology for the period September-November is estimated (Fig 6.9). In general, irrespective of the occurrence of climatic events, surface layers are fresher (salinity around 27) in the northwestern BoB (19°N, 86°E) compared to that in the central (around 31) and eastern BoB (29.5-30.5). In the northwestern Bay, however, there is a variation of 0.3 units between pIOD and nIOD events with pIOD having comparatively higher values (27.2). In the north central (19°N, 90°E) and eastern BoB (19°N, 92°E), surface waters are saltier during the nIOD event compared to that in the pIOD event. In the western BoB (10°N, 81°E), there is a difference of 0.7 in the surface salinity between the two events with pIOD years having comparatively saltier water (34). In the eastern bay (10°N, 94°E), the salinity is higher by 0.5 units in nIOD (33) compared to that in pIOD years whereas in the central Bay (10°N, 90°E), the differences between the two events are fairly marginal (0.2) but the surface layers are slightly saltier during pIOD years. In the equatorial region, surface

waters of the western (81°E) and eastern region (94°E) are slightly saltier during nIOD years compared to that in pIOD years, while the converse is true in the central equatorial region (90°E). In general, it is observed that the surface layers are saltier in the eastern BoB during the nIOD years (~0.3 units more than pIOD). Off the east coast of India, waters are saltier north of 10°N during the pIOD years.

6.3.2   El Niño/La Niña

The El Niño/Southern Oscillation (ENSO) is a well-known dominant mode of inter-annual variability. El Niño represents the warm phase of the ENSO cycle, with warming along the west coast of tropical South America (Fig. 6.10a). La Niña represents the cold phase with cooling of ocean waters off the west coast of Peru and Ecuador (Fig. 6.10b). To differentiate the El Niño/La Niña events, the Oceanic Nino Index (ONI) are utilized (Fig. 6.11). During the period 1950 to 2010, there were 17 El Niño and 16 La Niña events (Table. 2.2). The onset of an El Niño episode is defined when the 3-month average sea surface temperature departure exceeds 0.5°C in the east-central equatorial Pacific (between 5°N-5°S and 170°W-120°W).
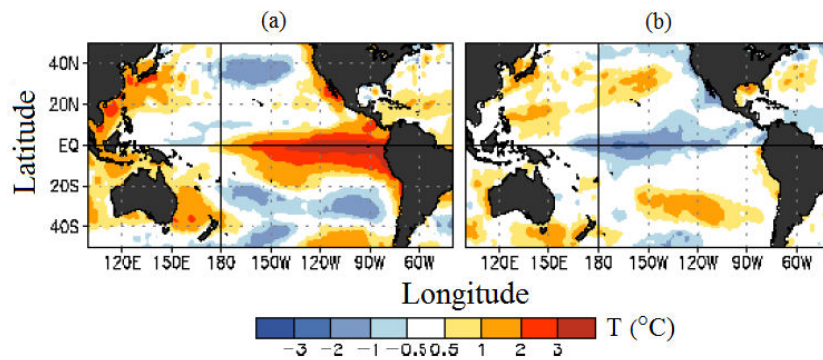
Fig. 6.10 Sea surface temperature (SST) anomaly maps for December-February during strong (a) El Niño and (b) La Niña episodes (cpc.ncep.noaa.gov).
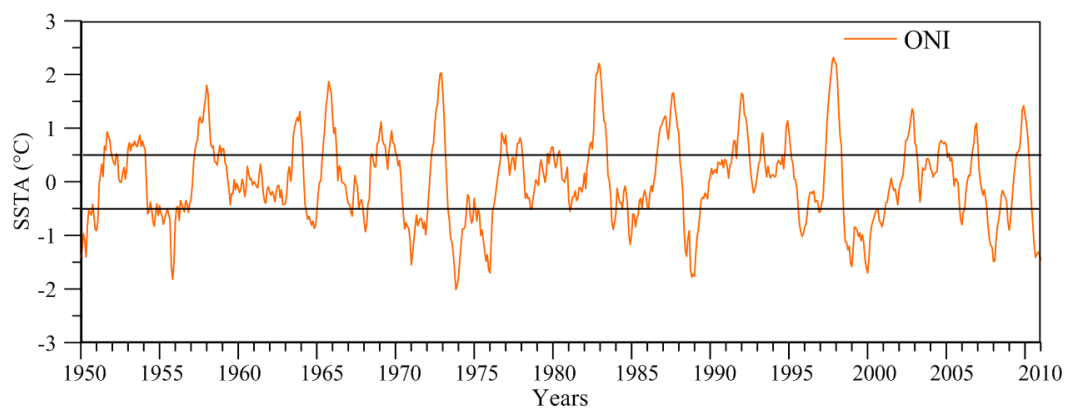
Fig. 6.11 Oceanic Niño Index (ONI). El Niño and La Niña years are represented by temperature anomaly above and below 0.5°C respectively.

(i)   Salinity variability in the BoB associated with El Niño/La Niña events

(a)   El Niño

The monthly composite of salinity anomaly during nine El Niño events (Table. 2.2) from May to December in the BoB are presented in Fig 6.12a. During June, negative ΔS start appearing in the northeastern BoB and this intensifies with a westward shift in July. Negative salinity anomaly (-0.2) is noticed along western BoB extending up to Sri Lanka during July-August, meanwhile increase in salinity indicated by positive ΔS start in July in the northeastern BoB. In September, low saline water occupies all along the east coast of India and comparatively saline water (positive ΔS) is present at the northern head bay and transported westward. Along the entire coastal region of BoB positive ΔS (0.8) is noticed during October-December. This positive anomaly could be associated with weak monsoon during El Niño years. In general anomalies are smaller in magnitude compared to pIOD.
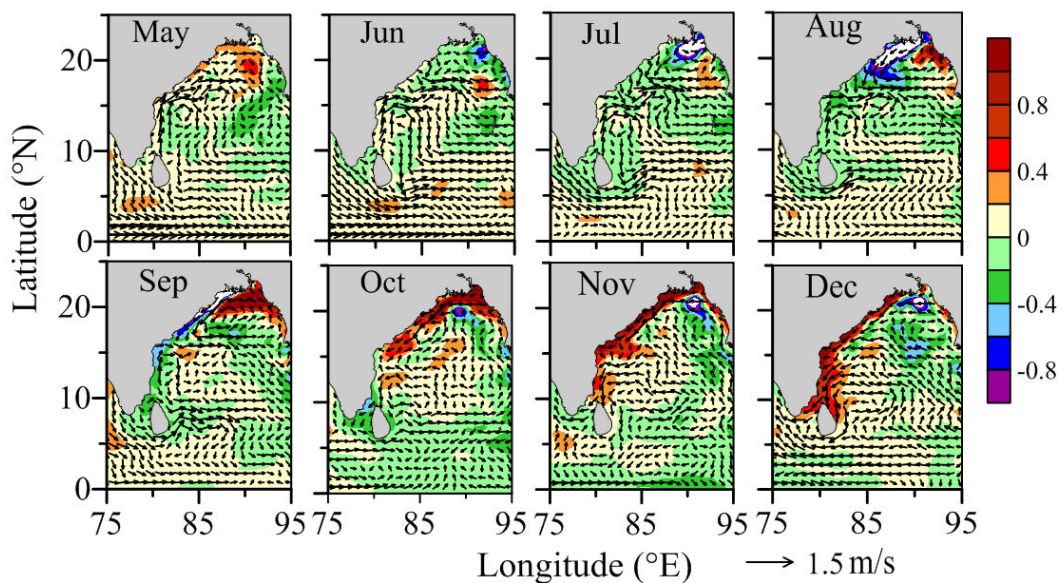
Fig. 6.12 (a) Composite maps of sea surface salinity anomaly (ΔS) overlaid with surface currents during El Niño

(b)   La Niña

The monthly composite of ΔS during the 10 La Niña events (Table. 2.2) from May to December in the BoB are presented in Fig 6.12b. In the entire BoB, negative salinity anomaly is noticed during May-August (-0.4). The negative salinity anomaly at the northwestern coastal BoB is replaced by positive values (0.8) in September and continues to exist till December. The southward extend of the positive anomaly is found to be limited to 15°N. At the same time, positive anomalies are observed in the offshore off the east coast of India and in the central BoB. The major difference

compared to El Niño is the dominance of negative salinity anomaly in the entire bay suggesting freshening of the Bay.
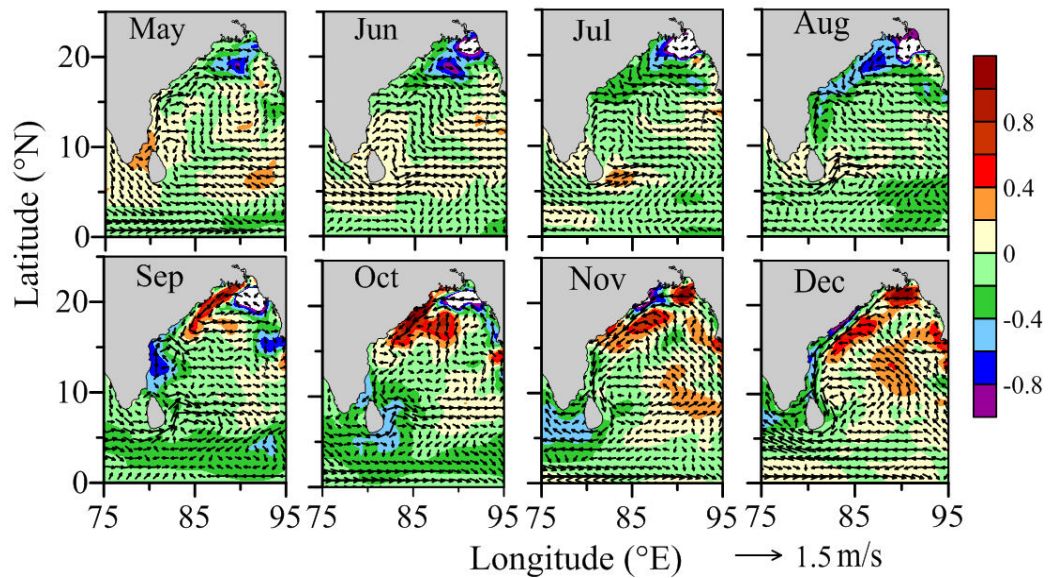
Fig. 6.12 (b) Composite maps of sea surface salinity anomaly (ΔS) overlaid with surface currents during La Niña.
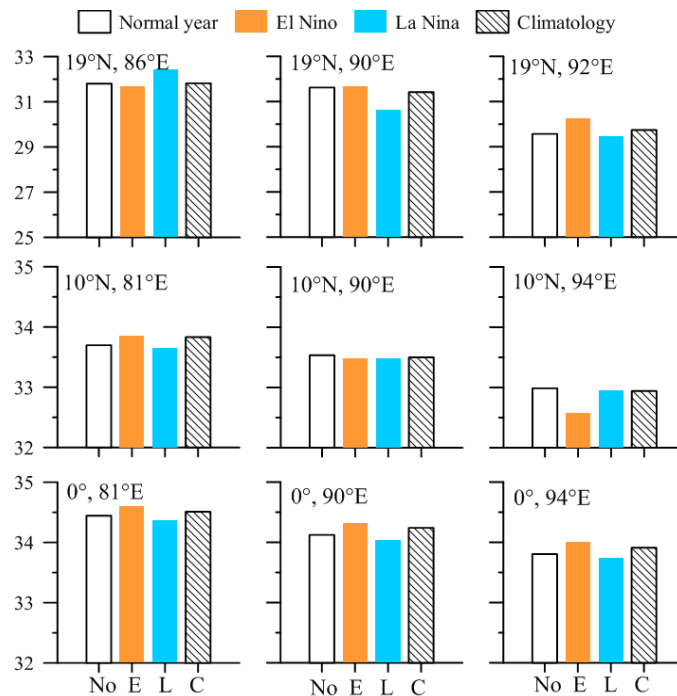
Fig. 6.13 Salinity in the northern, central and southern BoB during normal, El Niño, La Niña years and climatology averaged for June-September.

The salinity during normal year, El Niño, La Niña and climatology, salinity for the period June-September is averaged for nine stations (Fig. 6.13). In the entire BoB, surface waters are saltier during El Niño than in La Niña years in all regions except at 19°N, 86°E, and 10°N, 94°E which is in agreement with that in Fig. 6.12 a,

b. At 10°N, 90°E, there is no noticeable variation in salinity (33.5) between the two events while the maximum difference of 1 unit is observed at 19°N, 90°E.

6.3.3   Combined IOD and ENSO events

(a)   Co-occurred pIOD and El Niño events

The monthly composite of ΔS during eight co-occurred pIOD and El Niño events (Table. 2.2) from May to December in the BoB are presented in Fig 6.14 (a). The combined events are characterized by negative salinity anomaly (-0.2) in the entire equatorial belt, i.e. south of 10°N between May and December. The anomaly is minimum in the entire Bay in May, as indicated by the ΔS of ±0.2. A noticeable observation during July-September is very weak freshening in the northeastern BoB unlike that observed during pure pIOD (Fig. 6.8a).
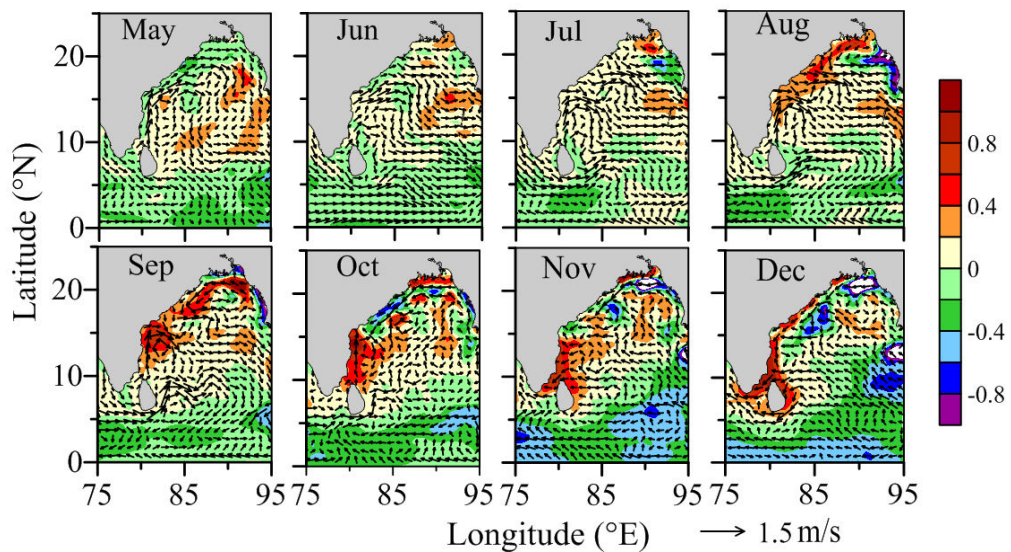
Fig. 6.14 (a) Composite maps of sea surface salinity anomaly (ΔS) overlaid with surface currents during co-occurred pIOD and El Niño events.

The negative anomaly observed in the western and northern periphery of the BoB is replaced by positive values in the northeastern Bay in July. Moreover, the prevailing northward current along the east coast of India brings saltier water from the Arabian Sea into the Bay circulated within the BoB. In addition, the prevailing eddies and coastal upwelling also contributes to the increase in salinity in the regions north of 10°N as seen as high salinity pockets. From September, the changes in the current pattern in the northwestern Bay bring freshwater of the northern Bay origin along the coastal belt of the east coast of India and thereby reducing the salinity in those regions. The remnant of the saltier water is transported southward confining along the

western coastal periphery of the basin and enters the Arabian Sea in December. North of the 15°N, the positive anomaly along the coastal belt of the east coast of India is replaced by negative values from October. This zone is much narrower and confined to the east coast than that in pure IOD event. Negative anomaly is noticed east of 85°E and south of 10°N (-0.6) in December which is in contrast to the positive anomaly noticed during the pIOD. In this case also, similar to that observed during positive dipole years, equatorial currents undergo change in direction from eastward to westward.

(b)   Co-occurred nIOD and La Niña events

The monthly composite of salinity anomaly in the BoB during six co-occurred nIOD and La Niña events (Table. 2.2) from May to December are presented in Fig 6.14b. In June, a pocket of positive anomaly, indicating saltier water is noticed in the northeastern bay (0.6). This pocket of saltier water is found transported to the western BoB in the subsequent months due to the prevailing cyclonic circulation. After reaching its maximum southward limit of 16°N in September, it starts dissipating / slightly shifted offshore, as the southward EICC which brings fresher water from the head bay dominates. Moreover, the difference in the period of initiation in freshening in the northeastern bay associated with summer monsoon makes pure nIOD different from the combined event. There appears to be a delay in the lowering of salinity as evident from negative ΔS in head bay only by August in comparison with that in June during pure nIOD event.

Another noticeable observation is the occurrence of negative salinity anomaly, even though weak (ΔS of -0.2), in the equatorial Indian Ocean. By October, as the downwelling Kelvin waves forms in the equatorial regions, there is a slight increase in the surface layer salinity in those regions. This saltier water is transported northward along the eastern periphery of the BoB as the coastally trapped Kelvin wave propagates along the coastal belt of the BoB. In December, a conspicuous feature is the occurrence of positive ΔS is the eastern periphery and negative ΔS in the western periphery. This contrasting behavior in the salinity distribution with saltier water in the eastern bay and fresher water in the western bay is typical for the BoB.
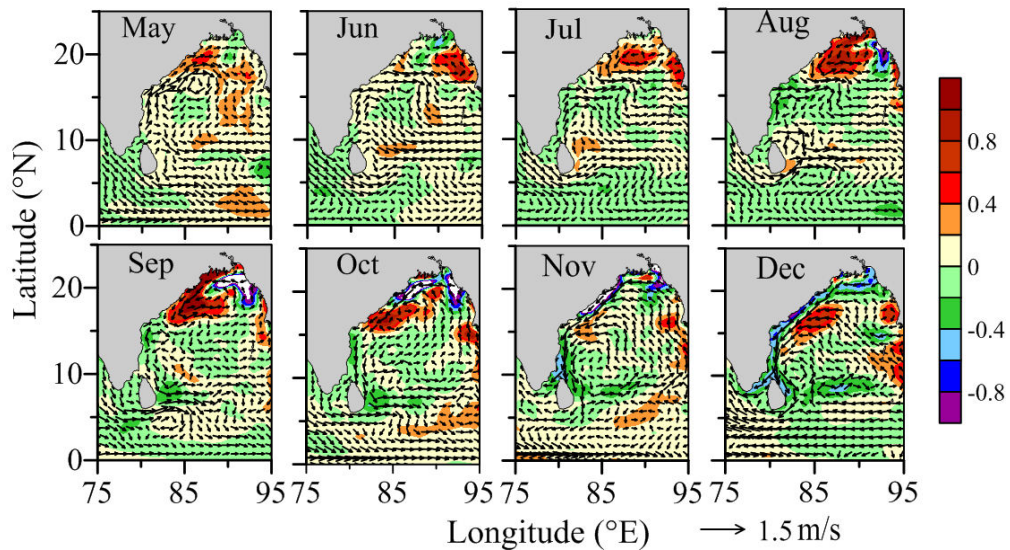
Fig. 6.14 (b) Composite maps of sea surface salinity anomaly (ΔS) overlaid with surface currents during co-occurred nIOD and La Niña events.

To understand the response of salinity in the BoB to all the events, salinity in six boxes representing different parts of the bay from May to December are presented (Fig. 6.15). In the northwestern bay surface water are saltier (33.5-34) than the northeastern bay (< 32) irrespective of the various climatic events till September. Afterwards it drops to its minimum in October-November. The differences in the salinity between the western and eastern periphery of the BoB indicate positive values from May till October and negative thereafter. The maximum difference of 4 units in the surface salinity in August suggests that the northern bay undergoes significant freshening during the monsoon season than in the northwestern bay. On the other hand, the negative difference during winter suggests comparatively saltier water in the eastern bay than in the western counterpart. Further, on a closer examination, it can be seen that in the northwestern bay, salinity is lowest during combined nIOD and La Niña and highest during El Niño while in the northeastern BoB, the minimum is observed during pIOD and El Niño (in August). In the central and equatorial bay, the salinity variations are not significant as in the northern bay. Moreover, the differences in salinity between the western and eastern bay are positive during May-December, except in the case of nIOD, where the difference is negative after October. This suggests that except during nIOD years and that also after October; the central-western bay is always saltier than the central-eastern bay. In the central-western bay, salinity (~34) is higher during pIOD and combined pIOD and El Niño events (September to December), whereas during normal years and rest of the events salinity is lower. In the central eastern BoB the salinity distribution is opposite to that in

western bay during September-December, where the difference is positive during pIOD, combined pIOD and El Niño and El Niño events, and negative during normal, nIOD and combined nIOD and La Niña events. In the southern BoB salinity higher than 33.5 is observed during all events from May to December, with western region having slightly saltier water. As a result, the difference in salinity between the western and eastern bay is always positive. Salinity difference is least during pIOD in southern bay.
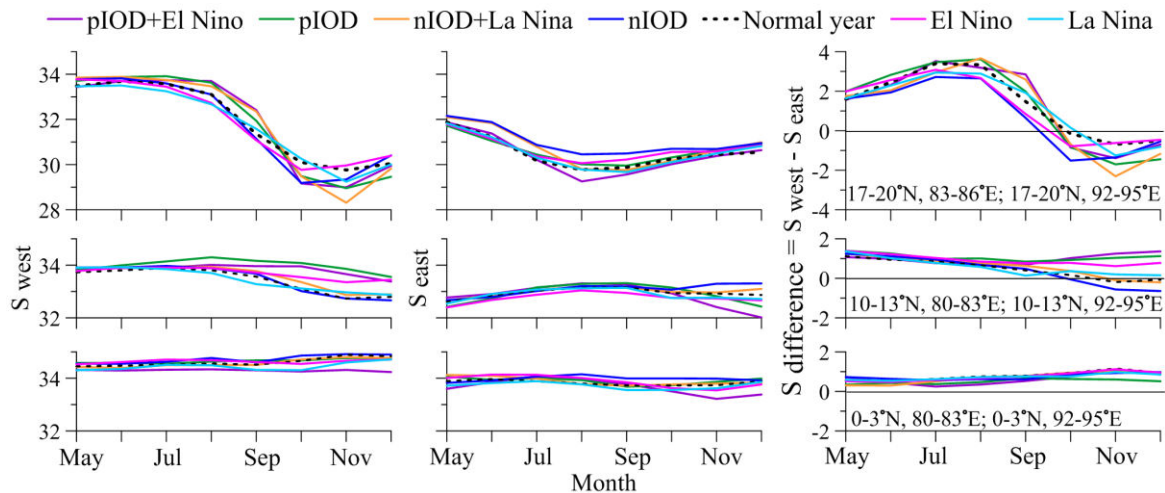
Fig. 6.15 Salinity difference between western and eastern BoB (boxes given in Fig. 6.1). Surface salinity during pIOD+El Niño (Violet line), pIOD (green line), nIOD+La Niña (Orange line), nIOD (Blue line), normal year (dotted line), El Niño (Magenta line) and La Niña (light blue line) in the north (17°-20°N), central (10°-13°N) and southern (0°-3°N) BoB.

6.3.4   Monsoon and salinity variability in the BoB

The different regimes of the summer monsoon are classified into Normal, Flood and Drought years based on the All-India Summer Monsoon Rainfall anomalies from IMD. Here the flood and drought monsoon events are compared to decipher the salinity variability during these events.

(a)   Flood monsoon

The monthly composite of ΔS during nine flood years (Table. 2.3) from May to December in the BoB are presented in Fig 6.16a. Flood monsoon is characterized by low saline water indicated by negative salinity anomaly during summer monsoon season. Negative salinity anomaly is noticed in the entire BoB during May-August. In August a patch of positive anomaly appear off the northeast coast of India.
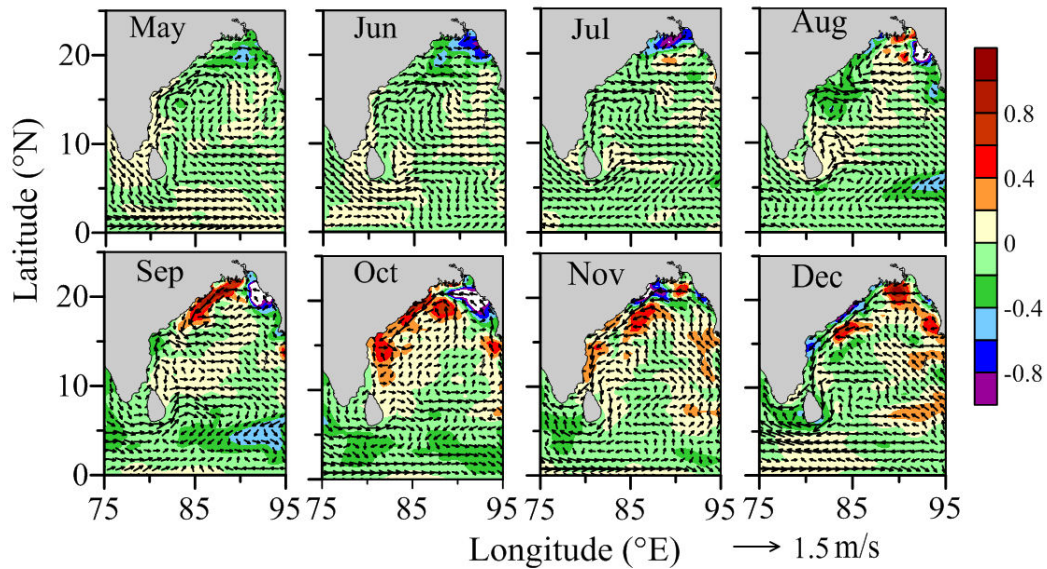
Fig. 6.16 (a) Composite maps of sea surface salinity anomaly (ΔS) overlaid with surface currents during flood years.

In September, a prominent zone of positive anomaly appears off the northeast coast India, which shifts to lower latitude with the progress of month. This may be due to the prevailing eddy activity in those regions, which played a major role in bringing the subsurface saltier water towards the surface as mentioned in the previous chapter. Also, the downwelling Kelvin wave also seems to play a key role in increasing the salinity in the eastern BoB, replacing the existing low salinity waters with the comparatively saltier waters from the equatorial BoB. The flood years resembles La Niña events with negative ΔS during summer monsoon season.

(b) Drought monsoon

The monthly composite of ΔS during fourteen drought years (Table. 2.3) from May to December in the BoB are presented in Fig 6.16b. Drought monsoon is characterized by the dominance of positive salinity anomaly in the entire bay, indicating saltier water during summer monsoon season, which is due to the reduction in the freshwater flux during these years. However, as observed in the previous section, pockets of comparatively saltier water is noticed at the head bay from June-October. During the period, September-November, the saltier water advect southward along the east coast of India due to the combined effect of eddies and associated circulation, reversal of EICC and southward propagating downwelling Kelvin wave. In December, the saltier water is found to enter into the southeastern Arabian Sea. The salinity anomaly in drought years is similar to that during El Niño but with increased magnitude.
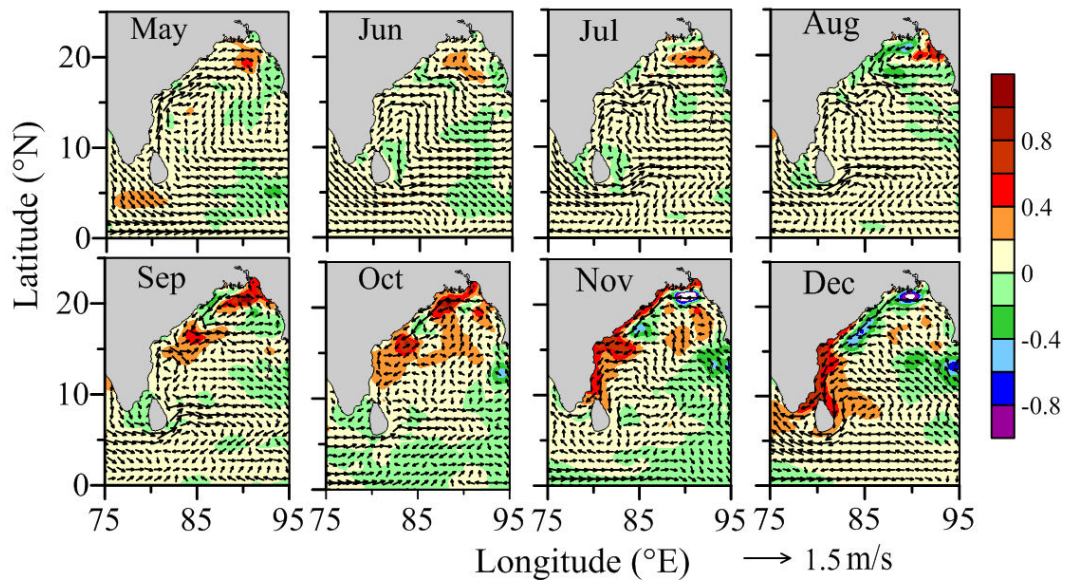
Fig. 6.16 (b) Composite maps of sea surface salinity anomaly (ΔS) overlaid with surface currents during drought years.

The response of salinity variations to climatic events likes Indian Ocean Dipole, El Niño/La Niña and different regimes of summer monsoon are described in this chapter. Over a period of 61 years (1950 to 2010), 13 pIOD, 17 nIOD, 17 El Niño, 16 La Niña, 9 floods and 15 droughts are identified. During October to December of the pIOD years, salinity in the western (eastern) central BoB is comparatively higher (lower) than that of normal years. During these events marked changes in the circulation pattern in the equatorial regions is noticed. On the other hand, during nIOD year's intensification of normal condition occurs with negative salinity anomaly (0.2) in the western boundary and positive anomaly in the eastern BoB (0.3). El Niño results in drought like condition and La Niña events are characterized by lowering of salinity (0.3) in many regions of the BoB similar to flood years. The salinity variations during these events can be attributed to the change in the circulation pattern and availability of freshwater in the head Bay.

Chapter 7

Summary and Conclusions

The Bay of Bengal (BoB) is a semi-enclosed basin in the tropical Indian Ocean which is land-locked in the north and forced by monsoon wind system. The unique feature of the Bay of Bengal is the large seasonal freshwater influx from rivers as well as excess precipitation over evaporation, which makes the waters of the upper layers less saline. The low saline water increases the near-surface stratification in the BoB thereby inhibiting the vertical mixing. The low salinity values are in phase with the seasonal cycle of river runoff in and around the BoB which later get advected by the prevailing circulation pattern. The sea surface salinity increases from about 20 unit at the head of the bay to ~34.5 psu at 5°N during summer monsoon. This heterogenous salinity distribution leads to frontal formation in the BoB. The stratification controlled by salinity also makes the bay less productive by hindering mixing of nutrients from subsurface layers. These features makes the bay dynamic and hence draws interest of researchers from around the world. In such a freshwater dominant environment, studies on salinity distribution in the BoB is very relevant and provides scope for its application in many aspects like marine life, climate models, acoustic propagation, cyclone prediction etc.

The inadequate salinity data prevented its study on a fine spatio-temporal coverage. The recent technologies have given a great momentum to make systematic and repeat measurements of the salinity in the BoB. The ARGO floats, moored buoy arrays (RAMA), field experiments, ocean reanalysis data (SODA), remote sensing of SSS (Aquarius) enable studies of global ocean surface salinity fields at fine spatio-temporal resolution. The thesis mainly focuses on improving the understanding of the salinity variability in the upper layers of the BoB utilizing these finer resolution datasets, with emphasis on the oceanic and atmospheric processes leading to this variability on different timescales. In addition, characterization of the watermasses, various processes that contribute to the saltening of the BoB and the salinity variability associated with the climatic events are addressed.

The sea surface salinity in the Arabian Sea (AS) and BoB on different spatio-temporal scales reveals that the BoB is warmer and fresher than AS by 0.7°C and 2 units mainly due to the increased freshwater flux than evaporation in the bay. This leads to the formation of a highly stratified surface layers and hence a barrier layer in the BoB. The increased freshwater flux also leads to a shallow mixed in the Bay. In the AS, the salinity structure consists of a prominent subsurface maximum whereas in

the BoB, the salinity increases from the surface towards deeper depth. Analysis of monthly salinity based on the existing climatology reveal a seasonal cycle in the sea surface salinity (SSS) with intense freshening of the northern part of the basin during the summer monsoon season, which subsequently spreads along the coastal periphery.

The seas surface temperature (SST) anomaly shows an increasing trend of ~0.5°C over a period of 61 years embedded with seasonal warming and cooling. The SSS anomaly also exhibits seasonal saltening and freshening associated with freshwater flux. Interestingly, it is observed that the BoB undergoes freshening by approximately 1.1 units between 1980 and 2001. These periods are characterized by occurrence of several (8 events) events like La Nina, combined pIOD-El Niño and flood years. Within 21 years, salinity drops by more than 0.7 units between 1990 and 2001 when nearly five climatic events occur during this period. Thereafter between 2002 and 2010, the upper 50 m continues to be comparatively warm (temperature in excess of 29°C) resulting in an increase in the SST by more than 1.2°C and SSS exhibits an overall increase of 1.2 units. This period coincides with occurrence of more number of El Niño events. The signatures of climatic events are observed in the sub-surface levels too but with reduced magnitude.

Along the coastal boundaries of the BoB, the spread in temperature, salinity and their vertical gradients is more in the regions covering the head bay, but exhibits a decreasing trend towards both western and eastern boundary. The lowest temperature (~24.5°C) and salinity (~15) is observed at the head bay which is the region of maximum river discharge. Correspondingly the respective gradients are highest at these regions. The stability parameter is 3-4 times greater at the head bay than along rest of the coastal regions. A noticeable observation at the head bay is the minimum spread in SLA associated with high stratification in those regions. This high stratification may also be one of the reasons for restricting the two Kelvin waves into the eastern BoB. Another region of low temperature (26.2°C), salinity (25) and high vertical stratification is in the eastern bay which is primarily due to the freshening by precipitation and the runoff from Irrawady. The spatial SST distribution show bi-modal pattern mainly confined to the north of 10°N with cooling during winter and warming in May. The SSS show contrasted pattern of low salinity in the northern bay and increases towards the south with seasonal variation. The influx of freshwater during summer monsoon makes the water low saline at the head bay and later during

winter, remnants of freshwater is advected along the western boundary. The freshwater and circulation plays a major role in the salinity modification.

The classification of surface watermass using the T-S analysis show existence of three prominent watermasses viz., NDW, TW and SBBW in the upper of the BoB. The NDW (T: 25-30°C, S: 17-31, σ_t< 19) is noticed at the surface layers between June and January, whereas TW (T: 25-30°C, S: 31-33, <19σ_t< 21) and SBBW (T: 25-30°C, S: 33-35, 21<σ_t< 22) are present throughout the year at different depth levels. The NDW, which is having maximum volume in November, owes its formation and sustenance to river discharge at head bay and gets advected by prevailing circulation pattern. The thickness of the watermass is more near the coast as they are regions of river discharge, but it reduces offshore. From the Turner angle, it is found that NDW region has diffusive convection due to thermal inversion and increasing salinity with increasing depth.

In general, the TW is noticed below the NDW; but in the absence of NDW, this watermass extends to the surface. During the summer monsoon, this watermass is confined to the coastal regions of the northern BoB below the NDW. The watermass undergoes large variability associated with the formation of cyclonic eddies in the BoB and lateral advection of saltier water from the south. The divergence at the centre of a cyclonic eddy uplifts the subsurface SBBW towards the surface thereby replacing TW and leading to its absence from this region. Turner angle show diffusive convection in the regions of TW with thermal inversion (-0.1 to -1.4°C) and increasing salinity (0.2 - 2) during December-February and is doubly stable during rest of the period.

The bottom water of the three, SBBW forms the major portion of the surface water and is found throughout the year at different depth levels. SBBW has minimum spatial extent in April-May. Its presence is affected by Ekman transport in the coastal regions during summer monsoon as it is brought to the surface. In winter in the central BoB due to formation of a cyclonic eddy it is uplifted to the surface. In December, it has maximum spatial extent at the surface. The thickness of SBBW gets modified by meso-scale eddies. The maximum volume of TW is in May and SBBW in March. The examination of volume occupied by each watermass reveals that, SBBW is almost twice the combined volume of TW and NDW

The fine resolution data collected from the SEAS helps to study the characteristics of watermass in this region with greater details. The low salinity plume appears in November in the coastal regions of the southern tip of India. The T-S-σ_t characteristics suggest the presence of SBBW in the SEAS during this period. In January, the SBBW could be traced upto 75°E and minimum salinity (~32.5) is noticed very close to the coast upto a depth of 50 m, whereas in the offshore region, its vertical limit is the upper 10 m. The reversal in direction of EICC to northward after January increases the core salinity. This watermass has minimum spread in February, indicating a highly homogeneous watermass structure in the entire coastal regions of the SEAS. But from March, salinity in the water column starts increasing and by May it becomes more or less homogeneous in salinity and its temperature vary from nearly 23°C to 30°C. In the deep water also similar features are observed.

The continuous freshwater influx can lead the BoB to be a freshwater basin. To prevent the bay from continuous freshening and to maintain its salt balance, the supply of saltier water into the bay is very much essential. The various processes that lead to the salinity increase in the surface layers, viz. coastal upwelling, divergence induced by eddies and their interaction, lateral advection from Arabian Sea, tropical cyclones, etc., are documented. The magnitude of saltening of the Bay due to these processes varies from north to south. In the near-shore regions of the east cost of India, the coastal upwelling due to Ekman transport plays a dominant role in increasing the salinity in the upper layers. On the other hand, in the open ocean, the divergence induced by cyclonic eddies and the mutual interaction between cyclonic and anti-cyclonic eddies contributes significantly to the salt water pumping. In the southern BoB, the lateral advection of saltier water from the AS increases the salinity. In addition, the formation of cyclones is another mechanism which can increase the surface salinity in the BoB. One of the salient features of the salt water pumping is the creation of a salinity front in the BoB.

The response of salinity variations to climatic events like Indian Ocean Dipole, El Niño/La Niña and different regimes of summer monsoon are examined considering the 61 years (1950 to 2010) of data. During this period, 13 pIOD, 17 nIOD, 17 El Niño, 16 La Niña, 9 floods and 15 droughts are identified. In presence of these events marked changes are noticed in the circulation pattern in the equatorial regions. During the pIOD years, salinity in the western (eastern) central BoB is

comparatively higher (lower) October to December than that of normal years. During nIOD year's intensification of normal condition occurs with negative salinity anomaly (0.2) in the western boundary and positive anomaly in the eastern BoB (0.3). El Niño results in drought like condition and La Niña events are characterized by lowering of salinity (0.3) in many regions of the BoB similar to flood years. The salinity variations during these events can be attributed to the change in the circulation pattern and freshwater influx in the head Bay

.

References

Agarwal N, Rashmi Sharma, Anant Parekh, Sujit Basu, Abhijit Sarkar, Vijay K Agarwal (2012) Argo observations of barrier layer in the tropical Indian Ocean. Advances in Space Research, 50, 642-654, https://doi.org/10.1016/j.asr.2012.05.021.

Akhil VP, Durand F, Lengaigne M, Vialard J, Keerthi MG, Gopalakrishna VV, Deltel C, Papa F and de Boyer Montégut C (2014) A modeling study of the processes of surface salinity seasonal cycle in the Bay of Bengal. Journal of Geophysical Research, 119, doi: 10.1002/2013JC009632.

Ali MM, Jagadeesh PSV and Jain S (2007) Effects of Eddies on Bay of Bengal Cyclone Intensity. Eos, Transactions, American Geophysical Union, 88, 93-95 doi: 10.1029/ 2007EO080001.

Ali MM, Sharma R and Cheney R (1998) An atlas of the North Indian Ocean eddies from TOPEX altimeter derived sea surface heights. Special publication, ISRO-SAC-SP-69(9), pp 6.

Anoopa PC, Pradeep Kumar T and Hareesh Kumar PV (2013) Arabian Sea Watermass characteristics in the southeastern Arabian Sea: pre-monsoon and monsoon scenario. In: National Symposium on Coastal Oceanographic Studies: Modeling and Observations, 227-232.

Anoopa PC and Hareesh Kumar PV (2015) Evolution of watermasses in the upper layers of the Bay of Bengal. Disaster Advances, 8, 12-24.

Babu MT, Prasanna Kumar S and Rao DP (1991) A subsurface cyclonic eddy in the Bay of Bengal. Journal of Marine Research, 49, 404-410.

Barnston AG, Chelliah M and Goldenberg SB (1997) Documentation of a highly ENSO-related SST region in the equatorial Pacific. Atmosphere-Ocean, 35, 367-383.

Benshila R, Durand F, Masson S, Bourdalle-Badie R, de Boyer Montégut C, Papa F and Madec G (2014) The upper Bay of Bengal salinity structure in a high-resolution model. Ocean Modelling, 74, 36-52.

Bhat GS, Gadgil S, Hareesh Kumar PV, Kalsi SR, Madhusoodanan P, Murty VSN, Prasada Rao CVK, Ramesh Babu V, Rao LVG, Rao RR, Ravichandran M, Reddy KG, Sanjeeva Rao P, Sengupta D, Sikka DR, Swain J and Vinayachandran PN (2001) BOBMEX-the Bay of Bengal monsoon experiment. Bulletin of American Meteorological Society, 82, 2217-2243.

Bruce JG, Johnson DR and Kindle JC (1994) Evidence for eddy formation in the eastern Arabian Sea during the northeast monsoon. Journal of Geophysical Research, 99, 7651-7664.

Cai W, Zheng XT, Weller E, Collins M and Cowan T (2013) Projected response of the Indian Ocean Dipole to greenhouse warming. Nature Geoscience, 6, 999-1007.

Carton JA, Giese BS and Grodsky SA (2005) Sea level rise and the warming of the oceans in the Simple Ocean Data Assimilation (SODA) ocean reanalysis. Journal of Geophysical Research, 110, C09006, doi:10.1029/2004JC002817.

Carton JA and Giese BS (2008) A Reanalysis of Ocean Climate Using Simple Ocean Data Assimilation (SODA). Monthly Weather Review, 136, 2999-3017.

Conkright ME, O'Brien TD, Boyer TP, Stephens C, Locarnini RA, Garcia HE, Murphy PP, Johnson D, Baranova O, Antonov JI, Tatusko R, Gelfeld R, Smolyar I,

(2001) World Ocean Database 2001, CD-ROM Data Set Documentation. National Oceanographic Data Center, Silver Spring, MD, pp 137.

Chaitanya AVS, Durand F, Mathew S, Gopalakrishna VV, Papa F, Lengaigne M, Vialard J, Ch Kranthikumar and Venkatesan R (2015) Observed year-to-year sea surface salinity variability in the Bay of Bengal during the 2009-2014 period. Ocean Dynamics, 65, 173-186.

Chamarthi S (1995) Numerical modeling of coastal upwelling along the east coast of India. Ph.D. Thesis, IIT-Delhi.

Chamarthi S and Sree Ram P (2009) Role of Fresh Water Discharge from Rivers on Oceanic Features in the Northwestern Bay of Bengal. Marine Geodesy, 32, 64-76. doi: 10.1080/01490410802662219.

Chamarthi S, Sree Ram P and Losyula L (2008) Effect of river discharge on Bay of Bengal circulation. Marine Geodesy, 31, 160-168.

Chen G, Wang D and Hou Y (2012) The features and interannual variability mechanism of mesoscale eddies in the Bay of Bengal. Continental Shelf Research, 47, 178-185.

Cheng X, Xie SP, McCreary JP, Qi Y and Du Y (2013) Intraseasonal variability of sea surface height in the Bay of Bengal. Journal of Geophysical Research, 118, 816-830.

Chowdary JS, Srinivas, Fousiya TS, Parekh A, Gnanaseelan C, Seo H and MacKinnon J A (2016) Representation of Bay of Bengal upper-ocean salinity in general circulation models. Oceanography, 29, 38-49, http://dx.doi.org/10.5670/oceanog.2016.37.

Cutler AN and Swallow JC (1984) Surface Currents of the Indian Ocean (to 25°S, 100°E): Compiled from Archived historical data (UK Institute of Oceanographic Sciences, Bracknell), Report No. 187, pp 8 and charts 36.

D'Addezio JM, Subrahmanyam B, Nyadjro ES and Murty VSN (2015) Seasonal variability of salinity and salt transport in the northern Indian Ocean. Journal of Physical Oceanography, 45, 19-47, http://dx.doi.org/10.1175/JPO-D-14-0210.1.

de Boyer Montégut C, Mignot J, Lazar A and Cravatte S (2007) Control of salinity on the mixed layer depth in the world ocean: 1. General description. Journal of Geophysical Research, 112(C6), C06011, doi: 10.1029/2006JC003953.

Delcroix T, McPhaden MJ, Dessier A and Gouriou Y (2005) Time and Space Scales for Sea Surface Salinity in the Tropical Oceans. Deep-Sea Research I, 52, 787-813. doi:10.1016/j.dsr.2004.11.012.

Dinesh Kumar PK, Steeven Paul Y, Muraleedharan KR, Murty VSN and Preenu PN (2015) Comparison of long-term variability of Sea Surface Temperature in the Arabian Sea and Bay of Bengal. Regional Studies in Marine Science, http://dx.doi.org/10.1016/j.rsma.2015.05.004.

Donguy JE and Meyers G (1996) Seasonal variations of sea surface salinity and temperature in the tropical Indian Ocean. Deep-Sea Research I, 43, 117-138.

Drushka K, Sprintall J and Gille ST (2014) Subseasonal variations in salinity and barrier-layer thickness in the eastern equatorial Indian Ocean. Journal of Geophysical Research, 119, 805-823, doi: 10.1002/2013JC009422.

Durand F, Shankar D, Birol F and Shenoi SSC (2009) Spatiotemporal structure of the East India Coastal Current from satellite altimetry. Journal of Geophysical Research, 114, C02013, doi: 10.1029/2008JC004807.

Endo S and Tozuka T (2015) Two flavors of the Indian Ocean Dipole. Climate Dynamics, doi 10.1007/s00382-015-2773-0.

Emery WJ and Meincke J (1986) Global water masses: summary and review. Oceanologica Acta, 9, 383-391.

Emery WJ and Thomson RE (2001) Data Analysis Methods in Physical Oceanography. Elsevier, pp 654.

Farge M (1992) Wavelet Transforms and their Applications to Turbulence. Annual Review of Fluid Mechanics, 24, 395-458.

Fousiya TS, Anant Parekh and Gnanaseelan C (2015) Interannual variability of upper ocean stratification in Bay of Bengal: observational and modeling aspects. Theoretical and Applied Climatology, doi 10.1007/s00704-015-1574-z.

Gallagher JF (1966) The variability of water masses in the Indian Ocean. Washington, DC, National Oceanographic Data Centre.

Giese BS and Ray S (2011) El Niño variability in simple ocean data assimilation (SODA), 1871-2008. Journal of Geophysical Research, 116, C02024, doi:10.1029/2010JC006695.

Girishkumar MS, Ravichandran M and McPhaden MJ (2013) Temperature inversions and their influence on the mixed layer heat budget during the winters of 2006-2007 and 2007-2008 in the Bay of Bengal. Journal of Geophysical Research, 118, 2426-2437, doi: 10.1002/jgrc.20192.

Gomes HR, Goes JI and Saino T (2000) Influence of physical processes and freshwater discharge on the seasonality of phytoplankton regime in the Bay of Bengal-The southwest and northeast monsoon, 1992-1993. Continental Shelf Research, 20, 313-330.

Goni GJ (2008) Tropical cyclone heat potential. In State of the Climate in 2007, Levinson DH and Lawrimore JH (editors). Special Supplement to the Bulletin of the American Meteorological Society, 89, S43-S45.

Gopalakrishna VV and Sastry JS (1985) Surface circulation over the shelf off the east coast of India during the southwest monsoon. Indian Journal of Marine Science, 14, 62-65.

Gopalakrishna VV, Murty VSN, Sengupta D, Shenoi SSC and Nilesh Araligidad (2002) Upper ocean stratification and circulation in the northern Bay of Bengal during southwest monsoon of 1991. Continental Shelf Research, 22, 791-802.

Gopalan AKS, Gopalakrishna VV, Ali MM and Sharma R (2000) Detection of Bay of Bengal eddies from TOPEX and insitu observations. Journal of Marine Research, 58, 721-734.

Grunseich Gary, Bulusu Subrahmanyam, Murty VSN and Benjamin S Giese (2011) Sea Surface Salinity Variability during the Indian Ocean Dipole and ENSO Events in the Tropical Indian Ocean. Journal of Geophysical Research, 116, C11013, doi: 10.1029/2011JC007456.

Han W and McCreary JP (2001) Modeling salinity distributions in the Indian Ocean. Journal of Geophysical Research, 106, 859-877.

Han W, McCreary JP and Kohler KE (2001) Influence of precipitation minus evaporation and Bay of Bengal rivers on dynamics, thermodynamics, and mixed layer physics in the upper Indian Ocean. Journal of Geophysical Research, 106, 6895-6916.

Han W and Webster PJ (2002) Forcing mechanisms of sea level interannual variability in the Bay of Bengal. Journal of Geophysical Research, 32, 216-239.

Hareesh Kumar PV, Madhu Joshi, Sanilkumar KV, Rao AD, Anand P, Anil Kumar K and PrasadaRao CVK (2009) Growth and decay of the Arabian Sea mini warm pool during May 2000: Observations and simulations. Deep-Sea Research, doi:10.1016/j.dsr.2008.12.004

Hareesh Kumar PV, Mathew B, Ramesh Kumar MR, Rao AR, Jagadeesh PSV, Radhakrishnan KG and Shyni TN (2013) Thermohaline Front off the east coast of India and its generating mechanisms. Ocean Dynamics, 63, 1175-1180.

Hareesh Kumar PV and Mathew B (1997) Salinity distribution in the Arabian Sea. Indian Journal of Marine Science, 26, 271-277.

Hareesh Kumar PV, Mohan Kumar N, Shyni TN and Rao AR (2013) Observed Variability of Thermohaline Fields, currents and eddies in the Western Bay of Bengal during BOBMEX-99. Marine Geodesy 36, 219-233, http://dx.doi.org/10.1080/01490419.2012.699505.

Hareesh Kumar PV and Sanilkumar KV (2004) Long period waves in the coastal regions of north Indian Ocean. Indian Journal of Marine Sciences, 33 (2), 150-154.

Hastenrath S and Lamb PJ (1979) Climatic Atlas of the Indian Ocean, Part 1: Surface Climate and Atmospheric Circulation. Wisconsin University Press, Madison, 97 charts, pp 19.

Howden SD and Murtugudde R (2001) Effects of river inputs into the Bay of Bengal. Journal of Geophysical Research, 106, 19825-19843.

Jain V, Shankar D, Vinayachandran PN, Kankonkar A, Chatterjee A, Amol P, Almeida AM, Michael GS, Mukherjee A, Chatterjee M and Fernandes R (2017) Evidence for the existence of Persian Gulf Water and Red Sea Water in the Bay of Bengal. Climate Dynamics, 48, 3207-3226.

Jensen TG (2001) Arabian Sea and Bay of Bengal exchange of salt and tracers in an ocean model. Geophysical Research Letters, 28, 3967-3970.

Jensen TG (2003) Cross-equatorial pathways of salt and tracers from the northern Indian Ocean: Modelling results. Deep-Sea Research, 50, 2111-2127.

Jensen TG (2007) Wind-driven response of the northern Indian Ocean to climate extremes. Journal of Climate, 20, 2978-2993.

Kurian J, Francois Colas, Xavier Capet, James C. McWilliams and Dudley B Chelton (2011) Eddy properties in the California Current System Journal of Geophysical Research, 116, doi:10.1029/2010JC006895.

Kurien P, Ikeda M and Valsala VK (2010) Mesoscale variability along the east coast of India in spring as revealed from satellite data and OGCM simulations. Journal of Oceanography, 66, 273-289.

La Fond EC (1958) On the circulation of the surface layers off the east coast of India. Andhra University Memoirs in Oceanography, 2, 1-11.

LaFond EC and LaFond KG (1968) Studies of oceanic circulation in the Bay of Bengal. Bulletin of the National Institute of Sciences of India, 38, 164-183.

Le Traon PY, Nadal F and Ducet N (1998) An improved mapping method of multisatellite altimeter data. Journal of Atmospheric and Oceanic Technology, 15, 522-534.

Li Junde, Chujin Liang, Youmin Tang, Changming Dong, Dake Chen, Xiaohui Liu and Weifang Jin (2016) A new dipole index of the salinity anomalies of the tropical Indian Ocean. Scientific Reports, 6, 24260, doi: 10.1038/srep24260.

Locarnini RA, Mishonov AV, Antonov JI, Boyer TP, Garcia HE, Baranova OK, Zweng MM, Paver CR, Reagan JR, Johnson DR, Hamilton M and Seidov D (2013) World Ocean Atlas 2013, Volume 1: Temperature. (Editor) Levitus S, (Technical editor) Mishonov A, NOAA Atlas NESDIS 73, pp 40.

Lucas AJ, Nash JD, Pinkel R, MacKinnon JA, Tandon A, Mahadevan A, Omand MM, Freilich M, Sengupta D, Ravichandran M and Le Boyer A (2016) Adrift upon a salinity-stratified sea: A view of upper-ocean processes in the Bay of Bengal during the southwest monsoon. Oceanography, 29, 134-145, doi.org/10.5670/oceanog.2016.46.

Lukas R and Lindstrom E (1991) The mixed layer of the western equatorial Pacific Ocean. Journal Geophysical Research, 96, 3343-3357.

Lu W, Yan X -Hai and Jiang Y (2015) Winter bloom and associated upwelling northwest of the Luzon Island: A coupled physical-biological modeling approach. Journal of Geophysical Research, 120, 533-546, doi:10.1002/2014JC010218.

Madhupratap M, Mangesh G, Ramaiah N, Prasannakumar S, Muraleedharan PM, De Souza, Sardesai SN and Usha M (2003) Biogeochemistry of the Bay of Bengal during summer monsoon 2001. Deep-Sea Research I, 50, 881-886.

Maneesha K, Murty VSN, Ravichandran M, Lee T, Yu W and McPhaden MJ (2012) Upper ocean variability in the Bay of Bengal during the tropical cyclones Nargis and Laila. Progress in Oceanography, 106, 49-61.

Mark M (1995) Orthogonal wavelet analysis: Inter-annual variability in the sea surface temperature. Bulletin of American Meteorological Society, 76, 2179-2186.

Martin JM, Burton JD and Eisma D (eds.) (1981) River inputs to ocean systems; United Nation Press, Geneva, pp. 384.

McCreary JP, Han W, Shankar D and Shetye SR (1996) Dynamics of the east Indian Coastal Current. 2. Numerical solutions. Journal of Geophysical Research, 101, 13993-14010.

McCreary JP, Kundu PK and Molinari RL (1993) A numerical investigation of dynamics, thermodynamics and mixed layer processes in the Indian Ocean. Progress in Oceanography, 31, 181-244.

Mignot J, de Boyer Montégut C, Lazar A and Cravatte S (2007) Control of salinity on the mixed layer depth in the world ocean: 2. Tropical areas. Journal of Geophysical Research, 112, C10010, doi:10.1029/2006JC003954.

Murtugudde R and Busalacchi AJ (1998) Salinity effects in a tropical ocean model. Journal of Geophysical Research, 103, 3283-3300.

Murty CS and Varadachari VVR (1968) Upwelling along the east coast of India. Bulletin of the National Institute of Sciences of India, 36, 80-86.

Murty VSN, Sarma YVB, Rao DP and Murty CS (1992) Water characteristics, mixing and circulation in the Bay of Bengal during southwest monsoon. Journal of Marine Research, 50, 207-228.

Murty VSN, Subrahmanyam B, Tilvi V and O'Brien JJ (2004) A new technique for the estimation of sea surface salinity using the Outgoing Longwave Radiation. Journal of Geophysical Research, 109, C12006, doi:10.1029/2003JC001928.

Narvekar J and Prasanna Kumar S (2014) Mixed layer variability and chlorophyll a biomass in the Bay of Bengal, Biogeosciences, 11, 3819-3843.

Neetu S, Lengaigne M, Vincent EM, Vialard J, Madec G, Samson G, Ramesh Kumar MR and Durand F (2012) Influence of upper-ocean stratification on tropical cyclone induced surface cooling in the Bay of Bengal. Journal of Geophysical Research, 117, C12020, doi: 10.1029/2012JC008433.

Nuncio M (2007) Role of eddies in the Bay of Bengal circulation and hydrography and in the distribution of nutrients and chlorophyll. Ph.D Thesis, Goa University, pp 118.

Nuncio M and Prasannakumar S (2012) Life cycle of eddies along the western boundary of the Bay of Bengal and their implications. Journal of Marine Systems, 94, 9-17.

Okubo A (1970) Horizontal dispersion of floatable particles in the vicinity of velocity singularity such as convergences. Deep-Sea Research 1, 17, 445-454.

Pant V, Girishkumar MS, Udaya Bhaskar TVS, Ravichandran M, Papa F and Thangaprakash VP (2015) Observed interannual variability of near surface salinity in the Bay of Bengal. Journal of Geophysical Research, 120, 3315-3329, http://dx.doi.org/10.1002/2014JC010340.

Pond S and Pickard G L (1983) Introductory Dynamical Oceanography. Pergamon Press, Oxford, pp 263

Potemra JT, Luther ME and O'Brien J (1991) The seasonal circulation of the upper ocean in the BoB. Journal of Geophysical Research, 96, 12667-12683.

Prasad TG (1997) Annual and seasonal mean buoyancy fluxes for the tropical Indian Ocean. Current Science, 73, 667-674.

Prasannakumar S, Muraleedharan PM, Prasad TG, Gauns M, Ramaiah N, de Souza SN, Sardesai S and Madhupratap M (2002) Why is the Bay of Bengal less productive during summer monsoon compared to the Arabian Sea? Geophysical Research Letters, 29, 2235, doi:10.1029/2002GL016013.

Prasannakumar S, Narvekar J, Ajoykumar, Shaji C, Anand P, Sabu P, Rejomon G, Jossia, J, Jayaraj KA, Radhika R and Nair KKC (2004) Intrusion of Bay of Bengal water in to the Arabian Sea during winter monsoon and associated chemical and biological response. Geophysical Research Letters, 31, L15304, doi:10.1029/2004GL020247.

Prasanna Kumar S, Nuncio M, Narvekar, Ajoykumar, Sardesai S, De Souza SN, Gauns M, Ramaiah N and Madhupratap M (2004) Are eddies nature's trigger to enhance biological productivity in the Bay of Bengal? Geophysical Research Letters, L07309, doi:10.1029/2003GL019274.

Prasannakumar S, Nuncio M, Ramaiah N, Sardesai S, Narvekar J, Fernandes V and Paul JT (2007) Eddy-mediated biological productivity in the Bay of Bengal during fall and spring intermonsoons. Deep-Sea Research Part I, 54, 1619-1640.

Qiu Yun, Wenju Cai, Li Li and Xiaogang Guo (2012) Argo profiles variability of barrier layer in the tropical Indian Ocean and its relationship with the Indian Ocean Dipole. Geophysical Research Letters, 39, L08605, doi:10.1029/2012GL051441.

Rahul S and Gnanaseelan C (2013) Net Heat Flux Over the Indian Ocean: Trends, Driving Mechanisms, and Uncertainties. IEEE Geoscience and remote sensing letters, 10, doi: 10.1109/LGRS.2012.2223194

Ramasastry AA and Balaramamurty C (1957) Thermal fields and oceanic circulation along the east coast of India. Proceedings of Indian Academy of Sciences, 46, 293-323.

Ramanathan KR and Pisharody PR (1972) Water balance- Indian Ocean in World Water Balance. Institute of Hydrologic Science, Genthbrugge, Belgium, 39-41.

Rao AD, Joshi M and Ravichandran M (2009) Observed low-salinity plume off Gulf of Khambhat, India, during post-monsoon period. Geophysical Research Letters, 36, L03605, doi:10.1029/2008GL036091.

Rao DP and Sastry JS (1981) Circulation and distribution of some hydrographical properties during the late winter in the Bay of Bengal. Mahasagar - Bulletin of National Institute of Oceanography, 14, 1-16.

Rao LVG and Jayaraman R (1968a) Vertical distribution of temperature, salinity and density in the upper 500 m of the north equatorial Indian Ocean during the north-east monsoon period. Bulletin of National Institute of Science of India, 38, 123-147.

Rao LVG and Jayaraman R (1968b) Hydrographical features of the southern and central Bay of Bengal during the transition period between winter and summer. Bulletin of National Institute of Science of India, 38, 184-205.

Rao CK, Naqvi SWA, Kumar MD, Varaprasad SJD, Jayakumar DA, George MD and Singbal SYS (1994) Hydrochemistry of the Bay of Bengal: Possible reasons for a different water-column cycling of carbon and nitrogen from the Arabian Sea. Marine Chemistry, 47,279-290, http://dx.doi.org/10.1016/0304-4203 (94)90026-4.

Rao RR and Sivakumar R (2003) Seasonal variability of sea surface salinity and salt budget of the mixed layer of the north Indian Ocean. Journal of Geophysical Research, 108, 3009, doi: 10.1029/2001JC000907.

Rao RR, GirishKumar MS, Ravichandran M, Rao AR, Gopalakrishna VV and Thadathil P (2010) Interannual variability of Kelvin wave propagation in the wave guides of the equatorial Indian Ocean, the coastal Bay of Bengal and the southeastern Arabian Sea during 1993-2006. Deep-Sea Research I, doi:10.1016/j.dsr.2009.10.008

Rao SA, Gopalakrishna VV, Shetye SR and Yamagata T (2002) Why were cool SST anomalies absent in the Bay of Bengal during the 1997 Indian Ocean Dipole Event? Geophysical Research Letters, 29, doi:10.1029/2001/GL014645.

Rao TVN (2002) Spatial distribution of upwelling off the central east coast of India. Estuarine Coastal and Shelf Sciences, 54, 141-156.

Ravichandran M, Vinaychandran PN, Joseph S and Radhakrishnan K (2004) Results from the first Argo float deployed by India, Current Science, 86, 651-659.

Robinson AR (1983) Eddies in Marine science. Springer-Verlag, Berlin, Germany, pp 609.

Rochford DJ (1964) Salinity maximum in the upper 100 meters of the north Indian Ocean. Australian Journal of Marine Freshwater Research, 15, 1-24.

Saji NH, Goswami BN, Vinayachandran PN and Yamagata T (1999) A dipole mode in the tropical Indian Ocean. Nature, 401, 360-363.

Sarma YVB, Rama Rao EP, Saji PK and Sarma VVS (1999) Hydrography and Circulation of the Bay of Bengal during withdrawal phase of the southwest Monsoon. Oceanologia Acta, 22, 453-471.

Sasmal SK (1989) Hydrography of northern Bay of Bengal during southwest monsoon. Mahasagar-Bulletin of National Institute of Oceanography, 22, 105-112.

Sastry JS, Rao DP, Murty VSN, Sarma YVB, Suryanarayana A and Babu MT (1985) Watermass structure in the Bay of Bengal. Mahasagar-Bulletin of National Institute of Oceanography, 18, 153-162.

Satya Prakash, Mahesh C and Gairola RM (2012) Observed Relationship between Surface Freshwater Flux and Salinity in the North Indian Ocean. Atmospheric and Oceanic Science Letters, 5, 163-169.

Sengupta D, Bharath RG and Anitha DS (2008) Cyclone-induced mixing does not cool SST in the post-monsoon north Bay of Bengal. Atmospheric Science Letters, 9, 1-6, doi:10.1002/asl.162.

Sengupta D, Bharath Raj GN and Shenoi SSC (2006) Surface freshwater discharge from Bay of Bengal runoff and Indonesian throughflow in the tropical Indian Ocean. Geophysical Research Letters, 33, L22609, doi: 10.1029/2006GL027573.

Sengupta D, Bharath Raj GN, Ravichandran M, Sree Lekha J and Papa F (2016) Near surface salinity and stratification in the north Bay of Bengal from moored observations. Geophysical Research Letters, 43, 4448-4456

Shankar D, (2000) Seasonal cycle of sea level and currents along the coast of India. Current Science, 78, 279-288.

Shankar D, Mc Creary JP, Han W and Shetye SR (1996) Dynamics of the East India Coastal Current. 1. Analytic solutions forced by interior Ekman pumping and local alongshore winds. Journal of Geophysical Research, 101, 13975-13991.

Shankar D, Vinayachandran PN and Unnikrishnan AS (2002) The monsoon currents in the north Indian Ocean. Progress in Oceanography, 52, 63-120.

Shankar D and Shetye SR (1997) On the dynamics of the Lakshadweep high and low in the southeastern Arabian Sea. Journal of Geophysical Research, 102, 12551-12562.

Shenoi SSC (2010) Intra-seasonal variability of the coastal currents around India: A review of the evidences from new observations. Indian Journal of Geo-Marine Sciences, 39, 489-496.

Shenoi SSC, Shankar D and Shetye SR (2002) Differences in heat budgets of the near-surface Arabian Sea and Bay of Bengal: Implications for the summer monsoon. Journal of Geophysical Research, 107, doi:10.1029/2000JC000679.

Shenoi SSC, Shetye SR, Gouveia AD and Michael GS (1993) Salinity extrema in the Arabian Sea. In: Monsoon Biogeochemistry (Ed.) Ittekkot and Nair, 37-49.

Shenoi SSC, Shankar D, Michael GS, Kurian J, Varma KK, Ramesh Kumar MR, Almeida AM, Unnikrishnan AS, Fernandes W, Barreto N, Gnanaseelan C, Mathew R, Praju KV and Mahale V (2005) Hydrography and water masses in the southeastern Arabian Sea during March-June 2003. Journal of Earth System Science, 114, 475-491.

Shetye SR, Gouveia AD, Shankar D, Shenoi SSC, Vinayachandran PN, Sundar D, Michael GS and Nampoothiri G (1996) Hydrography and circulation in the western BoB during the northeast monsoon. Journal of Geophysical Research, 101, 14011-14025.

Shetye SR, Shenoi SSC, Gouveia AD, Michael GS, Sundar D and Nampoothiri G (1991) Wind-driven coastal upwelling along the western boundary of the Bay of Bengal during the southwest monsoon. Continental Shelf Research, 11, 1397-1408.

Shetye SR, Gouveia AD, Shenoi SSC, Sundar D, Michael GS and Nampoothiri G (1993) The western boundary current of the seasonal subtropical gyre in the Bay of Bengal. Journal of Geophysical Research, 98, 945-954.

Sil S and Arun Chakraborty (2015) Diagnosis of upwelling and downwelling signals in the Bay of Bengal. International Education and Research Journal, 1, 7-18.

Subramanian V (1993) Sediment load of Indian Rivers. Current Science, 64, 928-930.

Thadathil P and Ghosh AK (1992) Surface layer temperature inversion in the Arabian Sea during winter. Journal of Oceanography, 48, 293-304.

Thadathil P and Rama Raju DV (1987) Intrusion of Bay of Bengal water into Arabian Sea along the west coast of India during north east monsoon. In Contributions in Marine Sciences, (Dr. SZ Qasim's 60th birthday felicitation volume), 237-244.

Thadathil P, Gopalakrishna VV, Muraleedharan PM., Reddy GV, Araligidad N and Shenoy SSC (2002) Surface layer temperature inversion in the Bay of Bengal. Deep Sea Research I, 49, 1801-1818.

Thadathil P, Muralidharan PM, Rao RR, Somayajulu YK, Reddy GV and Revichandran C (2007) Observed seasonal variability of barrier layer in the Bay of Bengal. Journal of Geophysical Research, 112, C02009, doi:10.1029/ 2006JC003651.

Thompson B, Gnanaseelan C and Salvekar PS (2006) Variability in the Indian Ocean circulation and salinity and its impact on SST anomalies during dipole events. Journal of Marine Research, 64, 853-880.

Torrence C and Compo GP (1998) A practical guide to wavelet analysis. Bulletin of American Meteorological Society, 79, 61-78, doi: 10.1175/1520-0477079,0061:APGTWA.2.0.CO;2.

Turner JS (1973) Buoyancy Effects in Fluids, Cambridge University Press, Cambridge, MA/USA, pp 367.

Tziperman E, Cane MA, Zebiak SE, Xue Y and Blumenthal B (1998) Locking of El Nino's peak time to the end of the calendar year in the delayed oscillator picture of ENSO. Journal of Climate, 11, 2191-2199.

Varadachari VVR, Murty CS and Reddy CVG (1968) Salinity maxima associated with some subsurface watermasses in the upper layers of the Bay of Bengal. Mahasagar-Bulletin of National Institute of Science Academy, 38, 339-343.

Varkey MJ and Sastry JS (1992) Characteristic Mixing Triangles in the Bay of Bengal. In: Physical Processes in the Indian Seas (Proc. First Convention, ISPSO, 1990), 47-50.

Varkey MJ, Murty VSN and Suryanarayana A (1996) Physical oceanography of the Bay of Bengal, In: Oceanography and Marine Biology: an Annual Review. (Ed) Ansell AD, Gibson RN and Barnes M, 1-70.

Venezian M, Griffa A, Garraffo ZD, and Chassignet EP (2005) Lagrangian spin parameter and coherent structures from trajectories released in a high-resolution ocean model. Journal of Marine Research, 63, 753-788.

Vidya PJ and Prasanna Kumar S (2013) Role of mesoscale eddies on the variability of biogenic flux in the northern and central Bay of Bengal. Journal of Geophysical Research, 118, 5760-5771, doi:10.1002/jgrc.20423.

Vinayachandran PN and Nanjundiah RS (2009) Indian Ocean sea surface salinity variations in a coupled model. Climate Dynamics, 33, 245-263, doi:10.1007/ s00382-008-0511-6.

Vinayachandran PN, Masumoto Y, Mikawa T and Yamagata T (1999) Intrusion of the southwest monsoon current into the Bay of Bengal. Journal of Geophysical Research, 104, 11077-11085.

Vinayachandran PN, Shankar D, Vernekar S, Sandeep KK, Amol P, Neema CP and Chatterjee A (2013) A summer monsoon pump to keep the Bay of Bengal salty. Geophysical Research Letters, 40, 1777-1782, doi:10.1002/grl.50274.

Vinayachandran PN and Kurian J (2007) Hydrographic observations and model simulation of the Bay of Bengal freshwater plume. Deep-Sea Research, Part I, 54, 471-486.

Vinayachandran PN, Murty VSN and Ramesh Babu V (2002) Observation of barrier layer formation in the Bay of Bengal during summer monsoon. Journal of Geophysical Research, 107, 8018, doi:10.1029/2001JC000831.

Vinayachandran PN, Neema CP, Mathew S and Remya R (2012) Mechanisms of summer intraseasonal sea surface temperature oscillations in the Bay of Bengal. Journal of Geophysical Research, 117, C01005, doi:10.1029/ 2011JC007433.

Vincent EM, Lengaigne M, Vialard J, Madec G, Jourdain N and Masson S (2012) Assessing the oceanic control on the amplitude of sea surface cooling induced by tropical cyclones. Journal of Geophysical Research, 117, C05023, doi:10.1029/ 2011JC007705.

Vincent E M, Lengaigne M, Vialard J, Madec G, Jourdain N and Masson S (2012) Assessing the Oceanic Control on the Amplitude of sea Surface Cooling induced by Tropical Cyclones. Journal of Geophysical Research, 117, C05023, doi: 10.1029/2011JC007705.

Webster PJ, Moore AM, Loschnigg JP and Leben RR (1999) Coupled ocean-atmosphere dynamics in the Indian Ocean during 1997-1998. Nature, 401, 356- 360.

Weiss J (1991) The dynamics of enstrophy transfer in two dimensional hydrodynamics. Physica D Nonlinear Phenomena, 48, 273-294. doi:10.1016/0167-2789(91)90088-Q.

Wilson EA and Riser SC (2016) An assessment of the seasonal salinity budget for the upper Bay of Bengal. Journal of Physical Oceanography, 46, 1361-1376, http://dx.doi.org/10.1175/JPO-D-15-0147.1.

Yaremchuk M, Yu Z and McCreary J (2005) River discharge into the Bay of Bengal in an inverse ocean model. Geophysical Research Letters, 32, L16605, doi:10.1029/2005GL023750.

Yu L, O'Brien JJ and Yang J (1991) On the remote forcing of the circulation in the Bay of Bengal. Journal of Geophysical Research, 96, 20449-20454.

Zweng MM, Reagan JR, Antonov JI, Locarnini RA, Mishonov AV, Boyer TP, Garcia HE, Baranova OK, Johnson DR, Seidov D, and Biddle MM (2013) World Ocean Atlas 2013, Volume 2: Salinity. Levitus S (Ed.), Mishonov A (Technical Ed.), NOAA Atlas NESDIS 74, pp 39.

List of Publications of the author

Journals (2)

1. Anoopa Prasad C and Hareesh Kumar PV (2017) On the possible mechanisms for saltening of the Bay of Bengal, (Accepted in Defence Science Journal)

2. Anoopa Prasad C and Hareesh Kumar PV (2015) Evolution of watermasses in the upper layers of the Bay of Bengal. Disaster Advances, 8, 12-24

Symposia / Conference: 6 (International: 2; National: 4)

1. Anoopa Prasad C, Anil Kumar K, Anand P, Raghunatha Rao A and Pradeep Kumar T (2015) Inter-seasonal variability of mixed and barrier layer in the southeastern Arabian Sea. World Ocean Science Congress, 5-8 Feb 2015, Kochi, pp 249.

2. Anoopa Prasad C, Raghunadha Rao A, Mohan Kumar N and Pradeep Kumar T (2014) Estimation of mixed layer depth- A statistical approach using satellite derived sea surface density. National Symposium on METOC, 30-31 Oct 2014, Kochi.

3. Anoopa Prasad C and Hareesh Kumar PV (2014) An investigation on the presence of low salinity watermass in the southeastern Arabian Sea during winter. National Seminar on Successes and Challenges in Ocean and Atmospheric Research, 9-11 Oct 2014, Andhra University, Visakhapatnam, pp 18.

4. Anoopa Prasad C, Pradeep Kumar T, Shyni TN and Hareesh Kumar PV (2013) Mesoscale variability of thermohaline fields in the Northern Arabian Sea using Argo profiles. National Conference of Ocean Society of India, 26-28 Nov 2013, IITM, Pune, 98-100.

5. Anoopa Prasad C, Pradeep Kumar T and Hareesh Kumar PV (2013) Arabian Sea Watermass characteristics in the southeastern Arabian Sea: pre-monsoon and monsoon scenario. National Symposium on Coastal Oceanographic Studies: Modeling and Observations, 9-10 May 2013, NPOL, Kochi, 227-232.

6. Pradeep Kumar T, Anoopa Prasad C and Hareesh Kumar PV (2012) Evolution of Arabian Sea Watermass and its inter-annual variability. Pan Ocean Remote Sensing Conference, 5-9 Nov 2012, Kochi, pp 436.